REPUBLIQUE ALGERIENNE DEMOCRATIQUE ET POPULAIRE
MINISTERE DE L'ENSEIGNEMENT SUPERIEUR ET DE LA RECHERCHE SCIENTIFIQUE

UNIVERSITE M'Hamed BOUGARA de Boumerdès

Faculté des Hydrocarbures et de la chimie

Département Gisements Miniers Et Pétroliers

Mémoire de fin d'études

En vue de l'obtention du diplôme :

MASTER

Présenté par :

BOUALOUACHE Ahmed

ATTABA Mohamed Amine

Filière : Hydrocarbures

Spécialité : Génie pétrolier -Forage des puits pétroliers

Thème

Conception optimisée de fluides de forage à base de nano-particules et contrôle amélioré de la filtration : Méthodologies de mapping inverse et algorithmes évolutifs

---

Devant le jury:

BENYOUNES Khaled	Prof	UMBB	Président
BELIMANE Zakaria	MAB	UMBB	Encadreur
MESSAOUD Nadia	MAB	UMBB	Examinateur

Année Universitaire : 2023/ 2024

SCIENTIFIQUE PEOPLE'S DEMOCRATIC REPUBLIC OF ALGERIA

MINISTRY OF HIGHER EDUCATION AND SCIENTIFIC RESEARCH

University M'Hamed Bougara of Boumerdès

Faculty of Hydrocarbons and Chemistry

Department of Mining and Petroleum Reservoirs

Final Year Project

For the attainment of the degree:

MASTER'S

Presented by:

BOUALOUACHE Ahmed

ATTABA Mohamed Amine

Major: Hydrocarbons

Specialization: Petroleum Engineering - Oil Well Drilling

Topic

Inverse Mapping and EAs Methodologies for Optimized Nano-based Drilling Fluid Design and Enhanced Filtration control

---

In front of the jury:

BENYOUNES Khaled	Prof	UMBB	President
BELIMANE Zakaria	MAB	UMBB	supervisor
SAIFI Redha	MAB	UMBB	Examiner

Academic Year: 2023/ 2024

Homage

To My Mother:

In every dawn, your unwavering love illuminated my path,
A beacon through the labyrinth of learning,
Your gentle strength, a fortress against doubt,
I owe the sunrise of this achievement to your unwavering faith.

To My Father:

With every step, your quiet resolve steadied my stride,
Guiding me through the wilderness of knowledge,
Your wisdom, a compass in the tempest of uncertainty,
I stand here today, anchored by your unwavering support.

To My Sister:

In the tapestry of shared dreams and whispered hopes,
Your belief wove threads of courage and resilience,

To All Who Once Believed:

To the teachers, mentors, and friends who sparked inspiration,
To the late nights and early mornings, whispered promises in solitude,
Each heartbeat, a testament to collective dreams,
In this tale of perseverance, your belief was the magic that lit the stars.
To . of a Once Upon a Time

Ahmed

Homage

“To my family, who imparted upon me a dignified education, especially to the most incredible person in the world, my dear mother. To my father, my pillar of strength and true friend. To my beloved sister Selma and brothers Faysal and Fouad.”

Mohamed Amine

Gratitude and Recognition

To start with We begin by expressing our deepest gratitude to Allah, whose guidance and blessings have illuminated every step of our journey.

We extend heartfelt thanks to the esteemed members of the jury, Professor Benyounes and Professor Messaoud, for considering our work. Their expertise and dedication are indeed invaluable.

Special appreciation goes to our advisor, Professor Belimane, whose unwavering support, encouragement, and scholarly guidance have been instrumental in shaping this thesis.

We are profoundly thankful to all who contributed to this endeavor, whether through academic insights, technical assistance, or moral support. Each contribution has played a crucial role in the development and completion of our thesis.

We are also grateful to all members of the faculty of hydrocarbons and chemistry whose resources, facilities, and conducive academic environment have fostered an atmosphere of learning and growth.

Lastly, we extend our thanks to all our friends from MAFP19 whose encouragement, understanding, and companionship have provided solace during challenging times and made this journey memorable.

Abstract

The incorporation of nanoparticles into drilling fluids has emerged as a promising technique to enhance filtration control in drilling operations. This study aims to determine the optimal composition of nano-enhanced drilling fluids by leveraging advanced modeling techniques. We developed two general Artificial Neural Network (ANN) models: the first predicts the filtrate volume of nanoparticle-based mud, while the second, comprising four sub-models, forecasts the rheological properties of the same mud. To identify the optimal nano drilling fluid composition, we employed inverse mapping with Evolutionary Algorithms (EAs), integrating a sharing mechanism to constrain the search space using the rheology model as a control.

Our models demonstrated robust performance, showing significant improvements in predicting both filtration and rheological properties of nano-enhanced drilling fluids. The data used for training and validation were derived entirely from laboratory experiments. Future work integrating these models with real field data could revolutionize drilling fluid design and application, potentially leading to more efficient and cost-effective drilling operations.

Keywords : Nanotechnology, Drilling Mud Artificial, Intelligence (AI), Filtration Control, Rheological Properties, Artificial Neural Networks (ANN), Predictive Modeling, Machine Learning, Nano-Enhanced Fluids.

Résumé

L'incorporation de nanoparticules dans les fluides de forage a émergé comme une technique prometteuse pour améliorer le contrôle de la filtration dans les opérations de forage. Cette étude vise à déterminer la composition optimale des fluides de forage enrichis en nanoparticules en utilisant des techniques de modélisation avancées. Nous avons développé deux modèles généraux de réseaux de neurones artificiels (ANN) : le premier prédit le volume de filtrat de la boue à base de nanoparticules, tandis que le second, comprenant quatre sous-modèles, prévoit les propriétés rhéologiques de cette même boue. Pour identifier la composition optimale du fluide de forage nano, nous avons utilisé la cartographie inverse avec des algorithmes évolutifs (EA), intégrant un mécanisme de partage pour restreindre l'espace de recherche en utilisant le modèle rhéologique comme modèle de contrôle.

Nos modèles ont montré des performances robustes, affichant des améliorations significatives dans la prédiction des propriétés de filtration et de rhéologie des fluides de forage enrichis en nanoparticules. Les données utilisées pour l'entraînement et la validation proviennent entièrement d'expériences en laboratoire. Un travail futur intégrant ces modèles avec des données réelles pourrait révolutionner la conception et l'application des fluides de forage, conduisant potentiellement à des opérations de forage plus efficaces et plus économiques.

Mots clés: Nanotechnologie, Boue de Forage, Intelligence Artificielle (IA), Contrôle de Filtration, Propriétés Rhéologiques, Réseaux de Neurones Artificiels (RNA), Modélisation Prédictive, Apprentissage Automatique, Fluides Améliorés par des Nanoparticules.

ملخص

أصبح إدخال الجسيمات النانوية في سوائل الحفر تقنية واعدة لتحسين التحكم في الترشيح في عمليات الحفر. يهدف هذا البحث إلى تحديد التركيبة المثلى لسوائل الحفر المحسنة بالجسيمات النانوية باستخدام تقنيات النمذجة المتقدمة. لقد قمنا بتطوير نموذجين عامين للشبكات العصبية الاصطناعية :(ANN) الأول يتنبأ بحجم الترشيح لطين الحفر القائم على الجسيمات النانوية، بينما يتنبأ الثاني، الذي يتكون من أربعة نماذج فرعية، بالخصائص الريولوجية للطين نفسه. لتحديد التركيبة المثلى لسائل

الحفر النانوي، استخدمنا رسم الخرائط العكسي مع الخوارزميات التطورية(EAs) ، ودمجنا آلية المشاركة لتقييد مساحة البحث باستخدام نموذج الريولوجيا كنموذج تحكم.

أظهرت نماذجنا أداءً قويًا، حيث حققت تحسينات كبيرة في التنبؤ بخصائص الترشيح والريولوجيا لسوائل الحفر المحسنة بالجسيمات النانوية. تم الحصول على البيانات المستخدمة في التدريب والتحقق من التجارب المخبرية بشكل كامل. يمكن أن يؤدي العمل المستقبلي الذي يدمج هذه النماذج مع بيانات ميدانية حقيقية إلى ثورة في تصميم وتطبيق سوائل الحفر، مما يؤدي إلى عمليات حفر أكثر كفاءة وفعالية من حيث التكلفة.

الكلمات المفتاحية ، التحكم في الترشيح، الخصائص الريولوجية طين الحفر، الذكاء الاصطناعي النمذجة التنبؤية، التعلم الآلي، السوائل المحسنة بالنانو شبكات العصبية ا(ANN) ، النمذجة التنبؤية، التعلم الآلي، السوائل المحسنة بالنانو.

Table of Contents

Table of Contents

Figures List

Tables List

Nomenclature

DF	Drilling Fluid
RH	Rheological properties
AV	Apparent viscosity
PV	Plastic viscosity
YP	Yield point
GS10S	10 seconds Gel strength
GS10M	10 min Gel strength
LPLT	Low pressure low temperature
HPHT	High pressure High temperature.
WBM	Water Based Mud.
OBM	Oil Based Mud.
ANN	Artificial Neural Network.
SVM	Support Vector Machine.
HIS	Hybrid Intelligent System.
GA	Genetic Algorithms.
PSA	Particle Swarm Algorithms.
CBR	Case Based Reasoning.
AI	Artificial Intelligent.
AARE	Average Absolute Relative Error.
NP	Nanoparticles.
AV	Average Velocity.
BOP	Blow Out Preventer.
CML	Controlled Mud Level.
ECD	Equivalent Circulating Density.
SBM	Synthetic Based Mud.
EDM	Emulsion Drilling Mud.
IEM	Invert Emulsion Mud.
PV	Plastic viscosity.
AV	Apparent Viscosity
YP	Yield Point
GS	Gel Strength.
NPT	Non-Predictive Time.
EOR	Enhanced Oil Recovery.
OOIP	Original Oil in Place.
IFT	Interfacial Tension
HPAM	Hydrolyzed Polycrylamide.

Nomenclature

SMCN	Sodium Carboxymethyl Cellulose
SDS	Sodium Dodecyl Sulfate.
NT	Non treated
GTL	Gas To Liquid.
CNG	Compressed Natural Gas.
PEG-600	Polyethylene Glycol.
PVP	Polyvinylpyrrolidone
MWCNT	Multiwalled carbon nanotube.
CT	Computed Tomography
Tanh	Hyperbolic Tangent.
ReLU	Rectified Linear Unit.
RBS	Radial Basis Function Network.
SOM	Self-Organizing Map.
SOFM	Self-Organizing Feature Map
BP	Back Propagation.
BWBM	Bentonite Water Based Mud.
LSNDM	Low Solids Non-Dispersed Mud.
SP- WBM	Salt Polymer –Water Based Mud.
RD	Relative Deviation.
MSE	Mean Squared Error.
RMSE	Root Mean Squared Error.
MAPE	Main absolute percentage error
MAE	Main absolute error
R2	coefficient of determination
INN	Inverted neural networks
GA	Genetic algorithm
EA	Evolutionary algorithm
ML	Machine learning
DL	Deep learning
M-FLT	Filtrate predictive model
M-RH	Rheology predictive model
M-AV	Apparent viscosity predictive model
M-PV	Plastic viscosity predictive model
M-YP	Yield points predictive model
M-GS	Gel strength predictive model
LSVM	Linear Support Vector Machine
PSO	Particle swarm optimization
FFBP	Feed forward back propagation

sigmoid	Sigmoid Function
Soft plus	Softplus Activation Function
Soft sign	Softsign Activation Function
Selu	Scaled Exponential Linear Unit
Elu	Exponential Linear Unit
Relu 6	Rectified Linear Unit 6
Silu	Sigmoid Linear Unit (also known as Swish)
SGD	Stochastic Gradient Descent
ADAM	Adaptive Moment Estimation
PMS-PROP	Root Mean Square Propagation
SBX	Simulated Binary Crossover
FR	Fuzzy Recombination
Blx	Blend Crossover
LCO	Linear crossover operator
UNDX	Unimodal normally distributed crossover
UM	Uniform mutation
NUM	Non uniform mutation
GM	Gaussian mutation
PM	Polynomial mutation
RM	Random mutation
RWS	Rolette wheel selection
SUS	Stochastic universal sampling
TS	Tournament selection
RBS	Rank based selection
SSS	Steady state selection

General Introduction

The oil and gas (O&G) industry is a fundamental component of the global energy sector, providing the primary source of energy for industrial, commercial, and residential use. The increasing complexity of hydrocarbon reservoirs, coupled with the demand for cost-effective and environmentally sustainable practices, necessitates continuous advancements in drilling technologies. Central to the success of drilling operations is the effective design and management of drilling fluids, commonly referred to as drilling muds, which perform critical functions such as lubricating the drill bit, transporting cuttings to the surface, and maintaining wellbore stability.

Drilling engineering, a multifaceted discipline, focuses on the design, optimization, and implementation of drilling processes. This field encompasses well planning, drilling fluid formulation, and wellbore stability management. Engineers in this domain are tasked with developing techniques and methodologies to enhance drilling efficiency, reduce operational costs, and mitigate environmental impacts. Among these tasks, the optimization of drilling fluid properties is particularly crucial, as these fluids must function effectively under the extreme pressures and temperatures encountered during drilling.

Within drilling engineering, mud drilling engineering is a specialized branch dedicated to the study and advancement of drilling fluid technologies. The formulation of drilling muds requires a precise balance of components to achieve optimal rheological properties, ensuring efficient cuttings transport, minimal fluid loss, and robust wellbore stabilization. The intricate interplay between the physical and chemical properties of the drilling mud and the geological characteristics of the formation necessitates a deep understanding of fluid dynamics and material science.

Recent technological innovations have introduced transformative approaches to enhancing drilling fluid performance. Nanotechnology, for instance, has emerged as a promising field, with nanoparticles being incorporated into drilling muds to improve filtration control, rheology, and thermal stability. The unique properties of nanoparticles enable them to effectively bridge microfractures and form a more resilient filter cake, thereby reducing fluid loss and enhancing wellbore integrity. Concurrently, artificial intelligence (AI) has revolutionized the design and optimization of drilling fluids. AI algorithms can analyze vast datasets and generate predictive models to determine the optimal mud composition for specific drilling conditions, significantly improving efficiency and cost-effectiveness.

The convergence of nanotechnology and AI represents a significant advancement in drilling fluid engineering. This work aims to develop an AI model capable of designing optimal nano-enhanced mud compositions for enhanced filtration control across various controlled conditions. By leveraging the predictive and optimization power of AI and the advanced functionalities of nanoparticles, this study seeks to create drilling fluid designs that meet the stringent demands of modern drilling operations, ultimately enhancing drilling efficiency.

To achieve that we developed predictive models using artificial neural networks (ANN) to forecast key aspects such as filtrate invasion and rheological behavior. Advanced techniques are then employed to refine the filtrate invasion model and integrate it with the rheological ANN model, allowing for a comprehensive analysis of different drilling fluid compositions. By merging these models, we identify the optimal drilling mud compositions, ensuring the desired properties for both filtration control and rheological characteristics. This systematic approach highlights the precision of scientific study and the advancements in drilling fluid optimization through AI and nanotechnology.

To explore this evolution and its future potential, this thesis embarks on a journey through five meticulously crafted chapters, each unraveling a unique facet of this exciting intersection:

Chapter 1 sets the stage with a comprehensive literature review. Here, we explore the rich tapestry of research conducted in the same era, highlighting the pioneering studies and groundbreaking discoveries that have shaped our understanding of drilling fluids and their evolution.

Chapter 2 delves into the core principles of drilling fluids. We navigate through the fundamental aspects of rheology and filtration, dissecting the intricate behaviors and properties that define effective

drilling muds. This chapter lays the groundwork, providing essential insights into the mechanisms that govern drilling fluid performance.

In ***Chapter 3***, we venture into the realm of nanotechnology. This chapter focuses on the integration of nanoparticles within the oil and gas sector, with a particular emphasis on their revolutionary impact on drilling muds. We explore the unique properties of nanoparticles and how their incorporation can enhance drilling efficiency and stability.

Chapter 4 shifts the spotlight to artificial intelligence and machine learning. We delve into the models and algorithms employed in this work, uncovering how AI and ML are transforming drilling operations. This chapter illuminates the cutting-edge techniques used to optimize drilling processes, from real-time data analysis to predictive maintenance.

Finally, ***Chapter 5*** is the culmination of our exploration—cracking the code with a thorough analysis and presentation of results. This chapter synthesizes the findings, drawing conclusions from the data and insights gathered throughout the research. It is here that we unravel the mysteries and showcase the transformative potential of combining nanotechnology and AI in the drilling sector.

Each chapter of this thesis contributes to a compelling narrative, weaving together history, science, and innovation to offer a comprehensive understanding of nano-based drilling fluids and the role of AI in modern drilling practices.

Literature Review

CHAPTER I

Chapter 1. Literature review

Introduction

The exploration and extraction of oil and gas are critical to meeting global energy demands. Drilling fluids, often referred to as drilling muds, play a pivotal role in the drilling process. In recent years, advancements in artificial intelligence (AI) and nanotechnology have opened new frontiers in the enhancement of drilling fluids. AI's ability to analyze vast amounts of data and predict optimal drilling parameters, combined with nanotechnology's potential to create materials with superior properties, offers promising solutions to longstanding issues in the industry. This literature review delves into the origin and evolution of these cutting-edge technologies, exploring how they are revolutionizing the field of drilling fluids. By examining current research and applications, we aim to provide a comprehensive understanding of the potential benefits and challenges associated with integrating AI and nanotechnology into drilling practices.

1.1 The Use of Nanoparticles in Drilling Mud

Drilling mud, or drilling fluid, is a crucial component in the drilling process for oil and gas extraction. Its primary functions include lubricating and cooling the drill bit, carrying cuttings to the surface, maintaining hydrostatic pressure to prevent well blowouts, and stabilizing the wellbore[1]. Traditional drilling fluids are composed of water, oil, or synthetic-based fluids combined with various additives to enhance their properties.

1.1.1 The Need for Advanced Drilling Fluids

The increasing complexity of drilling operations, such as deeper wells, higher temperatures, and more challenging geological formations, necessitates improvements in drilling fluid performance[2]. Traditional additives sometimes fall short in terms of thermal stability, rheological control, and filtration properties. This has led to the exploration of advanced materials, such as nanoparticles, to enhance the capabilities of drilling muds. ***Figure 1-1*** and ***Figure 1-2*** illustrates the nanoparticle topic distribution and coverage map, the research studies conducted in this field, and the yearly and industry-wise document distribution.

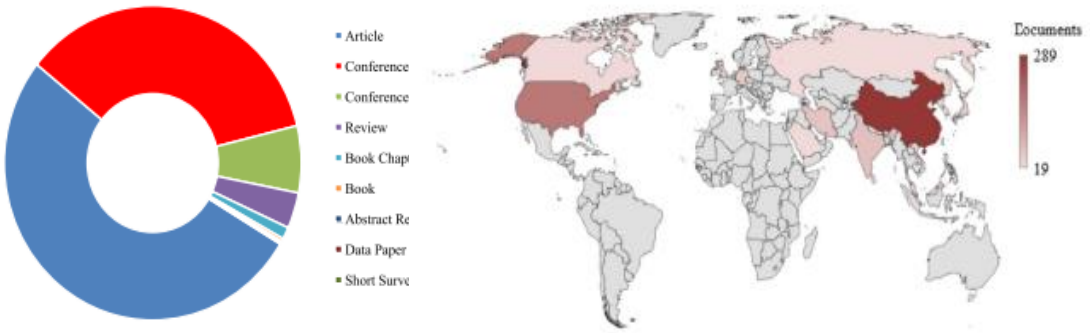

Figure 1-1 *Topic Distribution and Coverage Map [3]*

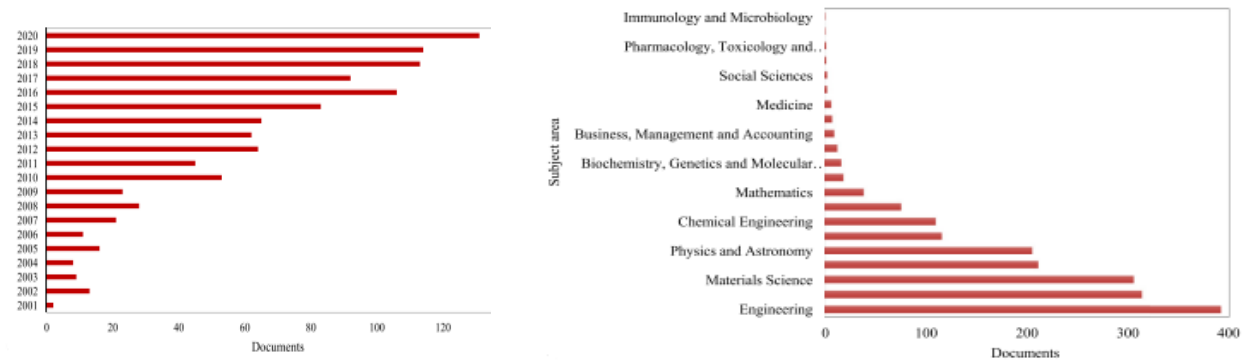

Figure 1-2 *Yearly and Industry-Wise Document Distribution[3]*

1.1.2 Emergence of Nanoparticles in Drilling Fluids

The concept of using nanoparticles in drilling muds arises from their unique properties at the nanoscale, which can significantly enhance fluid performance. Nanoparticles are particles between 1 and 100 nanometers (see ***Figure 1-3***)in size and exhibit high surface area to volume ratios, leading to enhanced reactivity and interaction with the fluid medium[4]. This idea was inspired by advancements in nanotechnology and its successful application in various fields such as medicine, electronics, and materials science.

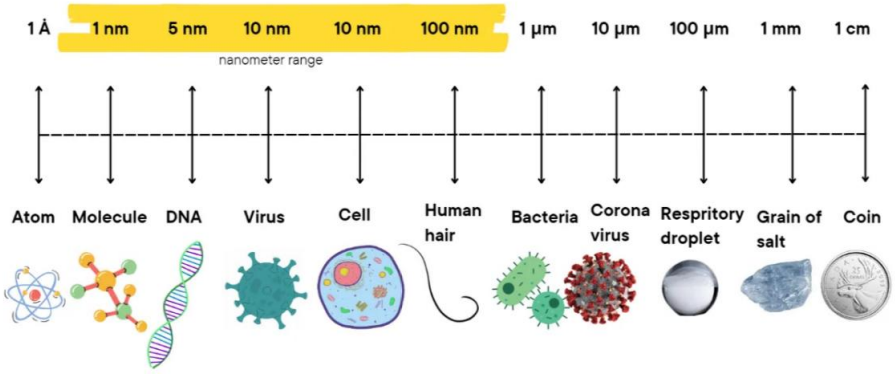

Figure 1-3 *Comparative Scale of Nanoparticle Sizes [5]*

1.1.3 Application and Benefits of Nanoparticles in Drilling Muds

Researchers have investigated various types of nanoparticles, including silica, titanium dioxide, aluminum oxide, and carbon nanotubes, for their potential benefits in drilling fluids[6]. The incorporation of nanoparticles can:

- **Improve Rheological Properties:** Nanoparticles can enhance the rheological performance of drilling fluids by improving their rheology and thixotropy, ensuring better suspension of cuttings and enhanced carrying capacity[5], [7].
- **Enhance Filtration Control:** The addition of nanoparticles can reduce fluid loss into the formation by forming a thin, impermeable filter cake on the wellbore walls[7]. This is critical in preventing formation damage and maintaining wellbore stability.
- **Increase Thermal Stability:** Nanoparticles can enhance the thermal stability of drilling fluids, making them more effective in high-temperature environments[3].

Numerous studies and field tests have reported positive outcomes from the use of nanoparticles in drilling fluids. For example, silica nanoparticles have been shown to improve the viscosity of water-based drilling fluids under high-temperature conditions[3]. This is particularly important for drilling

operations in challenging environments such as high-pressure and high-temperature wells (HPHT). Moreover, the addition of Fe2O3 nanoparticles with sizes ranging from 3 to 30 nm, nano silica and multi-walled carbon nanotubes in water-based drilling muds (WBM) has been shown to improve the rheology of the drilling fluid[3], [7].Additionally, the addition of SiO2 nanoparticles with a particle size of 50 nm has been found to reduce the thickness of the mud cake[7]. Also, the use of nano clay and nano silica has also been shown to improve the filtration properties of drilling fluids[3].IN terms of thermal stability, Titanium dioxide nanoparticles, for instance, has shown promising results in improving the thermal conductivity of water-based drilling fluids[5].

Table 1-1 Exemplary of studies that shows NPs effects on DFs

Author	NPs Type	Base fluid	Results' summary
Abdo et al (2016)	Sepiolite	Water	4.0 wt% of nano-sepiolite with 30-90 nm diameter in WBFs resulted in more stable rheological properties under various HPHT (77-365 F° and pressure up to 2,500 psi) conditions.
Agarwal et al. (2011)	Clay + silica	Oil	2.0 wt% of nanoclay individually, or mixed with 1 wt% nanosilica can improve the viscosity and gel strength of invert emulsion drilling fluids
Amanullah et al. (2011)	Not specified	Water	0.14wt% of nanoparticles in water-based drilling fluids showed superior gelling under LPLT condition
Anoop et al. (2014)	SiO2	Oil	2.0 vol% of nano-silica (SiO2) with 20 nm diameter in OBFs increased plastic viscosity at ambient condition and maintained stable rheological profile under HPHT (77-284 F° and pressure up to 6,000 psi) conditions.
Aftab et al. (2016)	ZnO	Water	1.0 gr of zinc oxide (ZnO) NPs in WBFs reduced filtrate loss under HPHT (150 and 250F°) conditions.
Barry et al. (2015)	Fe2O3	Water	The results showed decrease in fluid loss with the addition of ferric oxide (Fe2O3) NPs at LTLP conditions
Halali et al. (2016)	Carbon nanotubes	Water	0.8wt% of carbon nanotubes in WBFs reduced filtration loss under HPHT (248, 302, 347, 392F°) conditions.
Mahto et al. (2013)	Fly ash	Water	Experiments using fly ash NPs in WBFs achieved a 30% reduction in filtration loss. Increasing the concentration of the NPs and the size of the fly ash also decreases filtrate significantly
Taha et al. (2015)	Graphene	Water	5.0wt% of nano-graphene containing lubricant improved lubricity of the drilling fluids.

As set above, Nanoparticles have demonstrated significant potential in enhancing the performance of drilling mud, particularly under high-temperature conditions and one of the key advantages of incorporating nanoparticles is their ability to improve filtration properties. High concentrations of nanoparticles can form a more impermeable filter cake on the wellbore walls, which reduces filtrate invasion into the formation and helps maintain wellbore stability[8], [9], [10] . However, while a higher concentration of nanoparticles can effectively control filtration loss, it can also lead to increased friction and other rheological challenges[11]. This is because the presence of too many nanoparticles can alter the fluid's viscosity, making it more resistant to flow, which in turn increases the torque and drag on the drilling equipment.

1.1.4 Challenges and Future Directions

Despite the promising results, several challenges need to be addressed for the widespread adoption of nanoparticles in drilling fluids:

- **Dispersion and Stability:** Ensuring uniform dispersion and balance of nanoparticles in the drilling fluid over extended periods. An optimal concentration must be achieved to balance the improved filtration properties and minimize filtrate invasion while avoiding issues such as increased friction and altered rheological behavior. A balance must be struck between the benefits of filtration control and the potential drawbacks of increased friction and complex rheology[11] [9].Achieving this balance requires precise formulation and continuous monitoring to adapt to changing conditions.
- **Scale-Up and Field Implementation**: Laboratory results often differ from field conditions. Scaling up the use of nanoparticles from controlled environments to actual drilling operations poses significant technical and logistical challenges[3], [12].
- **Cost and Availability:** The production and incorporation of high-quality nanoparticles can be expensive, potentially offsetting the cost benefits gained from improved drilling performance[3], [12].
- **Environmental Concerns:** The environmental impact of nanoparticles, particularly their potential toxicity and long-term effects on ecosystems, requires thorough investigation and regulation[12].

In summary,

The incorporation of nanoparticles in drilling mud represents a significant advancement in drilling fluid technology, offering solutions to many challenges faced in modern drilling operations. While the initial results are promising, further research and development are necessary to address the associated challenges and fully realize the potential of this technology. Continued innovation and collaboration between academia, industry, and regulatory bodies will be crucial in driving the successful integration of nanoparticles into drilling practices.

1.2 The Use of Artificial Intelligence in Drilling Engineering

Artificial Intelligence (AI) has emerged as a transformative technology in various industries, including oil and gas. In drilling engineering, AI applications are revolutionizing traditional approaches by offering advanced data analytics, predictive modeling, and decision-making capabilities[13]. AI systems can analyze vast amounts of data from multiple sources in real-time, enabling proactive decision-making and optimization of drilling operations[14]. ***Figure 1-4*** Market Trends and Projected Estimates for Predictive Modeling and Operational Functions in Various O&G Industries in the future.

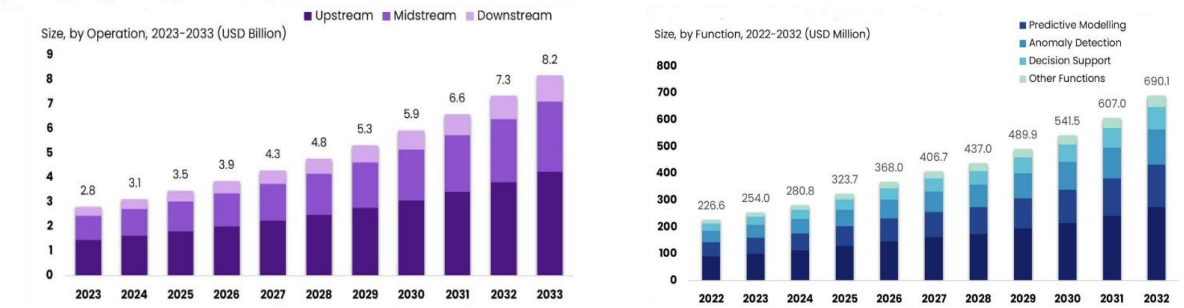

Figure 1-4 *Market Trends and estimated Projections for Predictive Modelling and Operational Functions in Various O/G Industries (2022-2033)[15] [16]*

1.2.1 AI Applications in Drilling Engineering

AI technologies are deployed across the entire drilling process, from planning and design to execution and post-drilling analysis(see ***Figure 1-5***). Some key applications include:

- **Predictive Maintenance:** AI algorithms analyze sensor data from drilling equipment to predict equipment failures before they occur, allowing for proactive maintenance and minimizing downtime[17].
- **Real-time Drilling Optimization:** AI-powered drilling optimization systems continuously analyze drilling parameters, formation characteristics, and downhole conditions to optimize drilling parameters in real-time, maximizing drilling efficiency and minimizing costs[17].
- **Formation Evaluation:** AI algorithms process and interpret downhole logging data to provide real-time insights into formation properties, facilitating accurate wellbore placement and reservoir characterization[14].
- **Risk Assessment and Mitigation:** AI models assess drilling risks by analyzing historical data, geological surveys, and real-time drilling data to identify potential hazards and develop mitigation strategies, enhancing safety and reducing operational risks[13].
- **Automated Decision Support Systems:** AI-based decision support systems assist drilling engineers in making complex decisions by analyzing multiple variables and recommending optimal courses of action[18].

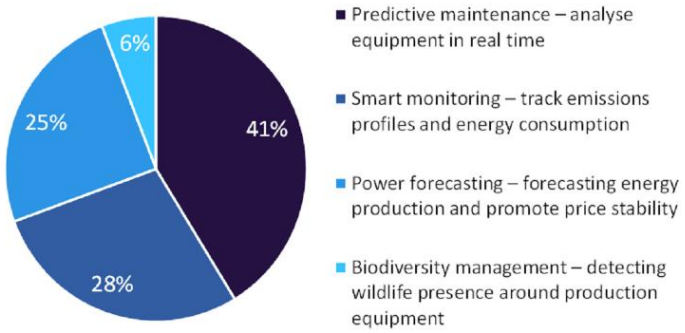

Figure 1-5 *AI vast applications in O/G sections[19]*

1.2.2 The Integration of AI in Drilling Mud Management

Drilling mud management is a critical aspect of drilling operations, and AI technologies offer several benefits in this area:

- **Optimized Mud Formulation:** AI algorithms analyze well data, geological information, and drilling parameters to recommend the optimal composition of drilling mud tailored to specific drilling conditions, maximizing performance and minimizing environmental impact[20].
- **Real-time Mud Property Monitoring:** AI systems monitor and analyze real-time drilling mud properties, such as viscosity, density, and filtration, to ensure mud performance meets operational requirements. Any deviations trigger automatic adjustments to maintain optimal mud properties[20].
- **Predictive Filtration Control:** AI models predict filtration behavior based on drilling parameters and mud composition, allowing for proactive adjustments to prevent filtration-related issues such as lost circulation and wellbore instability[17].
- **Environmental Impact Assessment:** AI algorithms evaluate the environmental impact of drilling mud formulations and operations by analyzing historical data and regulatory

requirements, helping operators comply with environmental regulations and minimize ecological footprint[17].

The integration of AI in drilling mud management has shown promising results in improving drilling efficiency, reducing costs, and enhancing environmental sustainability. Artificial Neural Networks (ANNs) dominate the field, being utilized in over 54% of the reviewed papers for predicting wellbore stability, optimizing drilling fluid properties, and enhancing drilling efficiency. Fuzzy Logic is employed to manage the uncertainty and ambiguity in drilling fluid properties, aiding in their prediction and optimization of drilling operations. Support Vector Machines (SVMs) are leveraged for their robustness against noise and ability to handle high-dimensional data. Hybrid Intelligent Systems (HIS) integrate multiple AI techniques to optimize drilling fluid properties and improve efficiency. Genetic Algorithms (GAs) and Particle Swarm Algorithms (PSA) are used to address complex optimization problems and enhance drilling efficiency, both showing resilience against noise. Case-Based Reasoning (CBR) is applied to predict drilling fluid properties and optimize operations, effectively managing uncertainty and ambiguity.

In relation to our current focus, several studies have demonstrated the application of Artificial Neural Networks (ANNs) in predicting the rheological properties of various drilling fluids. ***Tomiwa Oguntade et al*** [21]utilized an ANN from MATLAB to predict the rheological properties of water-based mud, including plastic viscosity, apparent viscosity, and yield point. Another research by ***Alsabaa et al.***[22]developed an ANN model for all-oil mud to predict plastic viscosity, yield point, behavior index, viscometer readings, and apparent viscosity. Moreover, ***Al-Azani et al*** [23]applied a BP-ANN model was applied to oil-based drilling fluid to predict plastic viscosity, apparent viscosity, and yield point in real-time. Lastly, an ANN model was used to provide rheological properties of an invert emulsion fluid, covering plastic viscosity, apparent viscosity, and yield point[24], more researches are displayed in ***Table 1-2*** Some studies of AI application in Dfs.

Table 1-2 Some studies of AI application in Dfs

Author	Purpose	Used model	Inputs	Outputs	Results
Gomma et al. (2020)	Real time RH prediction of over-balanced WBM	FFMLP	MW, MF, PV, YP	AV PV YP Flow behavior+consisteny index	AAPE=7.7% R^2 = 0.93
Gowida et al. (2019)	RH prediction of CaCl2 WBM	FFMLP	MW, MF	PV, AV, YP, Flow behavior+consisteny index	AAPE=2.4–3.9% R^2 = 0.97-0.99
Bispo et al. (2017)	AV prediction of WBM	FFMLP	T, concentration of barite, bentonite and Xanthan gum	AV	AAPE=10 %
Safari et al. (2014)	Hole ccleaning efficiency of foam drilling mud	FFMLP	Fluid composition and shale mineralogy	% Of shale recovery	RMSE=7.6-9.2 R^2 =0.85-0.9
Ahmadi (2016)	Drilling fuid density of OBM, WBM and SBM	GA	P, T	Mud density	RMSE=3.7084 AARE=2.144% R^2=0.9979
Tomiwa et al. (2019)	RH of a Solanum tuberosum formulated biopolymer improved WBM	FFMLP	Quantity of bentonite and solanum biopolymer	AV, PV, YP	RMSE =1.2522 R^2=0.9937

1.2.3 Challenges and Future Directions

Despite the significant benefits, several challenges remain in the widespread adoption of AI in drilling mud management:

- **Data Quality and Accessibility:** Access to high-quality, real-time data from diverse sources is essential for effective AI-driven decision-making. Ensuring data accuracy, reliability, and compatibility across different systems and platforms is a persistent challenge[25].
- **Algorithm Development and Validation**: Developing robust AI algorithms for mud management requires extensive training and validation using diverse datasets and real-world scenarios. Continuous refinement and validation are necessary to ensure algorithm accuracy and reliability[25].
- **Integration with Existing Systems:** Integrating AI technologies with existing drilling systems and workflows can be complex and require significant investment in infrastructure, training, and change management[25].
- **Regulatory and Ethical Considerations:** Addressing regulatory compliance, privacy, and ethical concerns surrounding AI adoption in drilling operations is crucial to ensure responsible and sustainable implementation[25].

In summary,

The integration of AI in drilling mud management represents a significant advancement in drilling engineering, offering unprecedented capabilities for optimization, efficiency, and environmental sustainability. While challenges remain, ongoing research and development efforts, coupled with collaboration between industry stakeholders and AI experts, are driving the evolution of AI technologies in drilling operations. With continued innovation and investment, AI is poised to revolutionize the future of drilling engineering, enabling safer, more efficient, and environmentally responsible energy extraction processes.

1.3 The Use of Artificial Intelligence in Nano-based Drilling Mud

The convergence of Artificial Intelligence (AI) and nanotechnology presents a promising frontier in drilling engineering. AI offers advanced data analytics and decision-making capabilities, while nanotechnology provides innovative solutions for enhancing drilling fluid performance. The integration of AI with nano-based drilling mud holds the potential to revolutionize drilling operations by optimizing fluid properties, improving efficiency, and minimizing environmental impact.

In the niche field of nanoparticle-based drilling mud integrated with AI that is considered trendy, the body of literature is not extensive, with relatively few articles available. Notably, ***Alireza Golsefatan and Shahbazi (2019)*** [26] pioneered the development of an AI model to predict the filtrate invasion of nanoparticle-enhanced drilling mud. Following this, ***Aleksander Lekomtsev et al. (2022)*** [27] advanced the field by employing ELM and PSO-LSSVM models to predict the filtration volume of drilling fluids containing various nanoparticles, achieving high accuracy in their predictions. Most recently, ***Gasser et al. (2023)*** [28]demonstrated the capabilities of an ANN model in predicting the filtrate invasion of nano-based mud, reporting an average absolute relative error (AARE) of less than 0.5% and a coefficient of determination (R^2) exceeding 0.99 across the dataset. These studies collectively highlight the significant potential of AI in enhancing the performance and predictability of nanoparticle-based drilling fluids.

In summary,

The integration of AI with nano-based drilling mud represents a significant advancement in drilling engineering, offering unprecedented capabilities for optimization, efficiency, and environmental sustainability. While challenges remain, ongoing research and development efforts, coupled with collaboration between industry stakeholders and AI experts, are driving the evolution of AI technologies in drilling operations. With continued innovation and investment, AI is poised to revolutionize the future

of nano-based drilling mud management, enabling safer, more efficient, and environmentally responsible energy extraction processes.

1.4 Roots and Realization

As detailed previously, finding the optimal concentration of nanoparticles (NPs) in drilling mud is essential for achieving peak performance. Also, a lot of AI models were created to predict both rheological properties and filtration loss of drilling fluids and those are the key elements that drive our innovative solution.

Ensuring uniform dispersion and balance of nanoparticles is essential. This process requires a delicate balance: maximizing the benefits of reduced filtrate invasion while mitigating the drawbacks of increased friction and rheological complications. Advanced AI-driven models are at the forefront of this optimization challenge. By meticulously analyzing a multitude of parameters, using these intelligent systems we aim to achieve the most effective nanoparticle concentrations, ensuring superior performance and minimizing adverse effects. This precise, data-driven approach not only enhances drilling efficiency but also represents the cutting edge of drilling fluid technology. taken this challenge head-on, this innovative optimization process forms the core of our thesis, promising to revolutionize the industry with smarter, more efficient drilling solutions.

Drilling Mud| Fundamentals and Essential Properties

CHAPTER II

Chapter 2. Drilling Mud: Fundamentals and Essential Properties

Introduction

Drilling wells in the oil and gas industry is a critical operation where drilling fluids, also known as drilling muds, play a pivotal role. These fluids account for approximately 20% of the total drilling costs ***(Agwu et al., 2015)***. During drilling, muds are pumped down the drill string to the drill bit to regulate formation pressure through the hydrostatic column of the mud. Drilling muds serve multiple essential functions, including suspending solids, removing cuttings, sealing formations, lubricating and cooling the drill bit, and preventing formation damage by managing subsurface pressure. There are two main types: oil-based fluids (OBMs) and water-based fluids (WBMs). Despite being more expensive, OBMs are preferred for challenging drilling conditions such as high temperatures, high pressures, reactive shale formations, and deep or directional wells ***(Zhong et al. 2019, Oseh et al. 2019; Li et al. 2016)***.

During the drilling process, as the mud filters into the formation, it carries fine solids and filtrate into permeable zones under pressure. This invasion of mud filtrate triggers the formation of a filter cake, which is essential for stabilizing the wellbore and protecting the formation from damage. The hole circulating system and mud-formation contact is described in ***Figure 2-1***.

> "In the world of drilling, the significance of drilling fluid is akin to the importance of water in sustaining life. It's indispensable." - ***Harold Hamm***

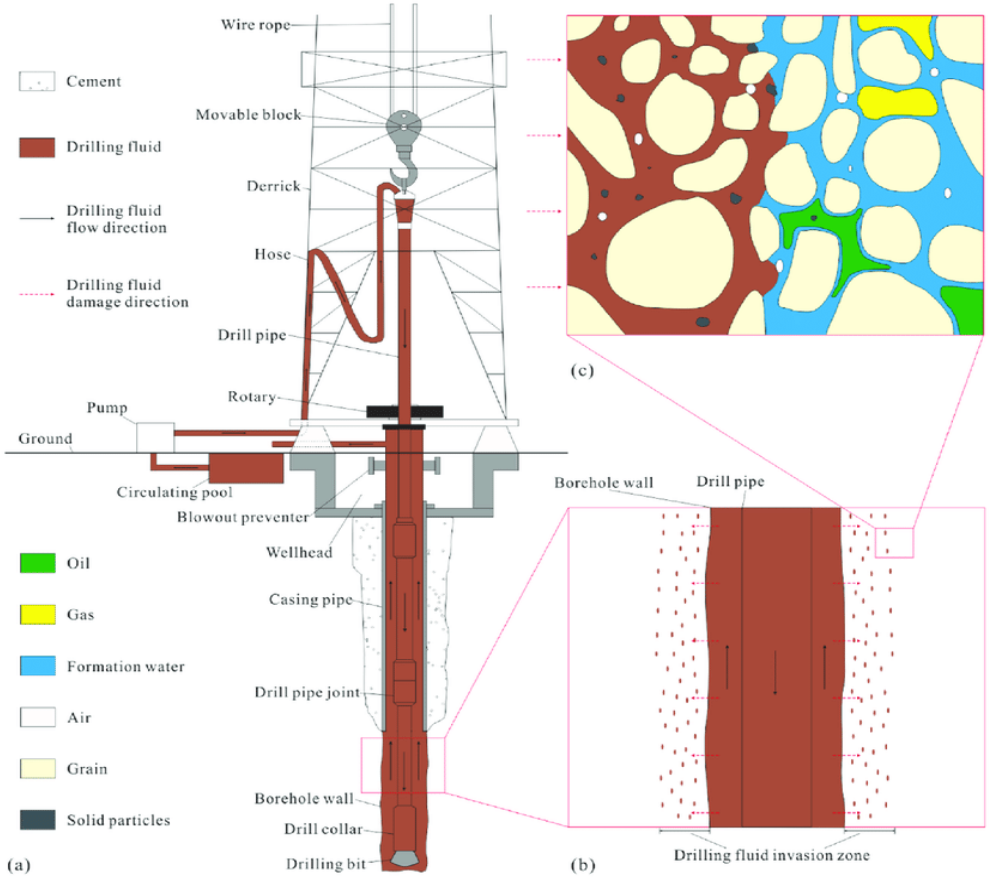

Figure 2-1 *Schematic diagram of drilling fluid cycle and formation contact* [29]

2.1 Functions of Drilling Fluids

Drilling fluids are essential to the success of any drilling operation. Their multifaceted roles ensure the safety, efficiency, and economic viability of drilling activities (see ***Figure 2-2***). Below are the key importance and functionalities of drilling fluids:

- ***Wellbore Stabilization:*** Drilling fluids maintain hydrostatic pressure to prevent well collapse and support the wellbore walls, preventing formation caving and sloughing. This stabilization is essential for maintaining the structural integrity of the well.
- ***Cuttings Transport and Removal:*** These fluids suspend and carry drill cuttings to the surface, preventing them from settling and causing blockages[30]. Effective cuttings transport ensures a clean wellbore, which is vital for smooth drilling operations[31].
- ***Cooling and Lubricating the Drill Bit***: By reducing friction and heat generated during drilling, drilling fluids cool and lubricate the drill bit, prolonging its life and that of other downhole equipment. This cooling and lubrication are critical for maintaining the efficiency and longevity of drilling tools[32].
- ***Controlling Formation Pressures:*** Drilling fluids balance formation pressures to avoid blowouts and maintain well control by exerting adequate downhole pressure[30]. This pressure control is fundamental for the safety and success of drilling activities.
- ***Filtration Control:*** The formation of a thin, impermeable filter cake on the wellbore wall minimizes fluid loss to the formation. Effective filtration control protects the formation and maintains drilling fluid performance[30].
- ***Supporting Core and Cutting Samples:*** Drilling fluids preserve the integrity of core samples for geological analysis and ensure accurate and reliable sampling of subsurface formations. This support is essential for obtaining high-quality geological data[33].
- ***Corrosion Inhibition:*** Protecting drilling equipment and casing from corrosion, drilling fluids extend the operational life of drilling infrastructure. Corrosion inhibition reduces maintenance costs and enhances equipment durability.
- ***Hole Cleaning:*** Ensuring the wellbore remains clear of obstructions, drilling fluids enhance drilling efficiency and prevent stuck pipe incidents. Effective hole cleaning is crucial for continuous and trouble-free drilling[31].
- ***Hydraulic Power Transmission:*** Drilling fluids power downhole motors and other hydraulic equipment, improving the efficiency of drilling tools and mechanisms. Hydraulic power transmission is vital for the operation of various downhole tools[34].
- ***Environmental and Safety Compliance:*** Formulating environmentally friendly and non-toxic drilling fluids ensures compliance with environmental regulations and safety standards. This compliance is essential for sustainable and responsible drilling operations[30].
- ***Formation Damage Prevention:*** Minimizing the invasion of drilling fluid into the formation protects reservoir integrity and optimizes production potential. Prevention of formation damage is key to maintaining the quality and productivity of the reservoir.
- ***Logging and Data Acquisition:*** Enhancing the accuracy of well logging and data collection, drilling fluids provide a medium for transmitting data from downhole sensors to the surface. This function is crucial for real-time monitoring and decision-making during drilling operations.

By addressing these critical functionalities, drilling fluids play a pivotal role in the overall success of drilling operations, contributing to improved efficiency, safety, and economic outcomes. Failure to meet these criteria can lead to solids settling, wellbore bridging, stuck pipe, hole fill, and loss of hydrostatic pressure, causing serious issues[35].

While a drilling fluid serves several critical functions, it is important to note that its effectiveness largely depends on its specific properties ***(Ljones, 2013).*** By adjusting the composition of these fluids, it is possible to achieve the desired properties for particular environmental conditions.

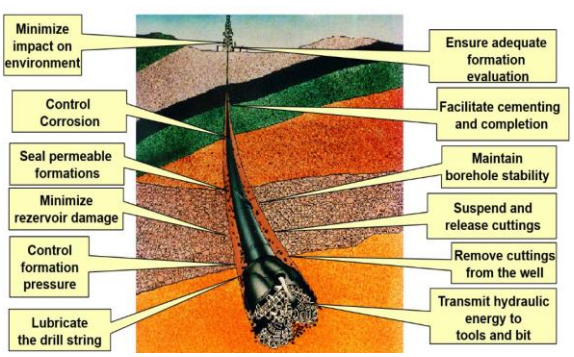

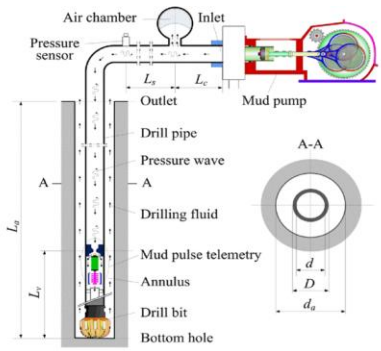

Figure 2-2 *Drilling mud functions and more detailed mud flow loop* [36]

2.2 Types and composition of drilling fluids

Various types of drilling fluids are used in the petroleum industry, each tailored to specific drilling conditions:

- **Water-Based Mud (WBM):** Predominant in drilling, WBM utilizes fresh or seawater as its continuous phase, along with clay and brine. It's widely used due to its availability and effectiveness in various drilling conditions.
- **Oil-Based Mud (OBM):** With oil (typically gas oil) as its continuous phase, OBM is employed when WBM is insufficient. Despite being costly, OBM delivers superior results due to its reverse-emulsions of saltwater in a continuous oil phase stabilized by surfactants.
- **Synthetic Based Mud (SBM):** Similar to OBM but less toxic and environmentally impactful, SBM comprises olefins, esters, and sometimes paraffins. It offers low kinetic viscosity, suitable for low-pressure conditions.
- **Emulsion Drilling Mud (EDM):** Comprising emulsion-based phases, EDM utilizes saltwater (brine) as the outer phase and oil as the inner phase. Surfactants are applied to make the two phases miscible, offering a cost-effective and environmentally friendly alternative.
- **Invert Emulsion Mud (IEM**): Resembling EDM in composition, IEM features an inverse phase distribution with oil as the outer phase and saltwater (brine) as the inner phase. It offers light viscosity and is suitable for high-temperature conditions.
- **Air Drilling Fluid:** Utilized for underbalanced pressure drilling, air drilling fluids are aerosols known for their high penetration rates and minimal formation damage. Understanding formation hydraulics is crucial for successful application.
- **Foam Drilling Fluids:** Comprising gas and liquid phases, foam drilling fluids are effective in underbalanced or deep-water wells. They offer faster drilling rates compared to water or oil-based fluids, making them suitable for specific drilling scenarios.

Going further, all types set above are tailored base on the specific objectives. The composition of drilling fluids is highly dependent on the specific requirements of the drilling operation. Engineers design drilling fluids to best performance based on real-time conditions.

Table 2-1 Types of Drilling fluids [37]

	family First			family Second		family Third
	Water-based			Oil-based	Synthetic-based	Gas-based
Application worldwide	50% of wells			10%	30% (mostly deep offshore)	10% of wells
Types/base	HPWM	Non-dispersed systems	Dispersed systems	Diesel or mineral low toxic oil	Ester, olefins, paraffins	Air, mist, foam, classical mud with nitrogen
Key reasons for selection	-improved rheology -well/hole stability -moderate temperature	-inhibition issues -high salinity -logistical challenges	-toPHole drilling -low cost and simple -spud mud	-high temperature -well/hole stability -torque and drag -better lubrication -increased ROP	-high temperature -well/hole stability -torque and drag -better lubrication -increased ROP -offshore disposal challenges	- underbalanced drilling -high penetration rate -low formation damage -no circulation loss - poorly fractured formations
Cost	Medium to high	Low	Low	high	High	High

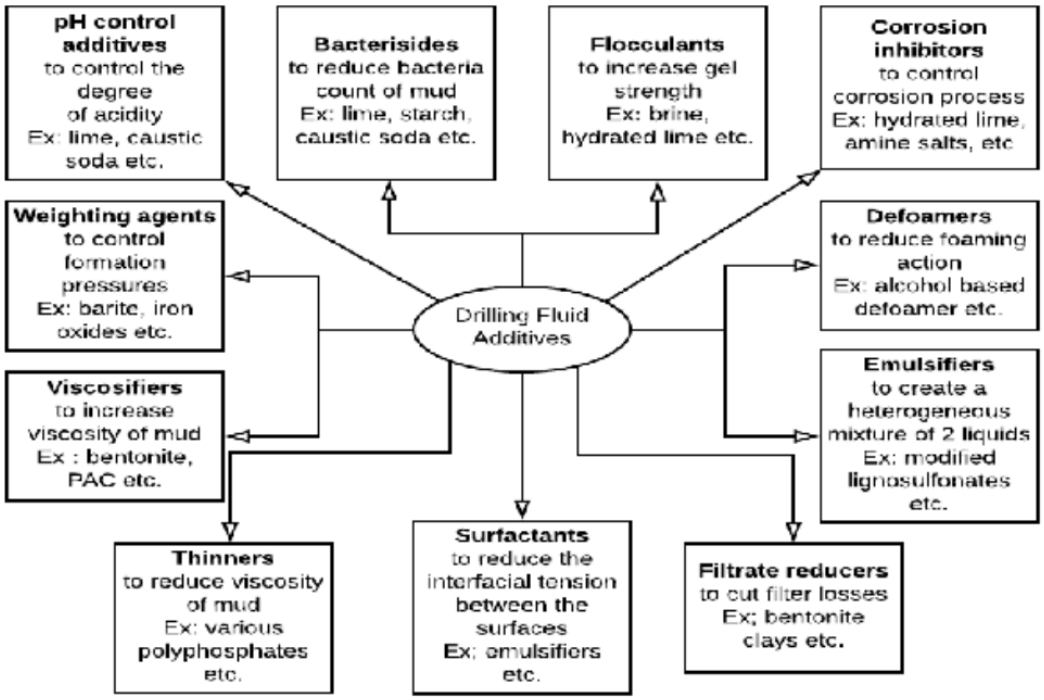

Figure 2-3 *Drilling fluid key components*[38]

2.3 Properties of drilling fluid

Drilling fluids, although accounting for only 5% to 15% of the total drilling cost, can be responsible for up to 100% of drilling problems. ***(Bloys et.al., 1994)***

Selecting an appropriate drilling fluid system involves initially choosing a mud family based on the rock formation characteristics while considering both financial implications and environmental impacts. Key factors influencing this choice include well design, formation pressure, rock mechanics, formation chemistry, and minimizing adverse effects on the producing formation. Environmental regulations, logistics, and cost are also crucial considerations[39]. Simulating down-hole conditions and optimizing fluid design play vital roles in reducing non-productive time and enhancing overall drilling efficiency.[39]

To meet these significant conditions, a drilling fluid must possess five fundamental properties: rheology, fluid loss, chemical properties, solid content, and density. For any drilling fluid type, these properties can be adjusted and optimized using various chemicals and additives. **(Bloys et.al., 1994).**

The properties of drilling fluids play a crucial role in their performance and effectiveness during drilling operations. These properties dictate the fluids' ability to meet operational requirements and are pivotal in selecting the appropriate fluid for specific geological conditions. In this section, we will explore the essential properties that define drilling fluids.

2.3.1 Density: Controlling Mud Weight for Effective drilling operations

Ensuring proper wellbore stability is critical in drilling operations, and this is primarily achieved through meticulous control of drilling mud density, often referred to as mud weight. Mud density plays a pivotal role in mitigating issues such as wellbore instability, which can result in challenges like hole collapse, formation damage, lost circulation, and stuck pipe [40]. This section will thoroughly examine the significance of density control, delve into the techniques employed for measuring and adjusting mud weight, and analyze how various drilling conditions impact mud density.

2.3.1.1 Understanding the Importance of Density Control

Maintaining optimal mud weight is crucial for ensuring effective wellbore stability during drilling operations. If the mud weight is too light, it may fail to exert sufficient hydrostatic pressure to balance the formation pressure[41] potentially causing formation fluid influx and leading to a blowout. Conversely, if the mud weight is too heavy, it can exert excessive pressure on the formation, resulting in issues like lost circulation, differential sticking, and other drilling challenges [46]. Therefore, achieving the right balance in mud weight is essential for safe and efficient drilling operations.

2.3.1.2 Measuring and Adjusting Mud Weight

Ensuring proper wellbore stability in drilling operations relies on precise measurement and control of mud weight. Typically, drilling engineers use instruments such as mud balances or mud scales to accurately determine the density of the drilling mud. These tools provide a straightforward method for assessing mud weight, allowing engineers to make necessary adjustments to achieve the desired density. Adjustments to mud weight involve adding weighting materials like barite or hematite to increase density, or incorporating water or low-density additives to decrease it [41]. Careful monitoring and control during the addition of these materials are crucial to maintaining consistent mud weight throughout the drilling process [42]. In challenging drilling environments, advanced drilling fluid systems such as oil-based or synthetic-based muds offer enhanced control over mud density[41]. When altering mud weight, it's essential to consider potential impacts on other critical mud properties. For instance, increasing mud weight with weighting materials can raise viscosity, affecting the hydraulic

efficiency of the drilling fluid. Therefore, achieving a balance between mud density and other essential properties is paramount to ensuring optimal drilling performance[42].

2.3.1.3 ***Factors Affecting Mud Density***

Several factors influence the required mud density for maintaining wellbore stability. Key considerations include the type of formation being drilled, the size of the wellbore, and the drilling depth. For instance, when drilling through highly permeable formations, a higher mud weight may be needed to prevent fluid influx. [42]. Likewise, drilling in narrow wellbores may necessitate a lighter mud weight to avoid exerting excessive pressure on the formation. Additionally, temperature and pressure variations at different drilling depths can significantly affect mud density[42]. As drilling depth increases, the hydrostatic pressure exerted by the mud column also rises. Consequently, adjustments in mud weight are necessary to maintain wellbore stability and balance the formation pressures effectively [42].

2.3.2 Solid content

The solid content in drilling fluids is a critical factor affecting the performance and efficiency of drilling operations. Managing solid content involves understanding its impact on various properties of the drilling fluid, including density, viscosity, and rheological behavior. Efficient solid control is essential for maintaining optimal drilling conditions and ensuring the longevity of equipment.

2.3.2.1 ***Impact on Bottom Hole Pressure (BHP)***

High solids content can significantly increase the density and viscosity of drilling mud, leading to elevated BHP. This increased pressure can cause hydraulic fracturing and mud losses into the formation. Effective control of mud density is crucial to avoid excessive BHP and prevent issues like thick filter cake formation, which can result in the drill string getting stuck due to differential sticking.

2.3.2.2 ***Effect on Plastic Viscosity (PV)***

Plastic viscosity (PV) is influenced by the concentration, size, and shape of solid particles in the drilling fluid. Higher PV indicates a higher percentage of solids or smaller particle sizes, leading to increased surface area and drag. High PV necessitates greater pumping pressure, raising the Effective Circulating Density (ECD) and complicating drilling operations. Efficient removal of drilled solids reduces PV, thereby improving drilling performance.

2.3.2.3 ***Influence on Yield Point (YP)***

The yield point (YP) measures the initial resistance of the fluid to flow, caused by electrochemical forces between particles. High solid concentrations increase YP, affecting the fluid's ability to lift cuttings and increasing swabbing effects. Maintaining appropriate YP and viscosity is essential for effective cuttings transport and minimizing operational issues. However, high YP can reduce the effectiveness of fine mesh shaker screens, requiring the use of coarser screens.

2.3.2.4 ***Impact on Rate of Penetration (ROP)***

Excessive solids in the drilling fluid negatively affect the rate of penetration (ROP) by increasing the mud's density and viscosity. This heightened density exerts greater differential pressure, slowing down ROP. Low viscosity mud promotes faster penetration by efficiently removing drilled cuttings. Keeping non-colloidal solid concentrations below 4% supports high ROP levels, ensuring efficient drilling progress.

2.3.2.5 ***Effect on Drag and Effective Circulating Density (ECD)***

Fluid rheology plays a vital role in solid transport and hole cleaning. Low viscosity fluids in turbulent flow are ideal for picking up solids, while high viscosity fluids with high YP/PV ratios are preferred when ECD is not a limiting factor. Maintaining low viscosity helps keep ECD within safe limits, as elevated viscosity due to increased low gravity solids (LGS) can raise ECD. Regular

monitoring of solid control equipment is necessary to minimize LGS and maintain efficient drilling operations.

2.3.3 Rheology of Drilling Fluid

The rheology of drilling fluids is a complex field that involves studying the deformation and flow of the fluid under various shear stresses and rates. Drilling fluids are typically non-Newtonian fluids, meaning their viscosity is not constant and depends on the shear rate.

2.3.3.1 Rheological properties

The rheological properties of drilling fluids are used to design and evaluate the hydraulics and assess the functionality of the mud system. Regular monitoring and adjustment of drilling fluid rheology is essential for maintaining wellbore stability, optimizing drilling performance, and minimizing equipment wear. Measurement techniques such as Marsh Funnel Viscosity, Rotational Viscometer, Gel Strength Measurement, and API Filtration Test can be used to assess the rheological properties of drilling fluids. Here are the definitions of the key rheological properties of drilling mud:

- ***Plastic Viscosity:***

Plastic viscosity is a measure of the resistance of the fluid to flow due to mechanical friction. It is typically measured at high shear rates and in lab, is calculated as the difference between the 600 RPM reading and the 300 RPM reading.

$$\mathrm{PV} = \theta_{600} - \theta_{300} \qquad 2\text{-}1$$

- Apparent Viscosity:

Apparent viscosity is a measure of the resistance to flow in a drilling fluid under specific conditions, typically taking into account the non-Newtonian nature of the fluid. In lab, it is calculated as half of the 600 RPM reading. Apparent viscosity is crucial for understanding how the fluid will flow under various conditions and is a key parameter in designing circulating systems for drilling operations.

$$\mathrm{AV} = \frac{\theta_{600}}{2} \qquad 2\text{-}2$$

- Yield Point:

The yield point is the minimum stress required for the fluid to flow. It reflects the electro-chemical or attractive forces in the mud under flow conditions. The yield point of the mud is essential as it indicates the fluid's ability to carry drilled cuttings out of the hole.

$$\mathrm{YP} = \theta_{300} - \mathrm{PV} \qquad 2\text{-}3$$

- Gel Strength

Gel strength is the shear stress of drilling mud measured at a low shear rate, usually with a viscometer after the mud has been static for periods specified by standard API procedures (10 seconds, 10 minutes, and 30 minutes) [42]. Proper gel strength is crucial to prevent downhole solids buildup and cuttings settling when circulation stops, which can cause significant operational issues. Adequate gel strength ensures a clean wellbore by allowing the drill bit to cut new formations rather than re-grinding settled cuttings, thereby increasing the rate of penetration [40]. However, achieving the right balance is essential: low gel strength can cause cuttings accumulation and barite sagging, while high gel strength can lead to pressure losses, formation fractures, and solids control problems. Vertical boreholes are less affected by high gel strength due to the longer interval for cuttings to settle, whereas horizontal wells need higher gel strength to hold cuttings in place until they can be transported out [41]. The optimal gel strength for horizontal wells should form quickly, reach an appropriate level, and remain stable. There is currently no established method for mathematically predicting gel strengths in any fluid system [41].

$$\mathrm{GS} = \theta_{\mathrm{gel}} \qquad 2\text{-}4$$

In summary, the rheology of drilling fluids is a complex field that involves understanding the deformation and flow of the fluid under various shear stresses and rates. Understanding these factors

and their impact on drilling mud rheology is crucial for optimizing drilling operations and preventing drilling problems. Regular rheological measurements and adjustments to the mud composition can help maintain the desired rheological properties and ensure successful drilling operations.

2.3.3.2 ***Rheological models***

Rheological models are mathematical tools that describe how drilling fluids behave under different shear stresses and shear rates. In the oil industry, the most commonly employed models are the Bingham Plastic and Ostwald de Waele (Power Law) models. However, in practice, many drilling muds are better represented by the Modified Power Law or Herschel-Bulkley models. These advanced models provide more accurate predictions of circulating pressure losses and other critical parameters in drilling operations.

Rheological models are essential in studying drilling fluids as they help stimulate their behavior under various conditions. Drilling fluids exhibit three flow regimes: plug flow, laminar flow, and turbulent flow [48]. To accurately represent these regimes, different rheological models are employed, including Newtonian, Bingham Plastic, and Power Law models. These models are vital for understanding and predicting the performance of drilling fluids in real-world applications.

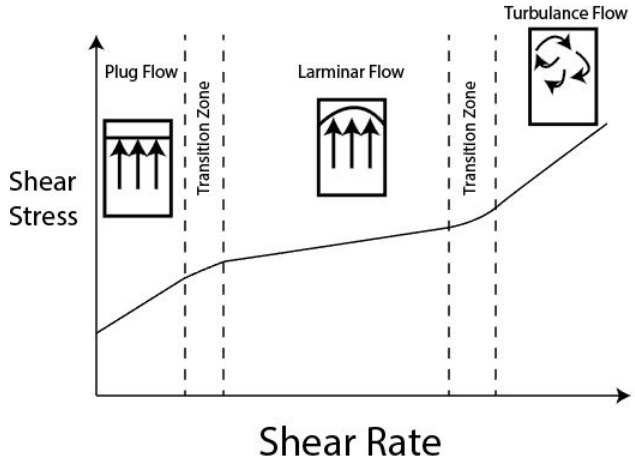

Figure 2-4 *Different DFs flow regimes*[43]

Rheological models are vital for understanding and predicting the behavior of drilling fluids during operations. Different models provide insights into how these fluids react under various conditions:

- **Newtonian Fluid Model**: This is the simplest model where the relationship between shear stress and shear rate is linear and passes through the origin. Newtonian fluids, such as light oil, water, and salt solutions, have particles no larger than the fluid molecules. However, Newtonian fluids do not accurately represent drilling fluids, as their viscosity remains constant regardless of the shear rate. Drilling fluids are much more complex, with behavior significantly influenced by interactions between fine particle suspensions in the mud [50].
- **Bingham Plastic Model**: This is the most commonly used model for non-Newtonian fluids. It assumes that shear rate is a linear function of shear stress, with the yield point or threshold stress being where shear rate is zero. The slope of the shear stress versus shear rate curve represents the plastic viscosity [50].
- **Power Law Model**: This model describes non-Newtonian fluid behavior where the shear stress versus shear rate curve, known as the "consistency curve," follows an exponential equation [50].
- **Herschel-Bulkley Model**: This more advanced model accurately predicts drilling mud rheology across the entire range of shear rates. It offers advantages over the Bingham Plastic and Power Law models by more precisely characterizing mud behavior under different shear conditions [50].

In summary, rheological models are critical for predicting drilling fluid behavior during operations. While the Bingham Plastic and Ostwald de Waele (Power Law) models are commonly used in the oil

industry, drilling muds often align more closely with the Modified Power Law or Herschel-Bulkley models. These models are essential for predicting circulating pressure losses and other key parameters in drilling operations.

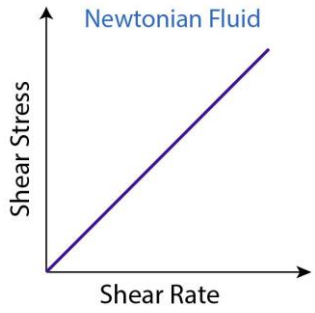

$\tau = \mu\dot{\gamma}$

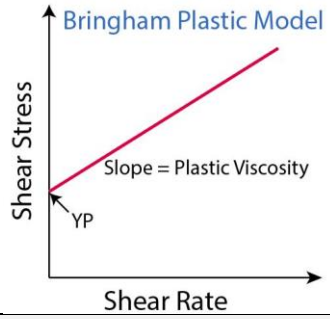

$\tau = \tau_0 + \mu_p \dot{\gamma}$

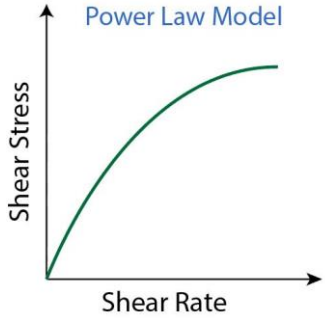

$\tau = K(\dot{\gamma}^n)$

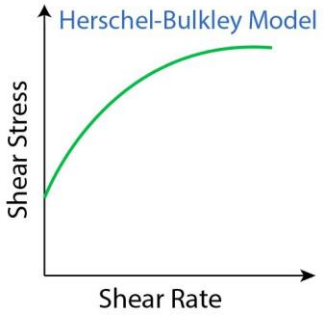

$\tau = \tau_0 + K(\dot{\gamma}^n)$

Figure 2-5 *Common RH models for drilling mud* [44]

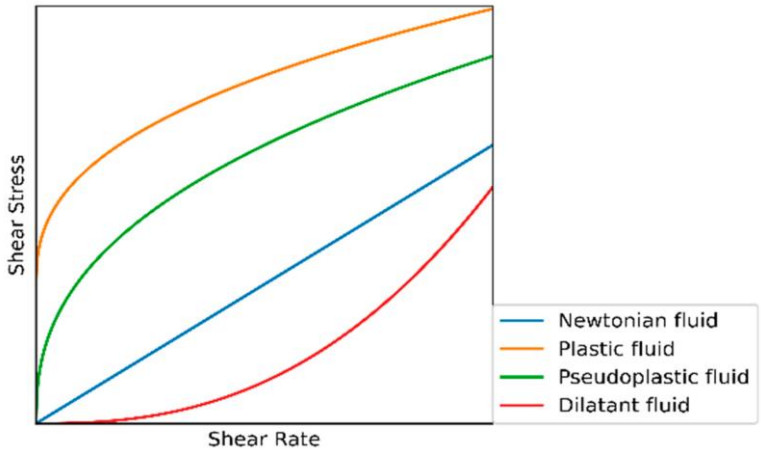

Figure 2 5 *Different types of fluids* [45]

2.3.4 Filtration properties

Drilling mud filtration is a critical aspect of well drilling operations, impacting well stability, productivity, and overall drilling efficiency. The filtration process involves the separation of the liquid phase of the drilling fluid (mud) from the solid particles as the fluid interacts with the formation. When differential pressure is applied, filtration takes place on the filter medium which, due to its permeability, allows a certain quantity of colloid to pass through.

2.3.4.1 ***Filtration Theory***

To understand how filtration occurs let's break it down, the drilling fluid, comprising a liquid phase and suspended clay particles, encounters hydrostatic pressure while interacting with porous and permeable formations. Simply, when the pore diameter of the formation exceeds that of the suspended clays, the fluid is entirely absorbed, leading to extreme cases of total losses where no mud returns to the surface[46]. Conversely, if the pore diameter is smaller than some suspended elements, filtration occurs, resulting in the deposition of these elements on the formation walls, creating a filter cake. The base liquid, or filtrate, then invades the formation. The permeability of this filter cake is crucial in determining the extent of filtration[46]. Effective management of drilling fluid properties is essential to minimize fluid loss and ensure wellbore stability, highlighting the importance of understanding the interaction between drilling fluids and formation characteristics. Filtration process can be categorized into below phases:

- **Initial Filtration (Spurt Loss):** When drilling mud is first introduced to a permeable formation, the liquid phase (filtrate) quickly invades the formation pores. This rapid initial invasion is known as spurt loss. The solids in the drilling mud start to deposit on the formation surface, beginning the mud cake formation process.
- **Mud Cake Formation:** As the spurt loss phase concludes, the filtration rate decreases and the mud cake begins to develop more uniformly. The process involves several steps:
- **Particle Deposition:** Solid particles from the drilling mud (such as clays, barite, and other additives) start to accumulate on the formation face, creating a thin layer.
- **Filtrate Flow:** The liquid phase continues to permeate into the formation, but now it has to pass through the developing mud cake, which acts as a filter.
- **Cake Growth:** As more solids deposit, the mud cake thickens. The rate of cake growth depends on the mud properties and the formation characteristics.
- **Steady-State Filtration:** Once the mud cake reaches a certain thickness, the filtration process reaches a steady state where the rate of filtrate invasion stabilizes. The mud cake now significantly reduces the permeability of the formation to the drilling fluid, thereby controlling fluid loss. The steady-state filtration rate is much lower than the initial spurt loss rate.

Table 2-2 *Characteristics of the filtering medium* **[47]**

Filter medium	Permeability K(D)	Diameter of particles causing obstruction (µm)	Concentration in particles at 2.5 cm(kg/m3)
Unconsolidated rock	< 0,1	< 2	-
Consolidated rock	0,100 – 1	10	2,85
Unconsolidated sand	1 – 10	74	14 to 28

The flow through the cake is theoretically governed by DARCY's law [47] which can be written in the form:

$$\frac{dv}{dt} = \frac{k \,.\, A \,.\, \Delta p}{\mu \,.\, Z} \qquad \textbf{2-5}$$

$\frac{dv}{dt}$ **:** Filtrate flow rate "cm3/s"**, k:** Permeability of the "DARCY" cake**, P:** Differential pressure "bar"**, Z:** Thickness of the cake "cm", **A:** Filtration surface "cm²", **t:** Time "s" and μ**:** Viscosity of the filtrate "CP".

2.3.4.2 ***Filtration types***

The filtration process can be divided into two classes: ***Figure 2-6*** describes the changes in filtrate volume as a function of time for static and dynamic filtration:

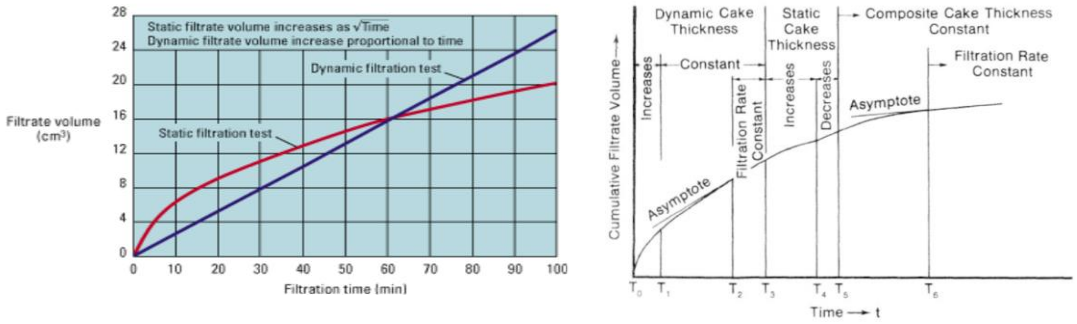

Figure 2-6 *Dynamic and static filtration*[48]

- ***Static filtration:***

occurs when mud does not circulate, and the drill string is out of the hole. filtration rates are controlled by cake permeance; cake thickness increases and filtration rate decreases continually with time; which, in turn, prevents further formation damage. ***Fergusson and Klotz 1954***[46] studied more particularly the case of drilling muds and they showed that the filtration of these fluids only partly followed the classical theory given by:

$$V = K\sqrt{t} \qquad 2\text{-}6$$

With: V: volume of the filtrate (cm3), K: permeability (mD) and t: filtration time (s).

The theory of static filtration in drilling fluids leads to the expression of the volume of filtrate collected QF. The fundamental equation that governs filtration is given by:

$$Qf = A\sqrt{\frac{2kp}{\mu}.r\,t} \qquad 2\text{-}7$$

Qf: Filtration volume "cm3", A: Surface area of the cake "cm2", k: Permeability of the "DARCY" cake, P: Differential pressure between the fluid and the "atm" formation, μ: Viscosity of the filtrate "cP", r: Ratio of the volume of filtrate to the volume of cake "Qf /Qc" and t: Time "s".

During static filtration, the cake continually thickens during the process. According to Darcy's law, the filtration speed through a cake of given porosity is of the following form:

$$\frac{\Delta V}{\Delta t} = \frac{K.\Delta P}{\eta.e.A} \qquad 2\text{-}8$$

with V: Filtered volume (cm3) for a time t, t: time (s), k: permeability of the cake (1D =1μm2), ΔP: differential pressure (Pa or psi), μ: viscosity of the fluid (cP), e: thickness of the cake (cm) after a time t, and A: Surface (cm2).

- ***Dynamic filtration***

Can be divided to two sets (see ***Figure 2-7***):

Dynamic filtration of drilling mud: occurs during drilling or mud circulation. Unlike static filtration, where mud particles settle without interference, dynamic filtration is influenced by the shearing action of mud at the wellbore wall. This shearing action impedes the accumulation of larger particles on the external filter cake surface, resulting in a variable filter cake thickness. Over time, an equilibrium is reached between the rate of particle deposition and erosion, which continues to fluctuate until a critical invasion rate is achieved.[46].

Dynamic Filtration from beneath the bit while drilling: No filter cake forms beneath the bit; instead, filtration is managed by the plugging of the formation ahead of the bit by mud particles. The

filtration process beneath the bit is influenced by the properties of the formation, the drilling speed, and the characteristics of the mud. In contrast, static and dynamic filtration are primarily controlled by the properties of the mud itself. [46].

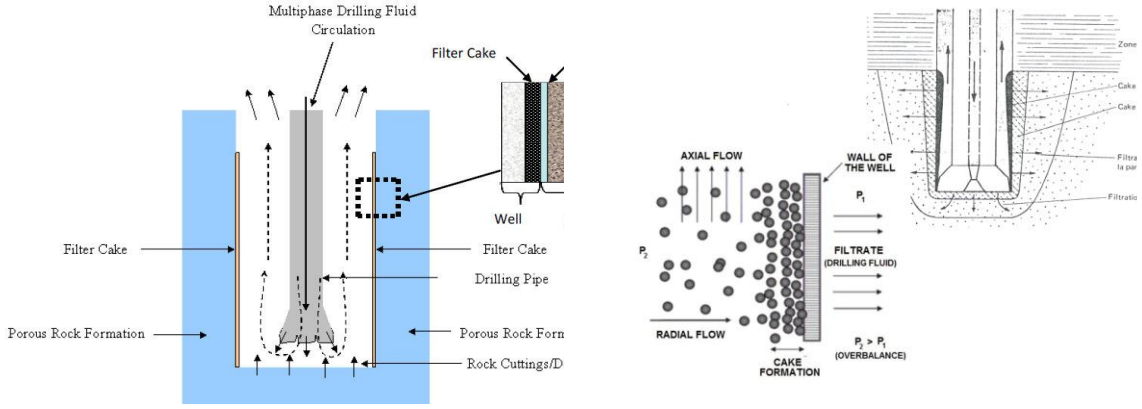

Figure 2-7 *The circulation of drilling fluid during the drilling process* [49]

2.3.4.3 ***Invasion of the Porous Medium and Formation of Cake***

Fractions of a second after the spurt invasion, drilling overbalance pressure forces more solid particles to invade the wellbore pores over a period of time. This second phase appears to be the most critical in wellbore stabilization because of the evolution of an internal filter cake followed by an external cake formation as displayed in ***Figure 2-8***.

Internal cake: An internal filter cake forms when appropriately sized mud particles accumulate in and around the wellbore at high concentrations, creating robust aggregates within the available pore network. This low permeability filter cake enhances near-wellbore stability by reducing permeability, mitigating filtrate invasion, moderating pore pressure increase behind the filter cake, and isolating formation fluids in reservoir or non-reservoir sections of the well. Additionally, when a permeable wellbore encounters a low permeability internal filter cake, it positively impacts effective stress, reinforcing the wellbore through the mud cake process. The formation of this internal cake hinges significantly on the characteristics of the filter medium. To effectively obstruct porous formations, the mud must contain particles sized just smaller than the widest pore openings to approximately one-third of these openings, along with smaller particles capable of blocking finer pores and interstices among coarser fractions already deposited[47].

External cake: The drag effect of the fluid causes compaction of the external filter cake, allowing smaller particles to penetrate deeper into it. While larger particles initially form the base of the external filter cake, the strong drag force pushes all particles towards the cake surface, leading to faster deposition of smaller particles. Moreover, increasing the overbalance pressure across a thin oil-based filter cake deforms water droplets within the mud water phase, thereby reducing the permeability of the external filter cake. As the mud filtration progresses, the growth rate of the external filter cake region eventually slows down until the filtration rate achieves pressure equilibrium with the formation. This results in the formation of a heterogeneous filter cake at the formation face, consisting of particles of various sizes, while allowing only small particles to pass through to the wellbore flow path[47].

- ***Mud Cake Properties***

  The effectiveness of the mud cake in controlling fluid loss depends on its properties:

  - ***Thickness:*** The thickness of the cake depends on the fluid content of the solid and also on the amount of liquid retained, any decrease in the filtration rate induces an increase in the cake's width. Thicker mud cakes generally provide better fluid loss control but can also pose risks such as differential sticking.

- ***Permeability:*** Lower permeability mud cakes are more effective in reducing filtrate invasion. permeability depends on the shape and dimensions of the particles deposited; it decreases: if the average diameter is smaller; if the granulometric distribution range is wider. Add that the colloidal elements play an important role. Flocculation and aggregation result in increased permeability.
- ***Strength and Stability:*** The mud cake must be strong enough to withstand the shear forces during drilling and stable enough to not erode or break down.
- ***Porosity and intergranular tension:*** The porosity is a function of the dimensions of the deposited particles and their granulometric distribution. As a result of the compaction, it increases from the lower to the upper part while the intergranular tension decreases.

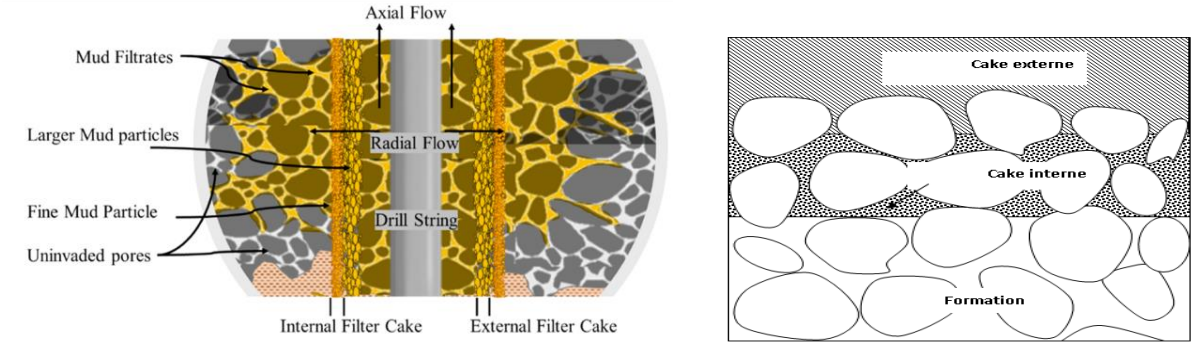

Figure 2-8 *Filtration of mud through the mud cake* [50]

2.3.4.4 ***Impact of mud filtration on wellbore, reservoir and overall drilling operations***

The invasion of mud filtrate into a reservoir result in the creation of distinct zones (see ***Figure 2-9***)around the wellbore. The invaded zone is where the filtrate penetrates the formation, altering its properties and potentially impacting logging and production. Beyond this, a transition zone may exist where the concentration of filtrate decreases until it merges with the unaffected formation. The infiltration of drilling fluids into the pore system of the formation affects its petrophysical characteristics, including porosity, permeability, and pore structure. Effective control of filtration is crucial to minimize formation damage, ensure wellbore stability, and optimize drilling efficiency by regulating the thickness and permeability of the filter cake.

Within these zones, several significant phenomena occur. Mud filtrate invasion into the reservoir increases water saturation in the near-wellbore zone, often referred to as the invaded zone or damaged zone. Conversely, oil saturation in this zone decreases, resulting in reduced effective permeability of the formation to oil. Consequently, the resistance to oil flow towards the wellbore increases, which can lead to decreased productivity of the well over time [51]**.**

In the invaded zone, the filtrate also alters the formation's resistivity, which can complicate the interpretation of well logs and affect reservoir evaluation. Capillary forces within the pores of the formation play a significant role, as they can draw filtrate deeper into the formation, exacerbating the invasion. This can lead to water blocking or oil trapping, reducing the permeability of the hydrocarbon-bearing zones and potentially decreasing production efficiency. Additionally, the filtrate can react with the formation's minerals, leading to changes in pore structure and further influencing the formation's permeability.

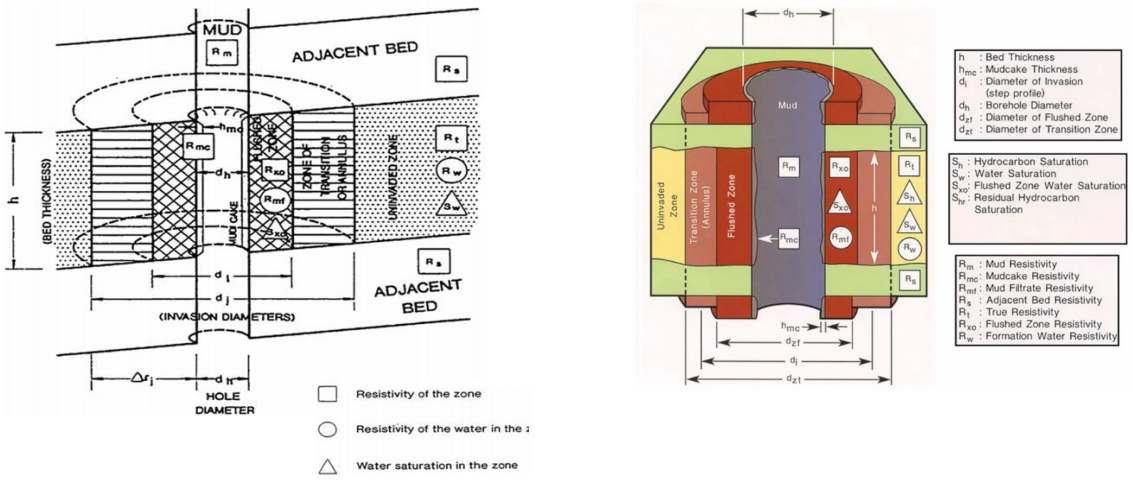

Figure 2-9 *Filtrate Invasion and contaminated zones*[52]

Table 23- *Filtration affects the wellbore and drilling operations[47]*

Aspect	Impact of Filtration	Consequences	Mitigation Strategies
Wellbore Stability	Formation of filter cake on wellbore walls	Provides support and stability to wellbore Prevents further fluid loss	Use appropriate mud weight and composition Monitor filter cake thickness
Fluid Loss	Fluid invades the formation due to filtration	Reduces hp Leads to well control issues Potential for lost circulation	Employ loss circulation materials Adjust mud properties to control fluid loss
Permeability Alteration	Mud filtrate invades formation, altering permeability	Formation damage Reduced reservoir productivity Increased skin factor	Optimize mud composition to minimize filtrate invasion Use chemical inhibitors and stabilizers
Differential Sticking	Thick filter cake increases risk of sticking	Drill string or casing may get stuck Increased non-productive time (NPT)	Maintain thin, impermeable filter cake Regular monitoring and adjustment of mud properties
Mud Cake Formation	Filter cake builds up on wellbore wall	Controls fluid loss Affects drilling parameters such as torque and drag	Monitor and manage filter cake properties Use appropriate additives to maintain desired mud cake characteristics
Well Control	Fluid loss due to filtration can lead to well control problems	Blowouts Loss of well control< Increased safety risks	Ensure adequate mud weight Employ well control measures and BOP systems

Drilling Efficiency	Changes in mud properties due to filtration affect drilling efficiency	Reduced rate of penetration (ROP) Increased torque and drag Higher energy consumption	Optimize drilling fluid properties Use real-time monitoring systems to adjust parameters
Reservoir Damage	Filtrate invasion can damage the reservoir	Reduced permeability Altered wettability Formation fines migration	Use low-filtration drilling fluids Apply pre-treatment chemicals to protect the formation
Environmental Impact	Uncontrolled fluid loss can lead to environmental contamination	Contamination of groundwater Regulatory non-compliance	Use environmentally friendly drilling fluids Implement effective containment and remediation measures
Cementing Operations	Filter cake can impact cement bond quality	Poor zonal isolation Compromised well integrity	Remove filter cake prior to cementing Use spacers and flushes to clean the wellbore

2.3.4.5 ***Factors Influencing Filtration and Mud Cake Formation***

- Formation Characteristics:

The penetration of mud filtrate into a reservoir is heavily influenced by key formation parameters such as porosity (ϕ) and permeability (k), as demonstrated by ***Jianhua Zhan et al.*** [53].***Figure 2-10*** from their research illustrates how permeability affects invasion depth (ri) over different time periods (t). The calculations used key input data: Sw=0.5, Cmf=280,000 mg/L, Cw=170,000 mg/L, T=80°C, a=3.75, m=1.8, and n=2.In formations with low porosity (ϕ=0.05), the invasion depths increase with time for various permeability values (k=0.01, 0.005, and 0.001 μm²). Higher permeability allows for deeper invasion depths due to better fluid flow capability. For example, after 25 days of invasion, depths were recorded as 1.16m, 1.31m, and 1.56m for permeabilities of 0.01, 0.005, and 0.001 μm² respectively. Conversely, formations with high porosity (ϕ=0.20) have larger pore volumes that require more mud filtrate to displace native fluids (water, oil, or gas), resulting in a slower invasion rate. For the same 25-day invasion period, depths were measured at 0.73m, 0.91m, and 1.08m for corresponding permeability values. Additionally, stable invasion depths are reached earlier in low porosity formations (around 75 days), while in high porosity formations, stable invasion depths are achieved later (beyond 125 days)..

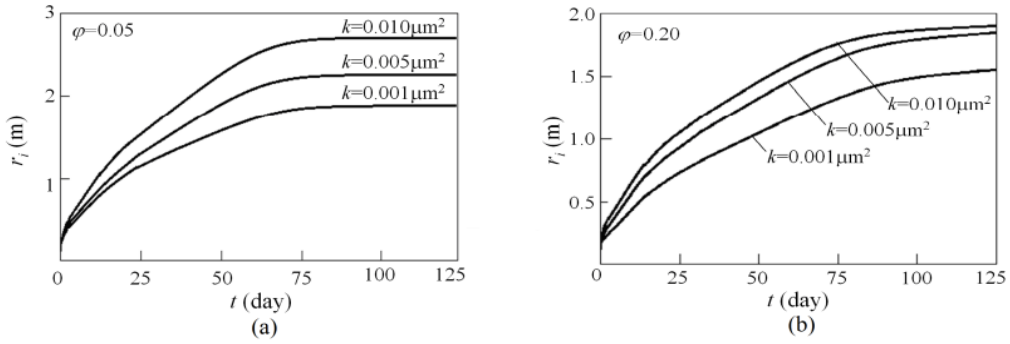

Figure 2-10 *Effects of permeability and porosity on invasion depth ri for (a) ϕ=0.05 and (b) ϕ=0.20*[53]

- Drilling mud properties

The composition and characteristics of drilling mud significantly impact its filtration properties. Drilling mud is a complex mixture of solids, liquids, and chemical additives. The types and concentrations of these components determine its ability to form an effective filter cake and control fluid loss. Solids such as clays and weighting materials provide the necessary density and viscosity, while polymers and bridging agents enhance filter cake quality by plugging formation pores and reducing permeability. Chemical additives, including pH adjusters and dispersants, maintain mud stability and optimize its interaction with the formation. The particle size distribution within the mud is crucial for forming a compact, impermeable filter cake, with a well-balanced range of particle sizes ensuring better filtration control. Overall, the careful selection and management of mud composition are vital for optimizing filtration performance and maintaining wellbore stability during drilling operations.

- Pressure Differential

The difference between the hydrostatic pressure of the mud column and the formation pressure drives the filtration process. Higher pressure differentials can increase fluid loss and affect the filter cake formation. ***Figure 2-12*** show the impact of temperature and pressure on drilling mud filtration process.

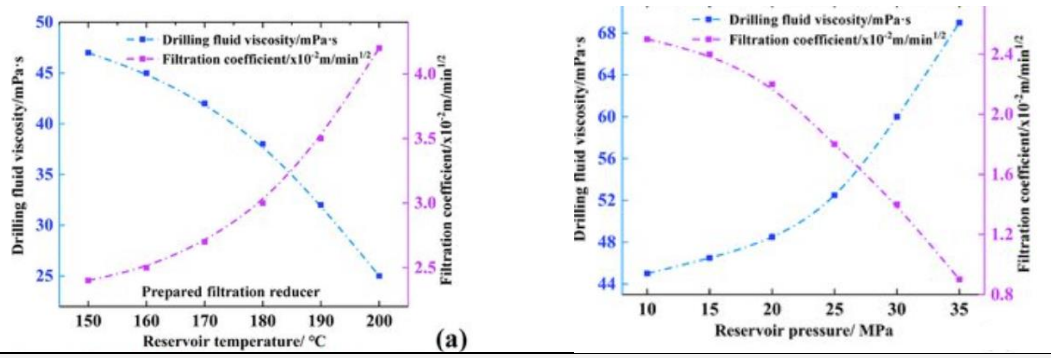

Figure 2-11 *Pressure, temperature and fluid viscidity impact on mud filtration*[54]

- Temperature:

Higher temperatures can affect the viscosity of the mud and the behavior of polymers and other additives which indeed results in so many impacts on fluid filtration. ***Haiqa,S, Inggarjati Qolbun.S*** and other investigated the effect of temperature in different mud filtration systems and the results are shown in ***Figure 2-12*** Impact of temperature on mud filtration systems

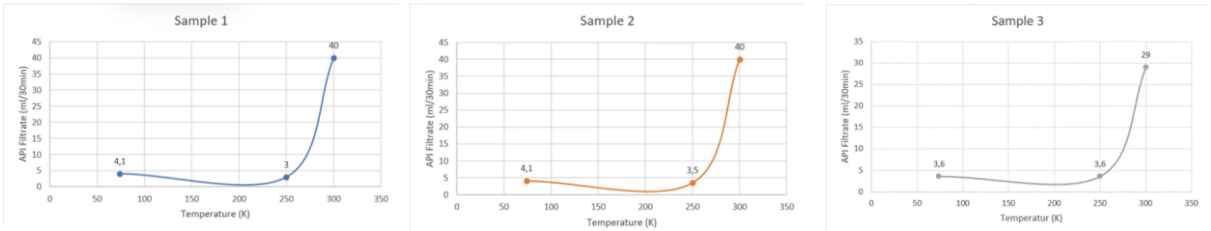

Figure 2-12 *Impact of temperature on mud filtration systems*[55]

This effect is primarily because higher temperatures reduce the viscosity of the drilling fluid, making it thinner and allowing it to flow more easily through the formation pores. Additionally, elevated temperatures can increase the mobility of the fluid's particles, enhancing their ability to penetrate the formation. The decrease in viscosity and increase in particle mobility together facilitate a higher rate of mud filtrate invasion into the reservoir rock, potentially leading to greater filtration losses and more significant formation damage.

- Time influence

(Larsen) found that if the sludge is filtered through filter paper at constant pressure and temperature, Qf is proportional to √ t. This is not always verified for all sludges, but it nevertheless represents the basis for the interpretation of filtration mechanisms.

$$V = a\sqrt{t} + q_0 \qquad \textbf{2-9}$$

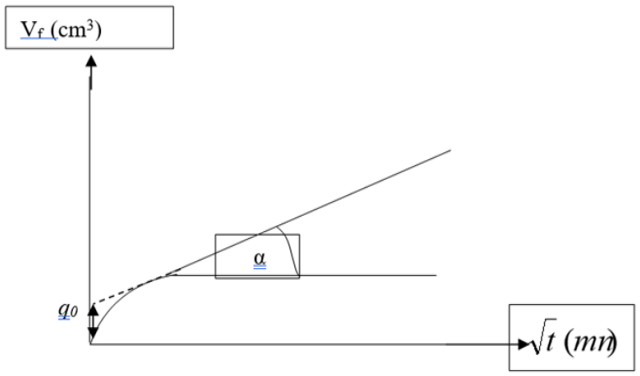

Figure 2-13 *Variation of cumulative filtrate volume as a function of time*

q0: y-intercept, volume of fine particles in the sludge, **a**: Slope of the flow line, this is the characteristic term of the mud.

In terms of drilling fluid behavior, initially, there is a rapid loss of fluid due to the high permeability of the formation, leading to the formation of a thin filter cake from solid particle deposition. As time progresses, this filter cake thickens, reducing permeability and slowing the rate of fluid loss. Eventually, an equilibrium state is reached where the filtration rate stabilizes, balancing the pressure differential with the resistance offered by the compacted filter cake. Under dynamic conditions, this equilibrium can fluctuate due to ongoing mud circulation and varying downhole conditions. In terms of drilling fluid behavior, initially, there is a rapid loss of fluid due to the high permeability of the formation, leading to the formation of a thin filter cake from solid particle deposition. As time progresses, this filter cake thickens, reducing permeability and slowing the rate of fluid loss. Eventually, an equilibrium state is reached where the filtration rate stabilizes, balancing the pressure differential with the resistance offered by the compacted filter cake.

2.3.4.6 ***Importance of Filtration Control***

Filtration control is crucial for several reasons:

- ***Wellbore Stability:*** Prevents excessive fluid loss that can destabilize the wellbore.
- ***Formation Damage Prevention:*** Minimizes mud filtrate invasion, reducing permeability impairment and formation damage.
- ***Maintaining Mud Properties:*** Helps in maintaining the rheological and chemical properties of drilling mud.
- ***Efficient Drilling:*** Reduces non-productive time by avoiding issues like stuck pipe, lost circulation, and differential sticking.
- ***Enhanced Production:*** Ensures optimal reservoir contact and prevents reduction in hydrocarbon flow by maintaining clean perforations and pore spaces.
- ***Cost Efficiency:*** Reduces treatment costs and the need for remedial actions by maintaining effective drilling fluid performance.

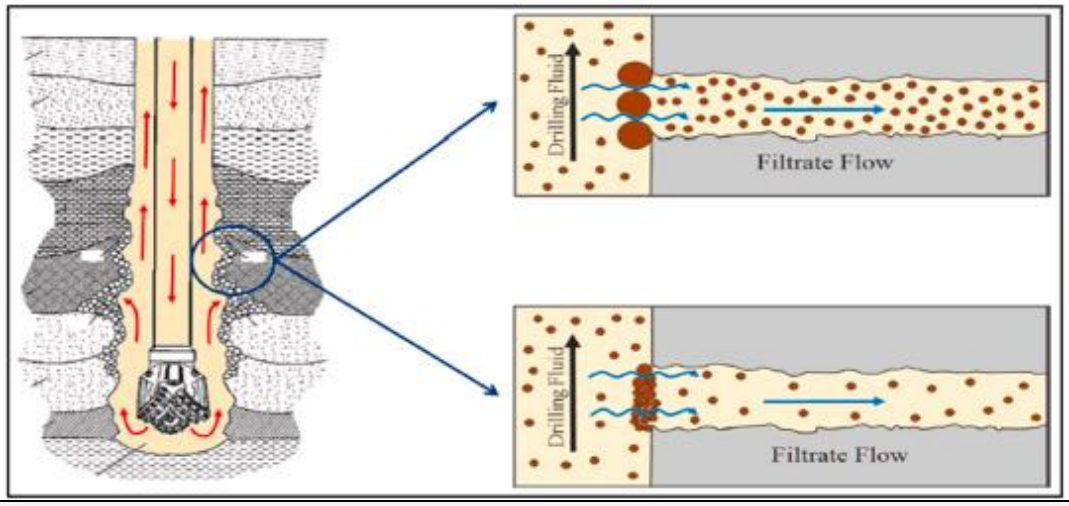

Figure 2-14 *Filtrate control impact by using filtrate reducer additives* [56]

Conclusions

The invasion process is intricately tied to both formation and fluid parameters. This study delves into the complex phenomenon of filtrate invasion in drilling operations, focusing particularly on the rheology of drilling mud and its significant implications for wellbore stability and formation integrity. Porosity and permeability play crucial roles in defining the characteristics of a formation and exert substantial influence on the invasion process. Effectively managing filtrate invasion is essential for ensuring the success of drilling operations. Integrating a deep understanding of rheological parameters and filtration is key to achieving this goal.

In summary, understanding and optimizing both rheological and filtration properties of drilling mud are essential for successful drilling operations. As highlighted by ***Ferguson and Klotz***:

"The performance of drilling operations lie under the performance of drilling fluid "

Ferguson and Klotz

Revolutionizing DFs| Integration of Nanoparticles

CHAPTER III

Chapter 3. Revolutionizing DFs: Integration of Nanoparticles

Introduction

Nanotechnology, epitomized by the precise manipulation and engineering of materials at the nanoscale, has emerged as a groundbreaking and transformative discipline with far-reaching implications across a spectrum of industries. Operating at dimensions of approximately 1 to 100 nanometers, this field harnesses the unique properties exhibited by materials at the nanoscale, revolutionizing fundamental understandings of matter and enabling the creation of novel structures and functionalities[57]. Its interdisciplinary nature converges expertise from physics, chemistry, biology, engineering, and materials science, fostering a collaborative environment where innovations flourish[58].

The essence of nanotechnology lies in its capacity to meticulously control and engineer materials at the atomic and molecular levels, affording unprecedented control over their properties and behaviors. By exploiting phenomena such as quantum confinement, surface effects, and size-dependent properties, nanotechnology transcends traditional boundaries, offering a playground where the laws of classical physics blur and the rules of quantum mechanics reign supreme[57].

In the oil and gas sector, the integration of nanoparticles into various field's sections has garnered considerable attention due to their unique physical, chemical, and mechanical properties[58]. This integration offers a promising avenue for enhancing drilling operations in terms of efficiency, cost-effectiveness, and environmental sustainability[58].

The application of nanoparticles in drilling mud serves as a strategic solution to address the complex challenges encountered during drilling processes by harnessing the distinctive attributes of nanoparticles, such as their large surface area-to-volume ratio, high reactivity, and tailored surface chemistry[59].

The origins of the ideas and concepts behind nanoscience and nanoparticles trace back to a pivotal talk given by physicist Richard Feynman titled "***There's Plenty of Room at the Bottom***." This landmark presentation occurred at an American Physical Society meeting held at the California Institute of Technology (Caltech) on December 29, 1959. It is worth noting that this occurred long before the term "nanotechnology" came into common usage.

3.1 Nanoparticles' structure

Nanoparticles, while sometimes considered simple molecules, are actually complex mixtures with unique behaviors. They possess a high surface area to volume ratio, leading to distinctive surface chemistry different from their core material[60]. For instance, silica nanoparticles have a SiO2 core but a surface layer with a different composition, significantly affecting their properties. The surface, about 0.4 nm thick, plays a crucial role, as it interacts first with the environment or biological systems. Surface functionalization is vital for maintaining nanoparticles' properties and preventing aggregation[60]. Functional groups or coatings, like surfactants, aid in dispersion and stability. Thus, nanoparticles consist of a functionalized surface, an optional shell, and a core, with the core material often defining their key properties[61].

3.1.1 Surface

The surface of nanoparticles can be functionalized with various metal ions, small molecules, surfactants, or polymers. For instance, base-catalyzed hydrolysis of tetraethyl orthosilicate creates particles with charged surfaces due to the deprotonation of SiOH groups, forming $SiO^- M^+$ (e.g., with sodium). This charge aids dispersion in aqueous media[61]. For materials without naturally charged surfaces, small molecules like citrate or thiopropanoic acid, which bind covalently and carry charges, can be used for stabilization. Surfactants, such as sodium dodecyl sulfate (SDS), also stabilize nanoparticles by forming micelles around them, although these systems are in equilibrium with free surfactant molecules [61]. Excessive dilution can destabilize these colloids by shifting the equilibrium.

Other surface-active molecules include long-chain compounds like amines, phosphines, carboxylates, and thiols, which bind to specific nanoparticle sites and extend into the dispersion medium for stability[61]. These are often applied during nanoparticle preparation and can be modified later. While typically stable in organic solvents, new materials with polyethylene glycol (PEG) are being developed for water dispersibility.

3.1.2 Shell

The shell of a nanoparticle is a layer of material that is chemically distinct from the core material. While the outer layer of any inorganic nanoparticle can differ from the core due to surface chemistry variations, a true shell has a completely different structure. Core/shell quantum dots, like those with cadmium selenide cores and zinc sulfide shells, are prime examples. Similarly, polymer nanoparticles such as polystyrene-polyaniline also demonstrate this structure. In some cases, shells form unintentionally, such as iron nanoparticles developing iron oxide layers upon exposure to air. These layers typically do not penetrate the entire particle, resulting in a core/shell structure rather than a uniform composition. Core/shell nanoparticles are generally created deliberately and are not likely to form accidentally[61].

3.1.3 The core

The core of a nanoparticle is its central region and often refers to the nanoparticle itself[61]. In physical sciences, the properties of nanoparticles are generally linked to the core's composition, and sometimes to both the core and shell. While the core's composition is crucial for determining a nanoparticle's physical and chemical properties, its role in ecotoxicology and environmental behavior is more complex and not solely dependent on the core. The core's properties can vary significantly, especially in inorganic nanoparticles that can exist in multiple phases, affecting their physical characteristics. Although nanoparticles can be synthesized in a single pure phase, they sometimes contain multiple phases, influencing their behavior and fate. Thus, the core's composition and phase are critical factors in understanding a nanoparticle's overall properties[61].

3.2 Nanoparticles' properties

The fate, behavior, and ecotoxicology of nanoparticles are closely tied to their intrinsic properties. Despite sometimes behaving more like molecules than larger colloidal suspensions, certain aspects of nanoparticles should not be overlooked.

3.2.1 Size-Dependent Properties

- **Large Surface Area**: Nanoparticles have a very high surface area-to-volume ratio compared to bulk materials. This increased surface area influences their chemical reactivity, adsorption capacity, and interaction with surrounding molecules.
- **Quantum Effects**: When nanoparticles are very small, quantum effects become significant. This includes quantum confinement (where electron behavior is restricted by particle size) and quantum tunneling (where particles can pass through barriers they would not overcome in classical physics).

3.2.2 Mobility properties

The process of diffusion in nanoparticles is influenced by gravitational forces, buoyancy, and Brownian motion, and can be described using Einstein's law of diffusion [62]:

$$Df = kT \qquad 3\text{-}1$$

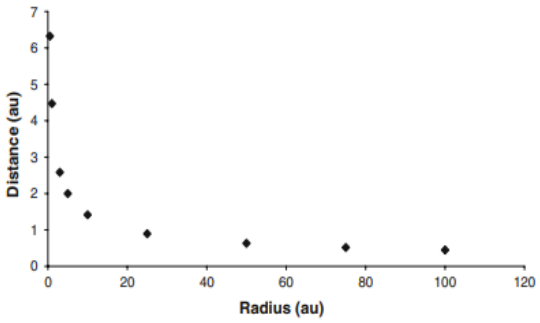

Figure 3-1 *The variation of diffusion rate on the radius of particles after 20 s* [62]

The diffusion coefficient D is influenced by several factors: $f$the frictional coefficient of the particle; k the Boltzmann constant; and $T$the temperature. The frictional coefficient f can be calculated using Stokes' law:

$$f = 6\pi\eta a \qquad 3\text{-}2$$

where η is the viscosity of the medium and, a is the particle radius.

Therefore, the diffusion coefficient (D) varies inversely with the particle's radius, indicating that the average displacement of a particle over time t is proportional to the inverse square root of its radius. For instance, a particle with a radius of 50 nm will travel a considerably shorter distance in the same time compared to a particle or molecule with a radius of 0.5 nm. This relationship is depicted in ***Figure 3-1*** a plot illustrating the average distances traveled after a fixed time by particles of different sizes, highlighting that smaller particle undergo much greater displacement than larger ones.

3.2.3 Surface energy and colloid stabilization

Nanoparticles, due to their small size and Brownian motion, tend to agglomerate and precipitate because of high surface energy upon collision. To stabilize nanoparticle dispersions, barriers are crucial. Charge stabilization involves a charged surface with associated counter ions, forming a Stern layer that repels like charges via Coulomb's law, preventing aggregation. Steric stabilization uses long molecules tethered to particles, creating a barrier through solvent interactions that hinder aggregation. Ionic strength affects charge-stabilized colloids significantly, shielding repulsion and promoting aggregation, unlike sterically stabilized systems which are more resilient[62].

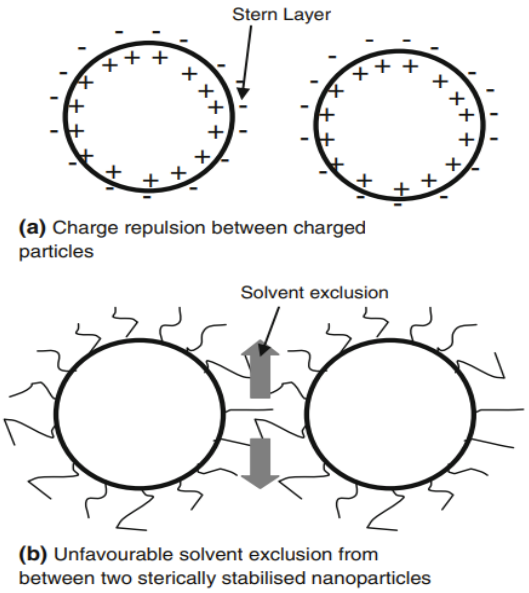

Figure 3-2 *(a) a charged stabilized nanoparticle and (b) a sterically stabilized nanoparticle* [62]

3.2.4 Optical Properties

- **Plasmonic Effects**: Certain nanoparticles exhibit plasmonic behavior, where their conduction electrons oscillate collectively in response to light. This results in unique optical properties such as localized surface plasmon resonance (LSPR), which can be tuned by controlling nanoparticle size, shape, and composition.
- **Photoluminescence**: Nanoparticles can emit light upon excitation due to quantum confinement effects. This property is exploited in applications like LEDs, biological imaging, and sensors.

3.2.5 Mechanical Properties

- **Enhanced Strength**: Nanoparticles can enhance the mechanical properties of composite materials when incorporated due to their high strength-to-weight ratio and reinforcement capabilities.
- **Ductility and Flexibility**: Some nanoparticles, especially those of metals, exhibit enhanced ductility and flexibility at the nanoscale, different from their bulk counterparts.

3.2.6 Chemical and Catalytic Properties

- **Enhanced Catalytic Activity**: Nanoparticles can act as highly efficient catalysts due to their high surface area and unique electronic properties. This is important in catalytic converters, fuel cells, and environmental remediation.

- **Surface Reactivity**: Nanoparticles often have highly reactive surfaces that can be functionalized with specific ligands or coatings to control their chemical reactivity and stability.

3.3 Nanoparticles' preparation

Nanoparticles are prepared using two main methods: top-down and bottom-up approaches. Top-down methods involve reducing larger material pieces to nanoparticles through techniques like lithography, etching, or ball milling. Conversely, bottom-up methods synthesize nanoparticles from simple molecules, controlling size through factors like concentration, surface functionalization, or using micelles for templating growth. Supersaturation governs bottom-up approaches, where material concentration increases until reaching a saturation limit, after which particles nucleate and grow. The reaction medium significantly influences particle properties and surface chemistry. While this explanation oversimplifies the process, it highlights the fundamental principles underlying nanoparticle synthesis.

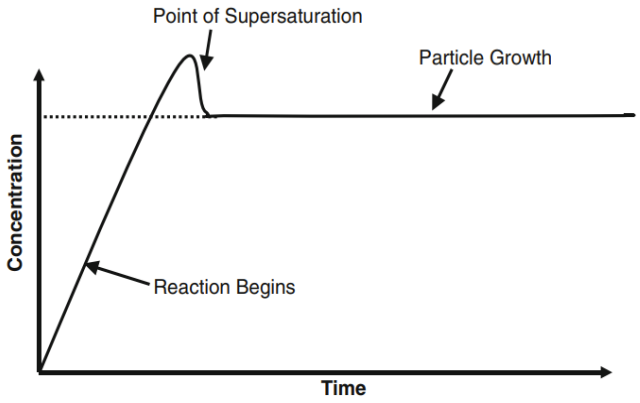

Figure 3-3 *Nanoparticle formation* [62]

Table 3 1- *Some key preparation aspect for nanoparticles*

Type of Nanoparticle	Preparation Method	Key Points
Metal Oxides (e.g., TiO2)	Stabilized precipitation (hydrolysis of titanium alkoxides)	Allows size control and surface functionalization. Methods include hydrolysis of titanium alkoxides and oxidation of titanium tetrachloride in flame.
	Flame pyrolysis (oxidizing titanium tetrachloride in a flame)	Rapid particle formation but limited surface functionalization. No in situ charge stabilization; stabilization occurs post-suspension in solvent.
Polymers	Emulsion polymerization (e.g., styrene in water with surfactant and initiator)	Rapid reaction forming nanoparticles within micelles. Particles are often charge stabilized due to trapped surfactants or grafted chains.
Nanowires and Nanotubes	Vapour-liquid-solid (VLS) method (e.g., carbon nanotubes)	Growth from metal nanoparticles via decomposition of precursor gases. Complex method specific to nanotubes; involves rapid absorption and extrusion of carbon.
Other Nanoparticles	micelle templating (e.g., cadmium sulfide)	Various methods involving precursor reactions (e.g., cadmium chloride and sodium sulfide). Surface may be hydrophobic; hydrophilic variants are possible.

3.4 Behavior in aquatic environment

Nanoparticles, due to their unique physical and chemical properties, exhibit distinctive behaviors in aquatic environments. Understanding these behaviors is crucial for assessing their environmental impact and potential risks. Here's a comprehensive overview:

3.4.1 Dispersion and Aggregation

Nanoparticles tend to agglomerate or aggregate in aquatic environments due to various factors such as electrostatic interactions, van der Waals forces, and surface chemistry:

- Electrostatic Interactions: Surface charge of nanoparticles influences their dispersion. Positively or negatively charged nanoparticles may repel or attract each other in solution, affecting their stability.
- Van der Waals Forces: Attractive forces between nanoparticles, especially when they come into close proximity, can lead to aggregation.
- Surface Chemistry: Functionalization of nanoparticle surfaces can alter their interactions with water molecules and other nanoparticles, influencing aggregation tendencies.

Example: Silver nanoparticles (AgNPs), widely used in consumer products, tend to aggregate in natural waters due to their high surface energy and interactions with ions and organic matter present in the environment.

3.4.2 Transport and Fate

The fate of nanoparticles in aquatic systems depends on their size, shape, surface chemistry, and the characteristics of the water body:

- Sedimentation and Settling: Larger nanoparticles or nanoparticle aggregates settle out of suspension over time, especially in calm or low-energy water bodies.
- Colloidal Stability: Nanoparticles that remain in suspension (colloidal stability) can be transported over long distances, potentially affecting ecosystems far from their original source.
- Bioavailability: Nanoparticles can interact with organisms and biomolecules, affecting their bioavailability and potential ecological impacts.

Example: Titanium dioxide nanoparticles (TiO2 NPs) used in sunscreens may enter aquatic environments through wastewater effluents. Their fate depends on water flow rates and the presence of natural colloids that can stabilize or destabilize them.

3.4.3 Transformation and Reactivity

Nanoparticles can undergo transformation processes in aquatic environments, altering their properties and behavior:

- Surface Coating Changes: Nanoparticles may acquire coatings from natural organic matter, altering their surface chemistry and environmental interactions.
- Chemical Transformation: Nanoparticles can undergo oxidation-reduction reactions, changing their speciation and toxicity.
- Photochemical Processes: Sunlight can induce chemical reactions on nanoparticle surfaces, affecting their stability and reactivity.

Example: Iron oxide nanoparticles used in groundwater remediation can undergo surface transformations in natural waters, influencing their effectiveness in removing contaminants.

3.4.4 Ecological Implications

Nanoparticles have the potential to impact aquatic ecosystems through various mechanisms:

- Toxicity: Some nanoparticles may exhibit toxicity to aquatic organisms due to their high surface area and potential for cellular uptake.
- Bioaccumulation: Nanoparticles can accumulate in aquatic organisms through dietary exposure, potentially biomagnifying up the food chain.

- Disruption of Ecosystem Functions: Changes in nanoparticle concentrations can alter microbial communities, nutrient cycling, and overall ecosystem health.

Example: Carbon nanotubes (CNTs) released into aquatic environments have been shown to affect the growth and development of aquatic organisms, impacting ecosystem dynamics.

3.5 Behavior in porous environment

The transport of nanoparticles (NPs) through porous media, such as soils or aquifers, is primarily influenced by their size, shape, and charge distribution. This process can be broken down into two main steps, as described by ***McDowell-Boyer et al. (1986)***[63]:

- ***Collision:*** This involves the NPs coming into contact with the surfaces within the porous media.
- ***Attachment:*** Once in contact, NPs may adhere to the soil or sediment grains (collectors). Attachment is heavily influenced by electrostatic interactions between the NPs and the soil surfaces.

The mechanisms leading to NP collision can be further categorized into:

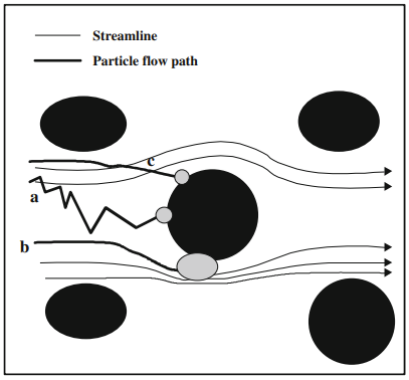

Figure 3-4 *Particle filtration by (a) diffusion, (b) interception and (c) sedimentation* [62]

- ***Surface Filtration:*** Larger NPs may be unable to penetrate into the media pores due to their size. Instead, they form a filter cake or surface mat above the media.
- ***Straining Filtration / Sieving:*** NPs that are small enough to enter the media can be mechanically removed as they encounter smaller pore spaces and are sieved out.

For small NPs physical and chemical forces are decisive. The collisions of small NPs with a collector occur as a result of three processes: diffusion, interception and sedimentation

Understanding these processes is crucial for predicting the behavior of NPs in natural environments and for designing effective strategies for their remediation or containment.

Table 3-2 Nanoparticles common behavior in Porous medium[64]

Nanoparticles Interaction Mechanism in Porous Media			
Nanoparticles-Pores			Nanoparticle-Nanoparticle
Surface Deposition	Mono-Particle Plugging	Multi-Particle Plugging	Aggregation and Gelation
• Van der Waals • Electrostatic • Hydrodynamic	• Size Exclusion or • Screening	• Straining or • Log-Jamming	• Van der Waals • Electrostatic • Hydrodynamic

Small nanoparticles (NPs) and their aggregates, typically less than 1 micron in size, are primarily transported through Brownian diffusion. As these NPs move along their flow path near soil materials, they can collide due to interception, where their velocity differs from that of the collector surface.

Additionally, agglomeration can occur based on differences in density, particularly for NPs denser than the transport medium, leading to sedimentation[64].

Additionally, nanoparticles (NPs) can be trapped within soil due to mechanisms such as pore size exclusion or sieving. The mobility of NPs is limited by factors like straining filtration and pore velocity. The concentration and size distribution of NPs in the nanometer range are affected by physico-chemical filtration processes. Notably, there is a minimum filtration size observed around 1 micron for NPs with a density close to 1 g/cm³, and approximately 0.2 microns for NPs with a density around 3 g/cm³. In these ranges, straining filtration is less effective, while physico-chemical filtration has not yet achieved its maximum efficiency.[62].

3.5.1.1 NPs Models for Porous environment

In 1937, ***T. Iwasaki*** [66]described the filtration process using a first-order kinetic model:

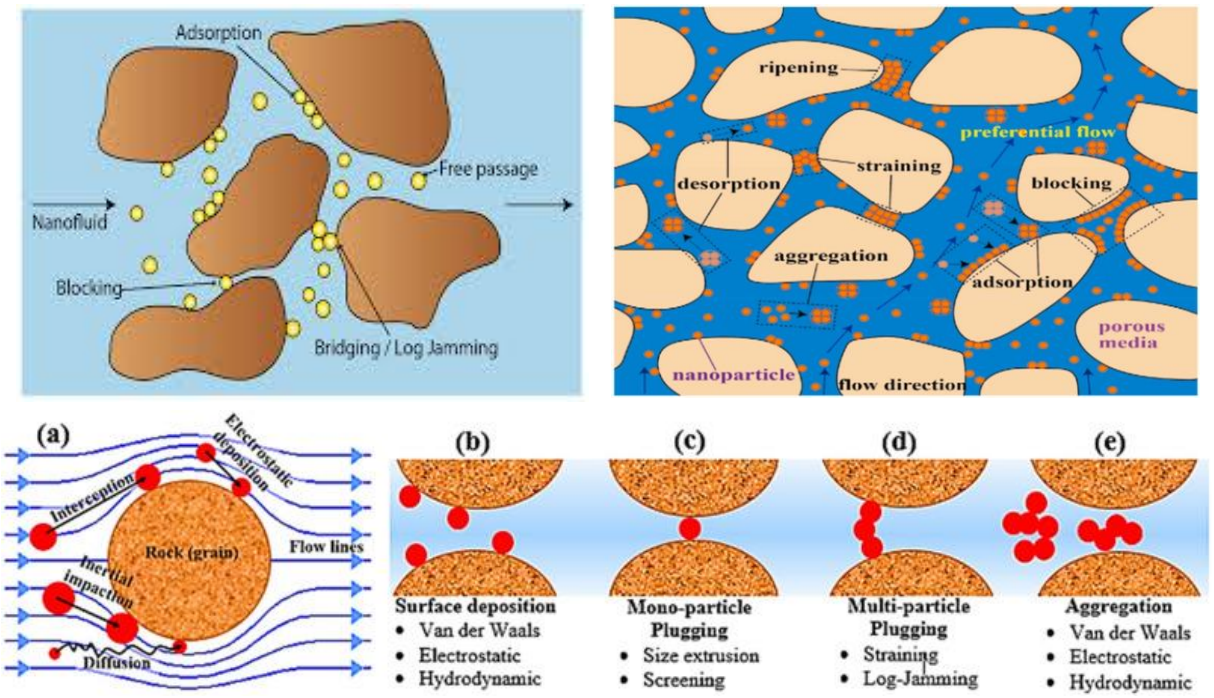

Figure 3-5 *Nano particles behavior in aqueous and porous medium* [65]

$$C_P = C_{0P} e^{(-\lambda \cdot \Delta x)} \quad \text{3-3}$$

$$R_T = -\frac{1}{\lambda} \ln\left(\frac{C_P}{C_{0P}}\right) \quad \text{3-4}$$

Where C_P is the nanoparticle ***(NP)*** concentration at the travel distance x, C_0 is the original ***NP*** concentration, k is the filtration factor in m^{-1}, R_T is the colloid travel distance in meters at a given retention rate. ***Figure 3-8*** represent the correlation between the filtration factor and travel distance.

Created by Yao in 1968[67], and further refined by Yao et al. in 1971[68] and Rajagopalan and Tien [69] in 1976, Filtration theory offers a systematic approach to compute the filtration factor and thereby simulate colloid transport in saturated media. This theory categorizes colloid filtration into four distinct mechanisms: sieving or straining, sedimentation, diffusion, and interception. These mechanisms can be mathematically described by the following equations: (Yao, 1968):

$$\lambda = \frac{3(1-n)\gamma}{2d_k}\alpha = \frac{\gamma}{d_k}\alpha \quad \text{3-5}$$

With

$$\gamma = \gamma_D + \gamma_I + \gamma_G + \gamma_S \quad \text{3-6}$$

$$\gamma_D = 0,9\left(\frac{k_B T}{\mu v_f d_p d_K}\right)^{\frac{2}{3}} \quad \text{3-7}$$

$$\gamma_I = \frac{3}{2}\left(\frac{d_p}{d_k}\right)^2 \quad \text{3-8}$$

$$\gamma_G = \frac{g d_p^2(\rho_p - \rho_W)}{18\mu v_f} \quad \text{3-9}$$

$$\gamma_S = 2,7\left(\frac{d_p}{d_k}\right)^{\frac{3}{2}} \quad \text{3-10}$$

To mitigate these limitations, ***Rajagopalan and Tien (1976)*** [69] introduced the Happel parameter AS and revised the equations to incorporate hydrodynamic retardation:

$$\gamma_D = 0,9A_S\left(\frac{k_B T}{\mu d_p d_k v_f}\right)^{\frac{2}{3}} \quad \text{3-11}$$

$$\gamma_I = A_S\left(\frac{4A_H}{9\pi\mu d_p^2 v_f}\right)^{\frac{1}{8}}\left(\frac{d_p}{d_k}\right)^{\frac{15}{8}} \quad \text{3-12}$$

$$\gamma_G = 0,00338A_S\left(\frac{(\rho_P - \rho_W)g d_p^2}{18\mu v_f}\right)^{1,2}\left(\frac{d_k}{d_p}\right)^{0,4} \quad \text{3-13}$$

$$A_S = \frac{(1-y^5)}{(1-\frac{3}{2}y+\frac{3}{2}y^5-y^6)} \quad \text{and} \quad y = (1-n)^{\frac{1}{3}} \quad \text{3-14}$$

where d_k = effective grain size in (m), n = porosity, c = elementary filtration rate, a = collision efficiency, γ_D = diffusion, γ_I = interception, γ_G = gravitation, γ_S = sieving, k_B = Boltzmann constant in (J K^{-1}), T = absolute temperature in (K), v_f = apparent flow velocity in (m s^{-1}) , d_p = colloid size in (m), g = gravitational acceleration in (m ^{2} s $^{-1}$), l = dynamic viscosity in (kg m^{-1} s^{-1}) , q_p = colloid density in (kg m-3) , q_W = fluid density in (kg m-3) , AS = Happel parameter and AH = Hamaker constant in (J). ***Figure 3-9*** shows the sum of the four different forces and the total filtration curve. A typical minimum in NP filtration in porous media can be observed at 1 (lm) for NPs with a density of (1 g/cm3).

Nevertheless, the aforementioned models do not account for a gas phase, which means using these equations for unsaturated soil systems requires caution and should only be considered preliminary estimates. In unsaturated soils, various factors such as preferential flow, fingering, macroporous flow, and retention or transport at the gas/water interface must be incorporated into transport predictions. While several modeling approaches have successfully addressed these mechanisms in laboratory experiments, there is currently no reliable method for accurately estimating NP filtration in unsaturated soil systems at field scales.

Equations 3–14 These models are only applicable under the condition that when nanoparticles (NPs) collide with each other or with soil grains, they attach to each other, which implies a collision efficiency (α) of 1 ***(eq 3-5)***. The charge carried by an NP is critical in NP filtration, influencing all factors related to the electrostatic forces between charged NPs.

In natural soils or sediments, most minerals exhibit a negative surface charge due to their inherent crystallographic properties or the adsorption of anionic polyelectrolytes like humic acid (HA). Similarly, nanoparticles (NPs) often carry a negative surface potential influenced by their surface groups and the chemistry of pore water. This negative charge results in repulsive forces and reduces the attachment factor (α). Conversely, when NPs and collector materials have opposite charges, attachment is

facilitated.Colloidal stability, which refers to the ability of NPs to remain dispersed, is crucial for NP transport ***(Stumm, 1992)*** [70]. The stability of NPs is influenced by several factors, including density, surface charge, surface chemistry, size distribution, water chemistry, and flow velocity in the water. The surface charge of nanoparticles (NPs) in soil or sediment is attributed to several mechanisms:

- ***Chemical Reactions at Different pH Levels:*** Functional groups (e.g., –OH, –COOH) on the surface of NPs undergo chemical reactions influenced by varying pH levels, resulting in variable charges. At the point of zero charge, NPs tend to destabilize and coagulate.
- ***Substitution of Ions with Different Charges*****:** Ions, such as Si/Al, can substitute into the crystal lattice of minerals, creating permanent charges on the surface.
- ***Adsorption of Hydrophobic Substances:*** Hydrophobic substances adsorbed onto NPs can alter their surface charge (Stumm and Morgan, 1996).

According to the DLVO theory (Derjaguin, Landau, Verwey, and Overbeek), NP stability is governed by the balance between van der Waals attractive forces and repulsive electrostatic forces.

In ***Figure 3-6*** the total interaction energy between two NPs or a NP and a collector can be calculated by the sum of the repulsive forces, i.e., the double layer force VDDL (Eq. 13) and the Born force VB , van der Waals force VA (***Ruckenstein and Prieve 1973)***[71]

$$V_{\mathrm{DDL}} = \frac{\varepsilon\varepsilon_0 d_{\mathrm{p}}}{2}\Psi_{\mathrm{P}}\Psi_{\mathrm{K}}\ln\left(1+e^{-\kappa h}\right) \qquad 3\text{-}15$$

$$V_{\mathrm{B}} = \frac{AH^6}{7560}\left(\frac{4d_{\mathrm{p}}+h}{d_{\mathrm{p}}+h^7}+\frac{3d_{\mathrm{p}}-h}{h^7}\right) \qquad 3\text{-}16$$

$$V_{\mathrm{A}} = \frac{A}{6}\left[\ln\left(\frac{h+d_{\mathrm{p}}}{h}\right)-\frac{d_{\mathrm{p}}}{h}\,\frac{h+\frac{d_{\mathrm{p}}}{2}}{h+d_{\mathrm{p}}}\right] \qquad 3\text{-}17$$

where ***VDDL*** = diffuse double layer repulsion in (J), ***VB*** = Born repulsion in (J), ***A*** = Hamaker constant in (J), ***h*** = NP-collector distance in (m), ***H*** = Born parameter in (m), ***j*** = Debye-Huckel parameter in (m^{-1}), ***WP*** = surface potential NP in (V), ***WK*** = surface potential collector in (V), ***dp*** = NP diameter in (m), e = relative dielectric constant, e^0 = absolute dielectric constant in (A s V-1 m -1).

If electrostatic repulsive forces are predominant, the approach and subsequent attachment of a nanoparticle (NP) to the collector surface are hindered by an energy barrier. This barrier is influenced by the expansion of the diffuse double layer, which can be altered by the ionic strength of the water and the surface charges of both the NP and the collector. Conditions favoring high surface charge and low ionic strength promote the stability and mobility of NPs in the medium.In scenarios where an energy barrier exists, characterized by the dominance of electrostatic repulsion, the filtration efficiency α in Eq. 3.5 will be less than 1. This signifies that not all NP collisions result in attachment, which can undermine the accuracy of filtration theory if the reduced collision rate is not accounted for. The theoretical efficiency of collision or attachment, Pcoll, is mathematically expressed by Eq. 3.18 (Ruckenstein and Prieve, 1973).

$$P_{\mathrm{coll}} = \exp -(V_{\mathrm{DDL}} + V_{\mathrm{A}})_{\frac{\max}{k_{\mathrm{B}}T}} \qquad 3\text{-}18$$

Figure 3-7 illustrates how collision efficiency decreases as the energy barrier increases. According to the findings in, an energy barrier exceeding 10 $\boldsymbol{KB_T}$ theoretically prevents NP attachment to a collector. This scenario would enhance NP transport within porous media and consequently diminish the filtration capacity of soil or sediment.

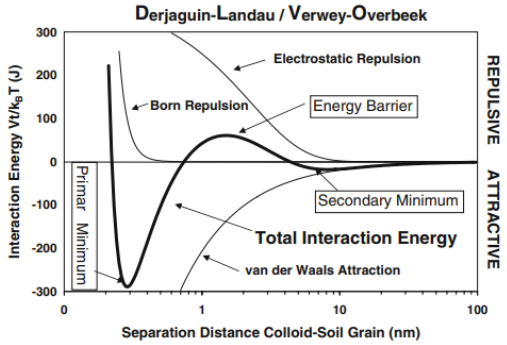

Figure 3-6 *DLVO model for total interaction energies between a spherical NP and a flat collector*

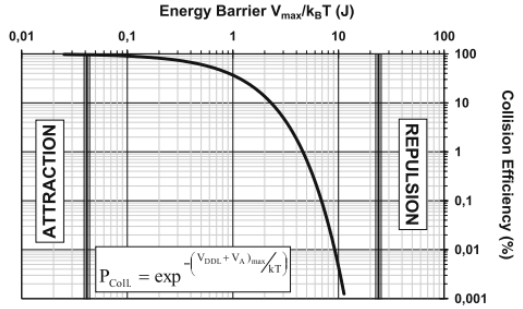

Figure 3-7 *Correlation between collision efficiency and energy barrier*

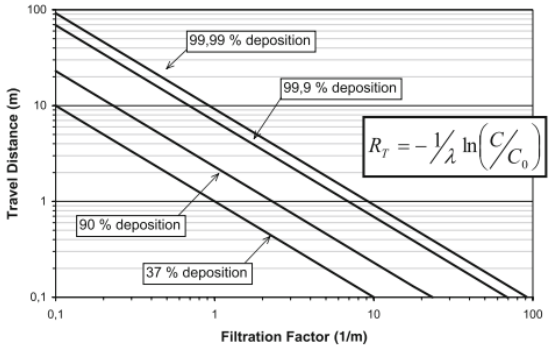

Figure 3-8 *Correlation between filtration factor and travel distance for a given deposition rate*

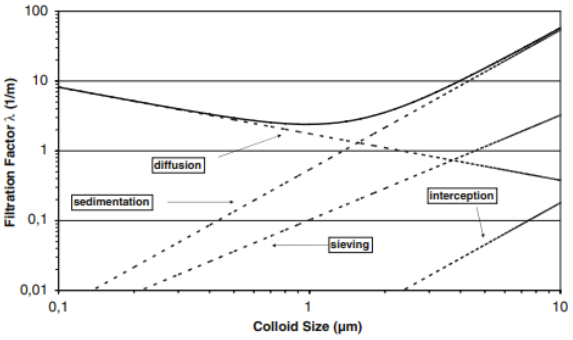

Figure 3-9 *Filtration theory modelling for diffusion, sedimentation and interception*

3.6 Advancements in Nano-technology for the O|G Sector

Nanoparticles have diverse applications in the oil and gas industry, contributing to enhanced efficiency, sustainability, and performance across various sectors. Some key applications are displayed in ***Figure 3-10*** below.

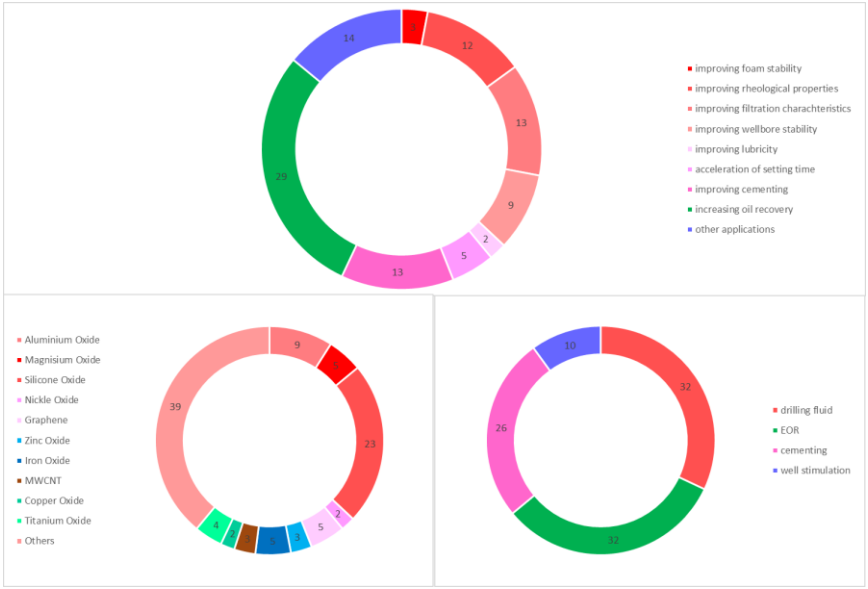

Figure 3-10 *Distribution of investigation for the application of different NPs in the oil and gas industry*[72]

3.6.1 Optimized Enhanced Oil Recovery Techniques

Nanoparticles have become essential in Enhanced Oil Recovery (EOR), significantly improving reservoir fluid behavior and displacement efficiency. Their ability to disperse in various fluids such as water, alcohols, surfactants, and polymers allows them to create effective nanofluids, nano-emulsions, and nano-catalysts[73]. This incorporation marks a paradigm shift in EOR strategies, addressing complex reservoir challenges by altering interfacial tensions, wettability, and fluid mobility, thus enhancing the extraction of trapped hydrocarbons[74]. The utilization of silica nanoparticles, renowned for their efficacy and prevalence, stands out as exemplary. These nanoparticles alone have demonstrated the potential to unlock an additional 20% of Original Oil in Place (OOIP), underscoring their unmatched impact on maximizing oil recovery rates[75].

Furthermore, recent field trials have highlighted the effectiveness of nano-Enhanced Oil Recovery (nano-EOR) techniques. Notable examples include: Petronas Carigali's Field Trial in Malaysia: Demonstrated up to a 15% increase in oil recovery, Saudi Aramco's Field Trial in Saudi Arabia: Showcased nano-EOR's adaptability in unconventional reservoirs and ConocoPhillips' Field Trial in the United States: Proved the utility of nano-EOR in mature reservoirs. These trials validate the theoretical benefits of nano-EOR, showing significant improvements in oil recovery and reservoir performance.[76] [77]

3.6.1.1 Nano-flooding

Using nanoparticles (NPs) as stand-alone fluids in enhanced oil recovery (EOR) is transformative, primarily through wettability alteration and interfacial tension reduction[78]. For instance, silica NPs shift wettability to water-wet conditions, trapping oil near pore walls and throats. They can reverse carbonate rock wettability, significantly reducing contact angles from 156° to 41°, and salinity enhances NP adsorption and release[79] [80]. Morteza Mansouri Zadeh et al. confirmed that nano-flooding after waterflooding increased oil recovery, with contact angle reducing from 82° to 52° and IFT from 18.5 to 14.9 (Mn/m) as nanofluid concentration increased from 0.02 wt.% to 0.05 wt.% [81]. Higher concentrations had no further impact on contact angle, thus, see ***Figure 3-11***. Moreover. Al-Anssari et al. confirmed silica nanofluids' ability to alter oil-wet carbonates to strongly water-wet conditions, suggesting their potential for CO2 sequestration, especially with anionic surfactants to stabilize NP suspension[82].In addition, Nanoparticles introduced during nano-flooding increase structural disjoining pressure, especially in the wedge film of nanoparticles, aiding in oil drop detachment from pore throats[83]check ***Figure 3-13*** for a mechanism's visualization. As shown in ***Figure 3-12*** Tariq Ali Chandio et al. demonstrated that injecting 2 PV of nanofluid after 2 PV of seawater increased oil recovery from 51.47% to 55.72%, highlighting again the nanofluid's effectiveness in altering interfacial tension and wettability[84].

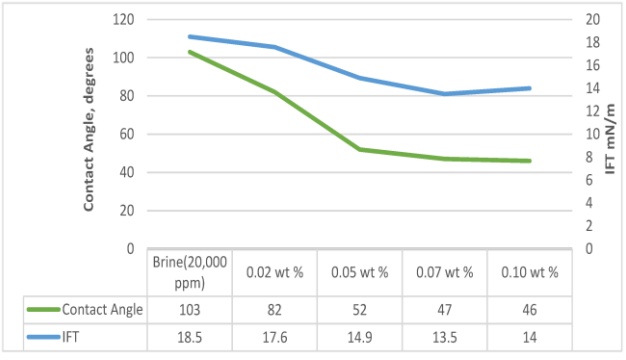

Figure 3-11 *Diagram of secondary oil recovery rate in core two due to flooding by seawater and nanofluid* [84]

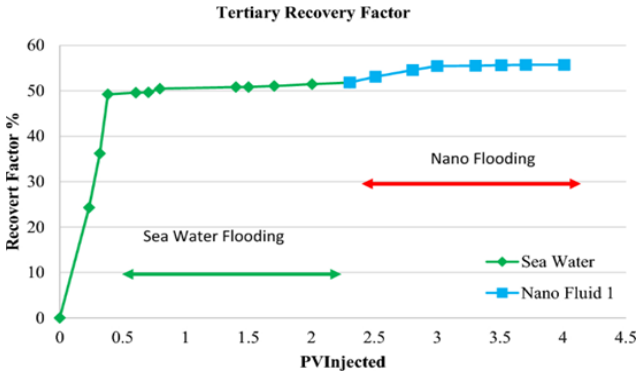

Figure 3-12 *Recovery (%OOIP) vs. Pore Volume injected* [81]

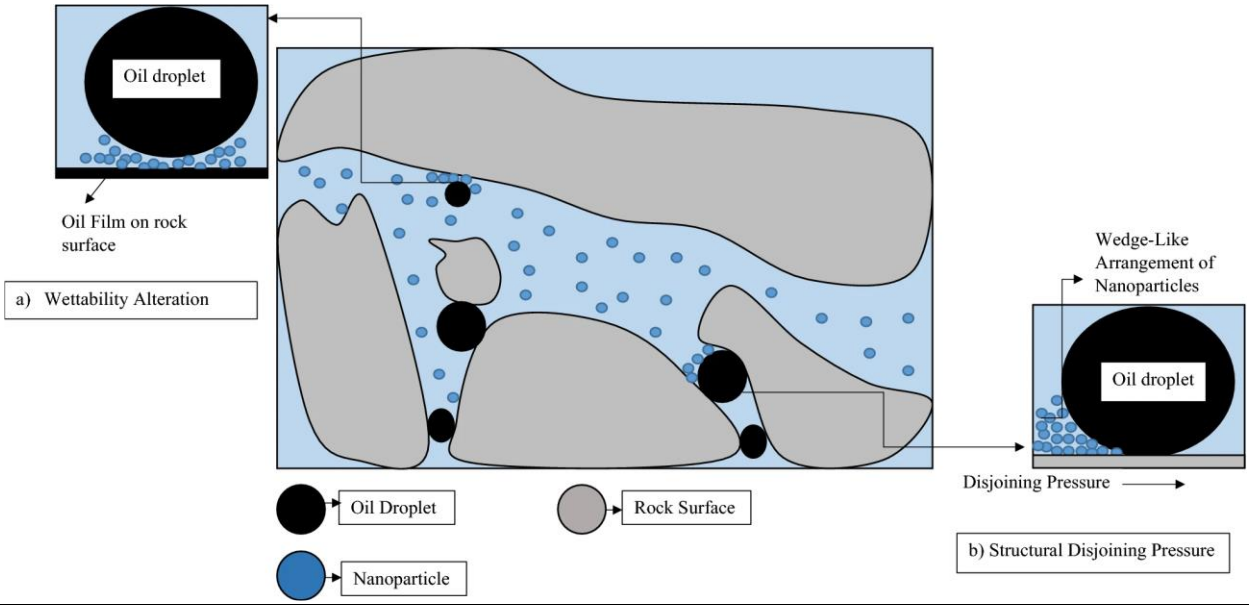

Figure 3-13 *Mechanism of NPs EOR. (a) Changing wettability and (b) structural pressure by NPs*[83]

3.6.1.2 ***Thermal N-EOR***

Nano-catalysts , including nickel-, iron-, and cobalt-based ones, are crucial in thermal Enhanced Oil Recovery (T-EOR) for reducing heavy oil viscosity and enabling aqua-thermolysis[85]. Their high surface-to-volume ratio enhances oil exposure and facilitates longer reactions[86]. Yi et al. demonstrated that nickel NPs effectively break carbon-sulfur bonds, though the effect diminishes over time, suggesting deeper reservoir placement for higher recovery factors[87]. Furthermore, ZnO NPs have proven to enhance oil recovery by 35.5% compared to conventional methods, significantly reducing viscosity at low concentrations[88]. Similarly, Fe2O3 and WO3 NPs at 0.2 (wt %) effectively reduce heavy oil viscosity to less than 40% during steam injection[89].

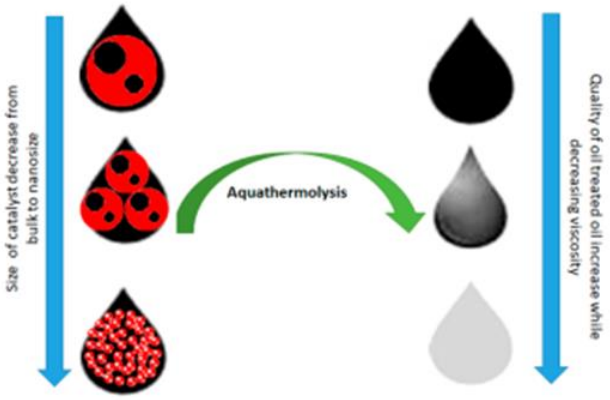

Figure 3-14 *Effect of catalyst size on aqua-thermolysis performance in oil treatment.*[90]

3.6.1.3 ***Chemical N-EOR***

The two primary branches of chemical flooding for enhancing oil recovery are polymer and surfactant flooding. As mentioned in the earlier section on nanofluids for EOR, various types of nanoparticles (NPs) can be employed to augment the viscosity of the displacing phase and decrease the interfacial tension (IFT) between oil and water. Consequently, recent reviews have extensively covered

the advancements in nano-assisted chemical EOR [86−89]. This section will delve into the progress made in both nano-polymer flooding and nano-surfactant flooding.

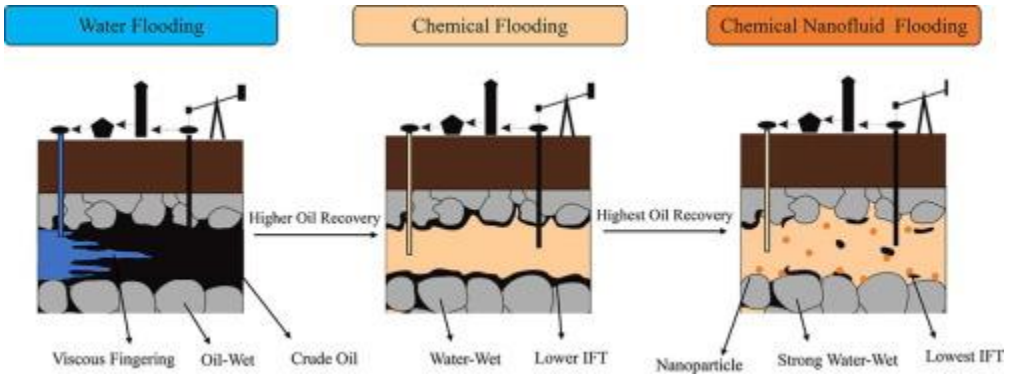

Figure 3-15 *C-Enhanced with and without nanomaterials* [91]

- Nano-polymer flooding

Combining polymers and nanoparticles (NPs) enhances the rheological properties of the displacing phase, aiming to reduce water coning/fingering and residual oil saturation[92]. NPs improve polymer stability in thermal, chemical, and mechanical aspects[93]. For instance, a nanocomposite of hydrolyzed polyacrylamide (HPAM) and silica NPs demonstrated superior stability and higher oil recovery compared to conventional HPAM[94] see ***Figure 3-17***. Moreover, the addition of silica NPs increased viscosity, reducing fingering and enhancing oil recovery[95]. Silica NPs also decreased polymer adsorption and shear thinning in sandstone due to ion-dipole interactions and physical cross-linking of polymer chains[96]. Also, Titanium dioxide NPs had been found to enhanced oil recovery through improved polymer viscosity[97]..In addition, Results of a core flooding test conducted by Gbadamosi et al., 2019 confirm that the SMCN particles could improve HPAM flooding and increase oil recovery factor by 33% more than ordinary HPAM flooding [98],results of the core flooding are shown in ***Figure 3-16***.

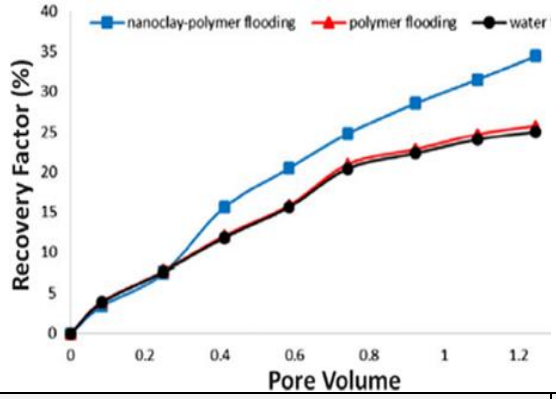

Figure 3-16 *Oil recovery versus pore volume injected for water flooding, polymer flooding and nanoparticle induced polymer flooding* [98]

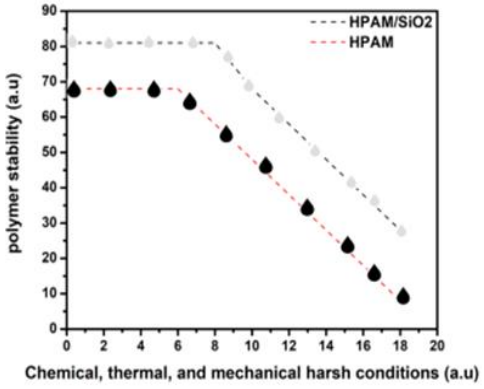

Figure 3-17 *. Stability of HPAM versus HPAM/SiO2.* [94]

- Nano surfactant flooding

While surfactants reduce interfacial tension between displacing and displaced phases, nanoparticles (NPs) further enhance this reduction[99]. NPs at the oil-surfactant/water interface contribute to additional interfacial tension reduction and may induce wettability alteration and capillary force decrease, which is ideal for EOR[100] . Silica NPs have been extensively studied in conjunction with surfactant flooding to enhance oil recovery. In one study using a five-spot glass micromodel, 2.2 wt% SiO2 NPs with sodium dodecyl sulfate (SDS) delayed breakthrough, enhanced sweep efficiency, and

shifted wettability, leading to 13% more heavy oil recovery compared to SDS alone [101]results are displayed in ***Figure 3-19***. In addition Surface-treated silica NPs demonstrated improved colloidal stability, IFT reduction, and wettability alteration [102] and TiO2 in SDS flooding showed nearly 5% incremental oil recovery due to breakthrough delay[103]. Moreover ,Alumina and zinc oxide NPs with SDS demonstrated varying IFT and oil recovery results, with zinc oxide NPs showing less IFT and achieving higher cumulative oil recovery, likely due to spontaneous emulsification[104] .

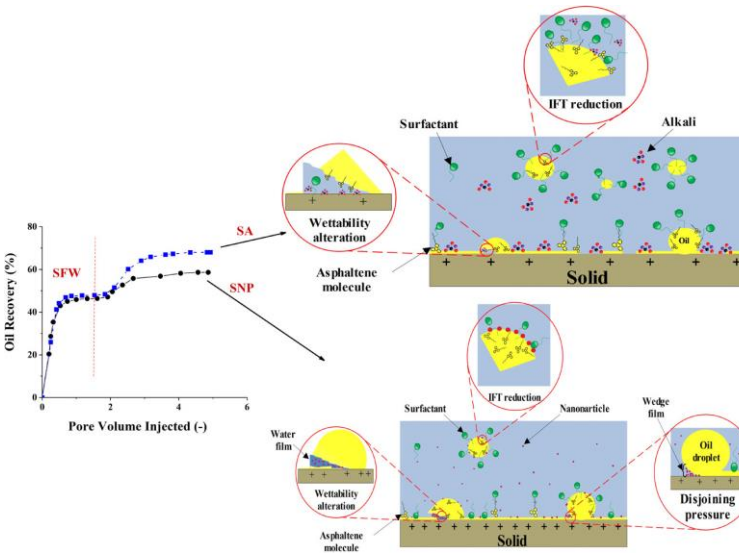

Figure 3-18 *NPs in enhancing surfactants effects* [105]

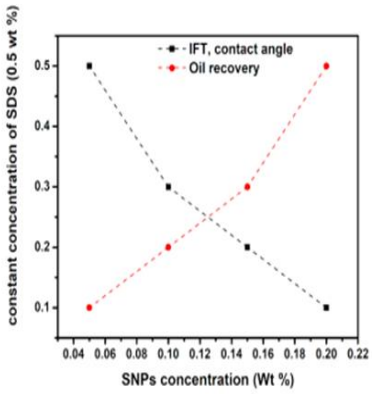

Figure 3-19 *Effect of adding silica NPs on IFT, contact angle, and oil recovery*[101]

In summary, nanoparticles in EOR are instrumental in modifying reservoir fluid properties, enhancing displacement efficiency, controlling wettability, reducing interfacial tension, and improving oil recovery rates by optimizing the interaction between injected fluids and trapped oil in reservoirs.

Still, Challenges include ensuring the stability of nanofluids, selecting the right nanoparticle size, tolerating harsh reservoir conditions, and addressing environmental concerns. Despite these challenges, nanoparticles show promising capabilities in improving EOR mechanisms.

3.6.2 Innovative Nano-Applications in Well Cementing

Oil-well cementing is crucial for providing zonal isolation and structural support for steel casings. However, fluid leakage remains a major challenge, leading to costly remediation and environmental issues[106]. Poor contact between cement and formation is a key factor contributing to leakage[107]. Shear bond strength between cement and formation is critical, with a minimum requirement of 100 psi [108]Nanoparticles show promise in enhancing cement efficiency by modifying properties such as strength and microstructure[109]. Nanoparticles in well cementing act as fillers, sealing gaps in the cement matrix and reducing porosity[110]. Challenges include nanoparticle dispersion, with optimal content ranging from 1-5% to avoid agglomeration[110].

In (Mtaki Thomas Maagi & Jun, 2020), The shear bond strength of specimens with varying NP dosages was evaluated after curing at 80°C for 3, 7, 14, and 28 days, showing that specimens containing nanoparticles exhibit significantly higher shear bond strength compared to controls. Shear bond strength increased gradually with NP type and curing age, reaching maximum values after 28 days. NS powders outperformed NT particles, likely due to enhanced pozzolanic activity and increased C–S–H gel formation[111], the results are shown below in ***Figure 3-20***. Optimal NP content was up to 3% bwoc, beyond which shear bond strength decreased due to reduced hydration rates and particle dispersion issues[112]. The optimal NP content in cement depends on various factors, including the nature of the nanomaterial. Studies indicate that optimal nanoparticle content in cement should be carefully

controlled. Low concentrations (1-5% bwoc) prevent agglomeration, while higher doses (up to 10% bwoc) can enhance performance if well distributed[113]. Smaller nanoparticles promote hydration but can decrease fluidity and strength due to agglomeration.

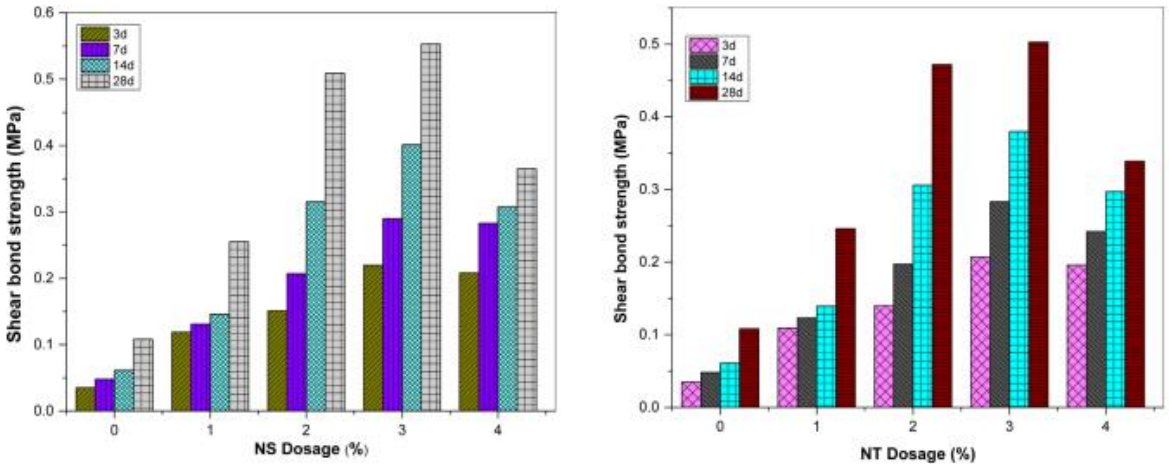

Figure 3-20 *Shear bond strength of the cement-formation interface NT and NS* [111]

3.6.3 Cutting-Edge Nanotechnology Solutions in Other Applications

Nanotechnology has a wide range of applications in the oil and gas industry majoring in the cited above, cementing and enhanced oil recovery (EOR). Here are some additional applications of nanotechnology in the oil and gas industry:

- ***Well stimulation And Hydrocarbons detection:*** Nanoparticles play a crucial role in well stimulation processes by enhancing reservoir permeability, increasing fluid flow, and improving overall well productivity. By modifying the properties of the reservoir rocks and fluids, nanoparticles facilitate increased fluid flow within the reservoir. This enhanced fluid flow helps in better mobilization of oil and gas, leading to improved recovery rates and overall, well productivity[114]. Nanoparticles can also be engineered to selectively bind to hydrocarbons, offering a promising avenue for developing sensors to detect leaks or monitor hydrocarbon concentrations in the environment. Several studies have delved into this area, showcasing the potential of functionalized nanoparticles for hydrocarbon detection[115].
- **Geothermal systems:** Nanotechnology has been identified as a promising approach to enhance the efficiency of geothermal energy systems by improving heat transfer processes[116].
- **Gas-to-Liquid (GTL) Production:** Nanotechnology can be used to develop nano catalysts and nanoscale membranes for GTL production, which can help address the problems associated with accessing stranded natural-gas resources[116].
- **Compressed-Natural-Gas (CNG) Transport:** Nanotechnology can be used to create nanostructured materials for CNG transport or long-distance electricity transmission [116].
- **Offshore Drilling Structural Materials:** Nanotechnology can be used to create lighter, stronger, and more corrosion-resistant structural materials in platforms for offshore drilling [116].
- **Environmental Protection:** Nanotechnology can be used to develop filters and particles with a nanostructure that allows them to remove volatile organic compounds from oil and gas production processes [116].
- **In-Situ Upgrading of Bitumen**: Nanotechnology can be used to convert bitumen and heavy-oil reserves into products cost-effectively by researching specifically designed adsorbents and catalysts to be introduced into the reservoir porous media in nanosized form [116].

- **Nanomaterial-Based Solutions:** Nanotechnology can be used to address technical challenges in the oil and gas industry, such as corrosive impurities, high temperatures and pressures, shock loads, abrasion, and other hostile environmental conditions[116].

In summary, the incorporation of nanoparticles in the oil and gas industry has shown promising results, offering significant. Despite this wide range of applications, the most important and widely applied use of nanoparticles is their incorporation into drilling fluids see ***Figure 3-10*** above.

3.7 Revolutionary D-Fluids: Nano-Tech Integration

One of the most valuable applications of nanoparticles (NPs) lies in their integration into drilling mud formulations. This strategic utilization of NPs plays a pivotal role in enhancing drilling operations across the oil and gas industry. By incorporating NPs into drilling mud, numerous benefits are realized, including improved lubrication, enhanced fluid stability, and effective formation damage mitigation[117]. NPs, with their high surface area-to-volume ratio and tailored surface properties, effectively reduce friction between the drill bit and the formation, leading to smoother drilling and decreased wear on equipment[118]. Additionally, NPs contribute to stabilizing drilling mud, preventing phase separation, and maintaining optimal viscosity under varying conditions, thus ensuring efficient cuttings transport and wellbore integrity[118]. Moreover, the inclusion of NPs aids in sealing microfractures and pore throats within the formation, mitigating the risk of fluid invasion and preserving reservoir productivity[118]. Overall, the incorporation of NPs into drilling mud represents a cornerstone in optimizing drilling performance, reducing operational costs, and advancing sustainable drilling practices.

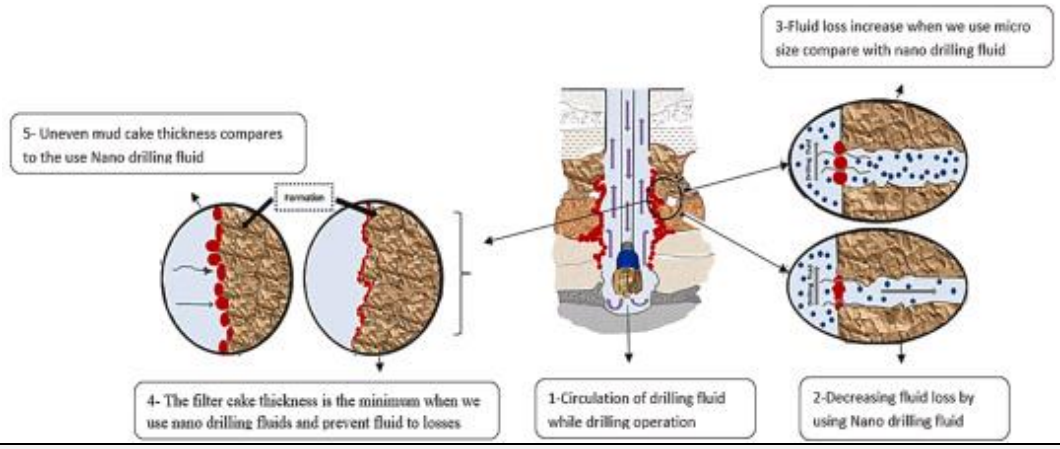

Figure 3-21 *NPs Drilling Fluids Versus Micro Drilling Fluids* [119]

3.7.1 different types of nanoparticles used in drilling fluids

Recent advancements in nanotechnology have significantly enhanced the performance of drilling fluids in the oil and gas industry. Various types of nanoparticles, including polymeric, ceramic, metal, and carbon-based nanoparticles, have been incorporated into drilling muds to improve their rheological, thermal, and filtration properties. The following table provides a summary of the different nanoparticles used in drilling fluids, highlighting their compositions, key benefits, and specific applications.

Table 3-3 *Common Incorporated NPs in DFs*

Nanoparticle Type	Example of application	Common Effects
Polymeric Nanoparticles		
Synthetic Polymer NPs	TiO2/PAM in WB drilling fluids	Improved fluid loss, mud cake thickness, and rheological properties
Ceramic Nanoparticles		
General Ceramic NPs	Magnesium aluminum silicate in WB drilling	Improved rheological, filtration properties, and thermal stability
Silica NPs	Natural gas hydrate drilling fluids	less hydrate formation
Zinc Oxide NPs	HSG removal from WBM	ZnO NPs performed better in HSG removal
Titanium Dioxide NPs	WB drilling fluids with TiO2 NPs	Improved stability, lubricity, mechanical properties
Cupric Oxide NPs	WBMs with CuO and ZnO NPs	Improved thermal properties, cooling efficiency, fluid loss control
Clay NPs	Drilling fluids with clay hybrid NPs	Reduced fluid loss, improved thermal stability
Metal Nanoparticles		
Iron-Based NPs	Drilling fluids under HPHT conditions	reduction in fluid loss
Calcium and Zirconium NPs	Drilling fluids with calcium NPs	Enhanced fracturing pressure
Silver NPs	WBMs with silver NPs and graphene nanoplatelets	Improved plastic viscosity, reduced fluid loss and yield point
Carbon-Based Nanoparticles		
Carbon NPs	WBMs with carbon NPs and ZnO nanowires	Delayed fluid sagging, improved fluid density

3.7.2 methods used to incorporate nanoparticles into drilling fluids

Nanoparticles can be incorporated into drilling fluids using various methods, including direct addition, surface modification, and encapsulation. Direct addition involves mixing nanoparticles into the drilling fluid without any further treatment. Surface modification involves altering the surface of the nanoparticles to improve their compatibility with the drilling fluid, such as by adding functional groups or coatings. Encapsulation involves enclosing the nanoparticles in a protective coating or matrix, which can improve their stability and control their release into the drilling fluid.

3.7.2.1 Direct Addition

Direct addition involves mixing nanoparticles into the drilling fluid without any further treatment. This method is straightforward and can be done by simply adding the nanoparticles to the drilling fluid. However, this method has some limitations. The nanoparticles may not be evenly distributed throughout

the drilling fluid, which can affect their performance. Additionally, the nanoparticles may not be compatible with the drilling fluid, which can lead to issues such as agglomeration or settling.

3.7.2.2 ***Surface Modification***

Surface modification involves altering the surface of the nanoparticles to improve their compatibility with the drilling fluid. This can be done by adding functional groups or coatings to the nanoparticles. The functional groups or coatings can improve the nanoparticles' ability to interact with the drilling fluid, making them more effective at improving the drilling fluid's properties. Surface modification can also help to prevent the nanoparticles from agglomerating or settling, which can improve their performance.

3.7.2.3 ***Encapsulation***

Encapsulation involves enclosing the nanoparticles in a protective coating or matrix. This can improve their stability and control their release into the drilling fluid. Encapsulation can also help to prevent the nanoparticles from interacting with the drilling fluid in an undesirable way, which can improve their performance. Encapsulation can be done using various methods, such as coating the nanoparticles with a polymer or encapsulating them in a liposome.

3.7.3 Nano-based Drilling Fluids: NPs and DF Stability

Nanoparticles (NPs) have been found to enhance the stability of drilling fluids, particularly in terms of filtration control and shale stability. The use of NPs in drilling fluids can improve the filtration performance, with some exceptions for certain types of NPs[120] .NPs can enhance shale stability through physical plugging, chemical inhibition, and electrostatic interactions between surface charges, minimizing clay swelling and improving wellbore stability in shale formations [121].

In addition to improving filtration control and shale stability, NPs can also enhance the thermal conductivity, stability, and rheological properties of drilling fluids, reducing viscosity and density while increasing heat transfer and preventing fluid loss and formation damage [120].However, it is important to note that the effectiveness of NPs in drilling fluids depends on various factors, such as concentration, size, and type of NPs, as well as the specific drilling conditions and formation characteristics[121].

3.7.3.1 ***WellBore Stability: Nano-Tech Influence***

One of the leading causes of non-productive time in drilling is wellbore instability[122]. This may lead to lost circulation and stuck pipe. It can create significant problems particularly when drilling through depleted formations or in deep water environment where operational drilling windows may be very small[122]. Wellbore strengthening should be considered in those cases, several types of nanoparticles have been tested as wellbore strengthening materials with good results so far, including field applications. Researches has shown that nano-materials significantly enhance wellbore stability in unstable formations. Xu et al. (2018) investigated the combination of polyethylene glycol and nano-silica, finding it effective as a shale stabilizer in water-based drilling fluids (WBD). Organic nanoparticles (NPs) like polystyrene, polyacrylamide, and polyethylene glycol have high colloidal stability and elastic modulus, allowing them to deform and fit various shale pore shapes, thereby improving drilling fluid stability in shale formations[123].Moreover, Liu et al. (2020) studied silica NP concentrations in Pickering emulsions for drilling fluids, concluding that NP additives enhance shale surface stability and prevent fractures[124]. Nakhaee, 2019[125] developed a nano-drilling fluid with different nano-ZnO concentrations, finding that positive charge, hydrophilicity, and size of NPs improve shale stability. Modified ZnO NPs were shown to block pore spaces in shale, as their positive charge allows them to be adsorbed by negatively charged shale particles.

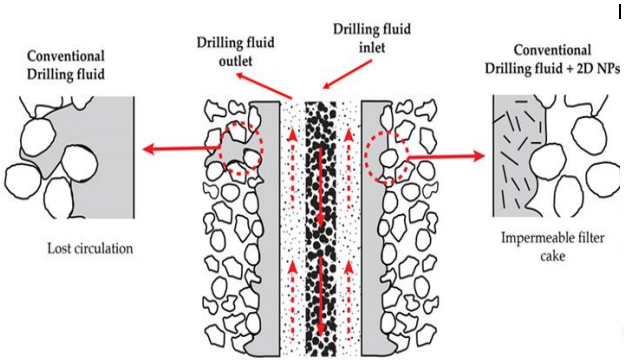

Figure 3-22 *Filtration process in well pores with conventional drilling fluid containing bentonite compared to the same fluid with added 2D nanoparticles.*[126]

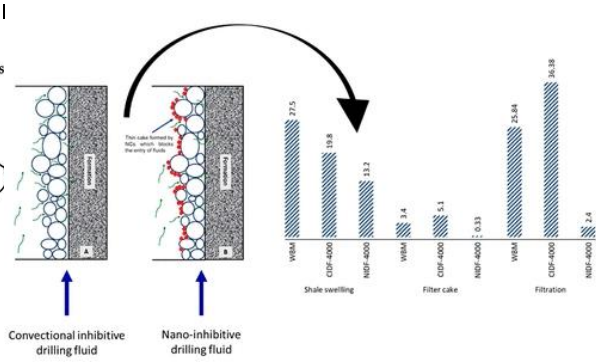

Figure 3-23 *Wellbore stability: nano fluid vs conventional*[127]

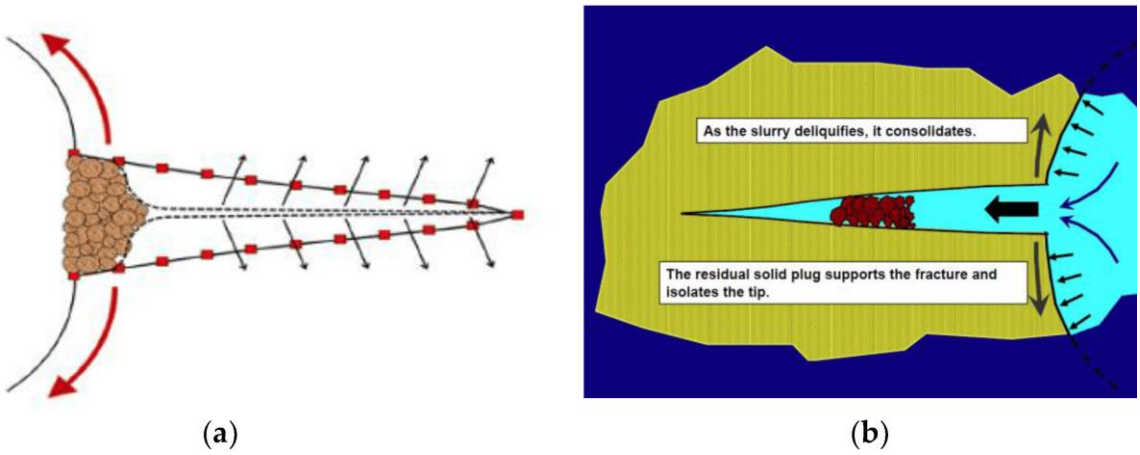

Figure 3-24 *Nano-materials in fractures, either (a) at the entrance of the fracture [58] or (b) by entering the fracture* [128]

3.7.3.2 ***Thermal Stability: Nano-Tech Influence***

The integration of nanoparticles (NPs) into drilling fluids represents a significant advancement in the quest for improved thermal stability, crucial for maintaining optimal rheological behavior in high-temperature drilling environments. NPs such as silica (SiO2), aluminum oxide (Al2O3), and titanium dioxide (TiO2) are particularly effective as they can withstand temperatures that cause conventional additives to fail[129]. The thermal conductivity of these NPs helps dissipate heat more uniformly throughout the drilling fluid, reducing the risk of localized overheating and thermal degradation.This area has garnered high interest from many researchers. For instance, Veisi et al. explored the effects of Al2O3, CuO, and Cu nanoparticles on drilling fluid properties. Their study revealed notable enhancements in thermal and rheological characteristics upon nanoparticle inclusion. Remarkably, the addition of 0.9 wt% Cu nanoparticles resulted in a substantial 15.6% improvement in heat capacity and a 12% enhancement in thermal conductivity[130].Further advancements were made by Ponmani et al., who developed nano-enhanced drilling fluids containing CuO and ZnO nanoparticles at various concentrations (0–0.5 wt%) in different base fluids, such as xanthan gum, polyethylene glycol (PEG-600), and polyvinylpyrrolidone (PVP). The results were compared to microfluid-enhanced drilling mud to reveal the effect of particle size. Their observations indicated that enhanced thermal conductivity properties were achieved with the addition of nanoparticles compared to micron-sized materials, and that higher concentrations of nanoparticles promoted better thermal conductivity properties[131], see

Figure 3-25 . These studies collectively underscore the critical role of NPs in advancing the thermal stability and performance of drilling fluids in high-temperature environments.

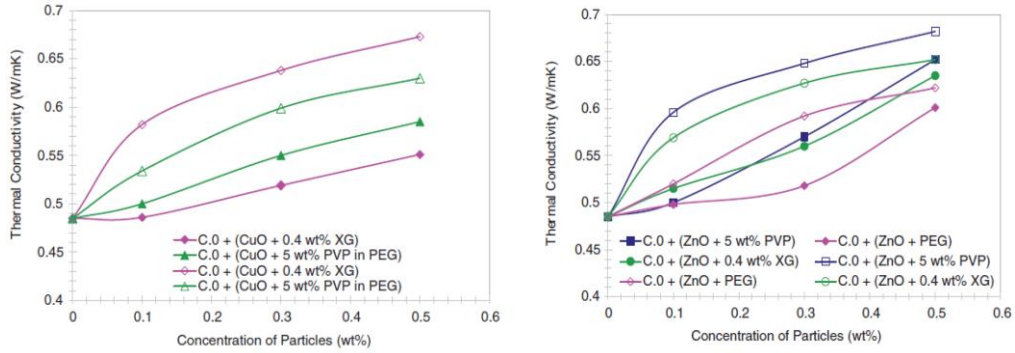

Figure 3-25 *Variation of thermal conductivity of nano-enhanced water-based mud (NWBM) and microfluid-enhanced water-based mud (MWBM) for (a) CuO/(b) ZnO*[131]

3.7.3.3 ***Rheological Properties: Nano-Tech Influence***

Nanoparticles (NPs) can significantly improve the rheological properties of drilling mud:

- ***Yield Point (YP) Improvement*** Nano-particles (NPs) significantly enhance the yield point (YP) of drilling mud by augmenting electrostatic interactions and reinforcing the structural network within the fluid. This enhancement improves the mud's ability to suspend cuttings and prevents sedimentation.
- ***Plastic Viscosity (PV) Enhancement*** NPs improve plastic viscosity (PV) by reducing the friction between solid particles and the fluid medium, leading to smoother flow characteristics and a more stable fluid. This reduction in friction results in better flow and handling properties of the drilling mud.
- ***Apparent Viscosity (AV) Increase*** The increased surface area and reactivity of NPs contribute to an enhanced overall viscosity and flow behavior of the drilling mud, thereby improving apparent viscosity (AV). This ensures the fluid maintains optimal performance under varying conditions.
- ***Gel Strength Enhancement*** NPs stabilize the mud structure and improve its thixotropic properties, significantly increasing gel strength. This stabilization ensures better cuttings suspension during drilling pauses, preventing settling and maintaining fluid integrity.

These enhancements collectively result in more efficient drilling operations, reduced equipment wear, and improved borehole stability, showcasing the critical role of NPs in advancing the performance of drilling muds.

Table 3-4 *Improvement Of RH properties with NPs LPLT AND HPHT Conditions*

Author	***Types of NPs***	***Base Fluid***	***Modified Properties***	***Experimental Conditions***	***Summary of results***
Nasser (2013)	Nanograp hite	Oil	Viscosity	LPLT	Nano-graphite with 40 nm diameter in OBFs increased fluid viscosity at LPLT condition.
Sadeghalv aad et al. (2015	TiO2	Water	PV, YP	LPLT	1 – 14 gr of the titanium oxide (TiO2) NPs were added to the water-based fluid formulation. Results indicated improvement in plastic viscosity and yield point under LPLT condition.

Srivatsa et al. (2012)	SiO2	Water	Viscosity	LPLT	2.5 wt% SiO2 WBFs increased viscosity under LPLT condition.
Song et al. (2016)	Cellulose nanoparticles	Water	PV, YP, GS	LPLT	3.5wt% of celluloses nanoparticles with 8.2 nm width and 321 nm length in WBFs increased rheological properties under LPLT condition.
Abdo et al (a) (2014)	ZnO	Water	PV, YP	HPHT at 109-370 F° and 150-18,500 psi	2.3wt% of the nanocomposite with 5-50 nm diameter resulted in more stable rheological properties under HPHT
Anoop et al. (2014)	SiO2	Oil	PV	HPHT at 77-284°F and Pressure-up to6,000 psi	2.0 vol% of nano6silica (SiO2) with 20 nm diameter in OBFs increased plastic viscosity at ambient condition and maintained stable rheological profile under HPHT
Mahmoud et al. (2016)	Fe2O3 SiO2	Water	PV, YP	High temperature (392, 410,428, 446Of°)	The formulation showed stable profiles at high temperature conditions

3.7.3.4 *Filtration Properties: Nano-Tech Influence*

Nanoparticles (NPs) significantly improve the filtration properties of drilling mud, addressing one of the critical challenges in drilling operations—controlling fluid loss into the formation. The process of improving mud filtration with NPs involves several mechanisms:

- ***Particle Bridging and Pore Blocking:*** When NPs are added to drilling mud, their small size and high surface area allow them to bridge across the pores and fractures in the formation. This bridging action creates a seal or filter cake on the wellbore walls, effectively reducing the permeability and preventing excessive fluid loss.
- ***Enhanced Filter Cake Quality:*** NPs help in forming a thin, low-permeability filter cake. Unlike conventional additives, NPs can create a more uniform and less porous cake due to their nano-scale size, which fills in the gaps and pores more effectively. This results in a filter cake that is less prone to spalling or breaking apart under pressure.
- ***Improved Particle Interaction:*** The high reactivity and surface energy of NPs enhance the interactions between mud particles and the formation. NPs can modify the surface properties of the filter cake, making it more hydrophobic or altering its electrostatic properties to improve adhesion and stability.
- ***Rheological Control:*** The presence of NPs also affects the rheological properties of the mud, such as yield point, plastic viscosity, and gel strength, which contribute to better suspension of solids and more efficient fluid flow. Improved rheology helps maintain the integrity of the filter cake by ensuring consistent deposition and minimizing erosion.
- ***Chemical Interactions:*** NPs can interact with other mud additives, enhancing their effectiveness. For instance, silica (SiO2) NPs can interact with polymers and clays in the mud to form a more cohesive and robust filter cake structure. Additionally, NPs like magnesium oxide (MgO) and iron oxide (Fe3O4) can provide chemical stability, further enhancing the filtration properties of the mud.

The overall benefit of using NPs in improving mud filtration is the reduction of fluid invasion into the formation, which minimizes formation damage, maintains wellbore stability, and enhances overall drilling efficiency. This leads to fewer problems related to differential sticking, loss of circulation, and formation fracturing, ultimately reducing operational costs and improving the success rate of drilling projects.

Table 3-5 *Improvement of filtration properties with NPs LPLT AND HPHT Conditions*

Author	***Types of NPs***	***Base Fluid***	***Modified Properties***	***Experimental Conditions***	***Summary of results***
Akhtarmanesh et al. (2013))	SiO2	Water	Fluid Loss Shale inhibition	LPLT	30wt% of silica nanoparticles with 35 nm diameter in WBfs showed a reduction of fluid filtrate observed through the pore plugging test.
Barry et al. ***(2015)***	Fe2O3	Water	API fluid loss HPHT fluid loss	LPLT and HPHT	The results showed an increase in fluid loss with the addition of ferric oxide (Fe2O3) NPs at LTLP conditions.
Contreras et al. (2014)	Iron Calcium	Oil	Filter cake Fluid loss	LPLT and HPHT	Iron showed higher reduction of filtration loss than samples with calcium-based NPs. It also concluded that LCM works better with iron-based NPs but not with calcium at HPHT conditions
Liu et al. ***(2016)***	Cellulose nanoparticles	Water	Fluid loss Shale inhibition	LPLT	2.0wt% of silica (SiO2) NPs in WBFs reduced filtration loss at low temperature (21 to 43oF) conditions.
Taha et al. ***(2015)***	Graphene	Water	Fluid loss Friction coef	LPLT and HPHT	tested 1, 2, 3, 4 and 5 wt% of graphene NPs in a 10 ppg WBF and resulted in reduced API fluid loss of up to 30%.but higher c leads to higher friction coef
William et al. ***(2014)***	CuO ZnO	Water	Fluid loss	LPLT and HPHT	The results showed that fluid loss and filter cake thickness decreased significantly under LPLT and HPHT
Zhang et al. ***(2015)***	Not specifiesd	Oil	Fluid loss	HPHT	2.0wt% of NPs in OBFs effectively significantly reduced fluid loss and filter cake thickness under HPHT condition at 194oF

3.7.3.5 ***Nanoparticles for Mitigating Temperature Effects on Drilling Fluids' Filtration***

The effect of temperature in drilling mud filtration is set in previous chapter, nanoparticles can prevent those effects, those Majestics particles can enhance fluid filtration in drilling mud even at high temperatures through several mechanisms that leverage their unique properties, such as high surface area, thermal stability, and reactivity. High-temperature resilience: Many NPs, such as silica (SiO2), titanium dioxide (TiO2), and aluminum oxide (Al2O3), have high thermal stability see section. This means they can maintain their structural integrity and functional properties at elevated temperatures where conventional additives might degrade. This stability ensures that the NPs continue to full-fill their part see section effectively block pores and maintain a robust filter cake under high-temperature conditions.

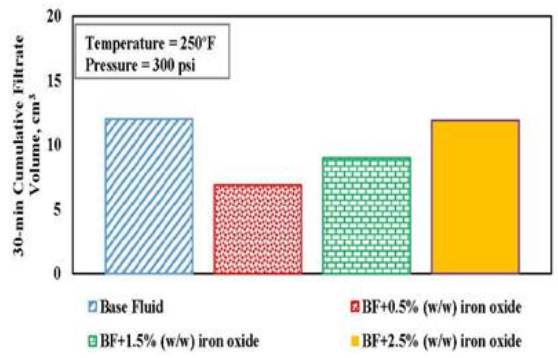

Figure 3-26 *Benefits of integrating Fe2O3 in DFs for HPHT conditions* [132]

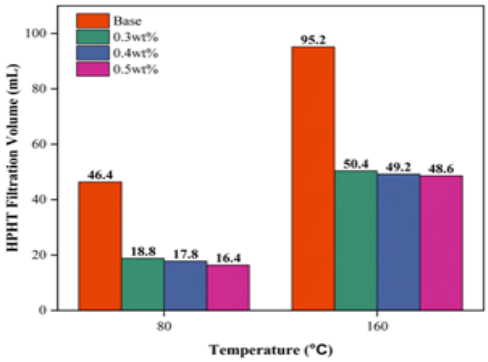

Figure 3-27 *Effects of temperature in DFs with different NPs concentrations*[132]

3.7.3.6 *Effect of concentration of Nanoparticles on Mud Filtration*

The concentration of nanoparticles (NPs) in drilling mud significantly affects its filtration properties, with optimal levels needed to achieve the best performance. At low NP concentrations, the enhancement in filtration might be minimal as there aren't enough particles to effectively bridge the pores and form a robust filter cake. As the concentration increases, NPs can efficiently fill the gaps and seal the pores, creating a dense, low-permeability filter cake that significantly reduces fluid loss and enhances wellbore stability. However, excessively high NP concentrations can lead to issues such as increased viscosity and potential agglomeration of particles, which can adversely affect the rheological properties and overall performance of the mud. Therefore, a balanced NP concentration is critical to maximize the benefits of improved filtration while maintaining optimal mud rheology and operational efficiency.

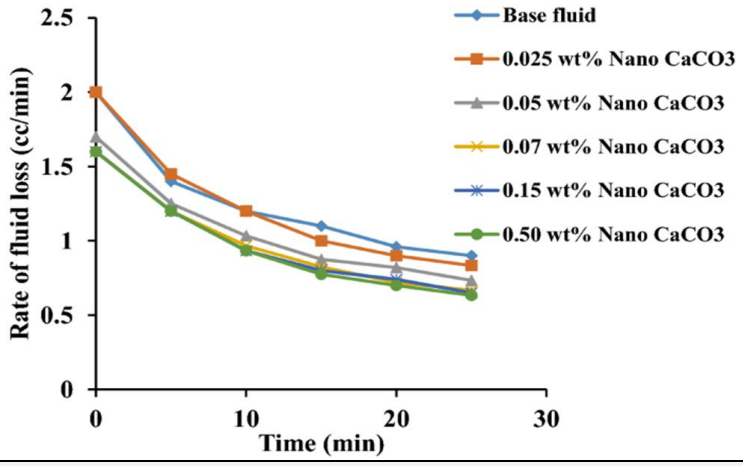

Figure 3-28 *Effects of CaCo3 NPs on DFs filtrate volume*[132]

3.7.3.7 *The Impact of Optimal Nanoparticle Concentration*

From sections above, the idea that pioneer our work is more confirmed, Higher concentrations of NPs can lead to improved filtration control, especially at elevated temperatures, by reducing fluid loss capacity and enhancing rheological properties but achieving the optimal concentration in drilling mud requires a careful balance to minimize filtration loss while maintaining desirable rheological properties. This involves systematically determining the concentration at which NPs effectively seal pores and form a robust, low-permeability filter cake, significantly reducing fluid loss. Simultaneously, the concentration must be controlled to prevent excessive viscosity increases and particle agglomeration, which can negatively impact the flow characteristics and stability of the drilling mud. By fine-tuning the NP concentration, it is possible to enhance the filtration control capabilities of the drilling mud without compromising its ability to suspend cuttings and flow efficiently, ensuring both operational effectiveness and wellbore integrity.

AI and ML for Optimal Drilling Performance

CHAPTER IV

Chapter 4. AI and ML for Optimal Drilling Performance

Introduction

Machine learning is a powerful tool that enables computers to learn from data and make predictions or decisions without being explicitly programmed. In the oil and gas industry, machine learning has found numerous applications, particularly in drilling operations and drilling fluid management. In drilling operations, machine learning models have been developed to optimize performance, solve technical problems, and reduce costs. Several models also have been applied to various aspects of drilling fluid, such as predicting drilling fluid properties, estimating rheological properties, and determining shear stress and filtration criterions.

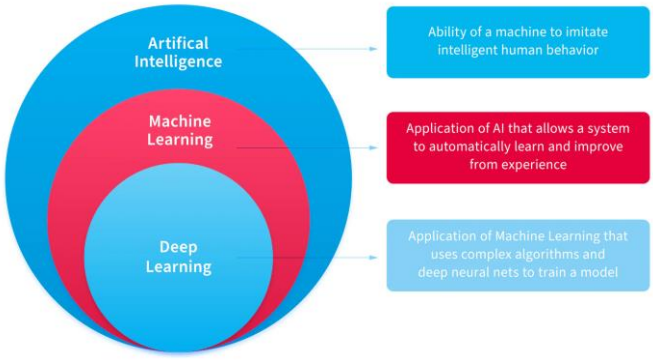

Figure 4-1 *AI, ML and Deep Learning* [133]

"Artificial intelligence is here and being rapidly commercialized, with new applications being created not just for manufacturing but also for energy, healthcare, and oil and gas. This will change how we all do business" **Joe Kaeser**, former CEO of Siemens, noted the transformative impact of AI across multiple sectors, stating,

4.1 Advanced Techniques: AI, ML, and Deep Learning in Drilling Operations

4.1.1 Artificial Intelligence (AI)

AI refers to the simulation of human intelligence in machines that are programmed to think and learn like humans. It encompasses a broad range of techniques and approaches aimed at enabling machines to perform tasks that typically require human intelligence, such as decision-making, problem-solving, and pattern recognition[134]. In drilling engineering, AI can be applied to automate processes, optimize drilling parameters in real-time, predict equipment failures, and improve overall efficiency and safety.

4.1.2 Machine Learning (ML)

Machine Learning is a subset of AI that focuses on the development of algorithms and statistical models that enable computers to learn from and make decisions or predictions based on data. Unlike traditional programming where rules are explicitly defined, ML algorithms learn patterns and relationships from data without being explicitly programmed[134]. ML algorithms are used in drilling engineering to analyze vast amounts of data collected from sensors, historical drilling operations, geological surveys, etc. They can optimize drilling processes, detect anomalies, predict equipment maintenance needs, and improve drilling performance based on real-time feedback.

4.1.3 Deep Learning (DL)

Deep Learning is a specialized subset of ML inspired by the structure and function of the human brain called artificial neural networks (ANNs). DL algorithms learn hierarchical representations of data, typically through many layers of interconnected nodes (neurons), allowing them to model complex

patterns and relationships in large datasets[134]. DL techniques, particularly deep neural networks, can be used in drilling engineering for tasks such as image recognition (e.g., identifying subsurface structures from seismic data), natural language processing (e.g., analyzing text reports and logs), and predictive modeling (e.g., forecasting drilling performance based on various parameters). They excel in tasks where large amounts of data are available and complex patterns need to be extracted.

4.2 Machine Learning Foundations for Engineering Applications

4.2.1 Machine Learning Categories

Machine learning algorithms can be categorized into three main types:

4.2.1.1 Supervised Learning

This type involves known output or response variables, where the algorithm maps input features to the output. It includes:

- **Regression**: Used when predicting continuous output variables.
- **Classification**: Used when predicting output variables with multiple classes or labels.

4.2.1.2 Unsupervised Learning

In this approach, there is no explicit output variable, and the algorithm identifies hidden structures and relationships in the data. Examples include clustering, dimensionality reduction, and associative rule learning.

4.2.1.3 Reinforcement Learning

These algorithms learn by associating rewards or penalties with decision sequences to achieve a defined objective. Modeled using the Markov decision process (MDP), reinforcement learning involves trial-and-error to optimize actions. An example application is robotics for industrial automation.

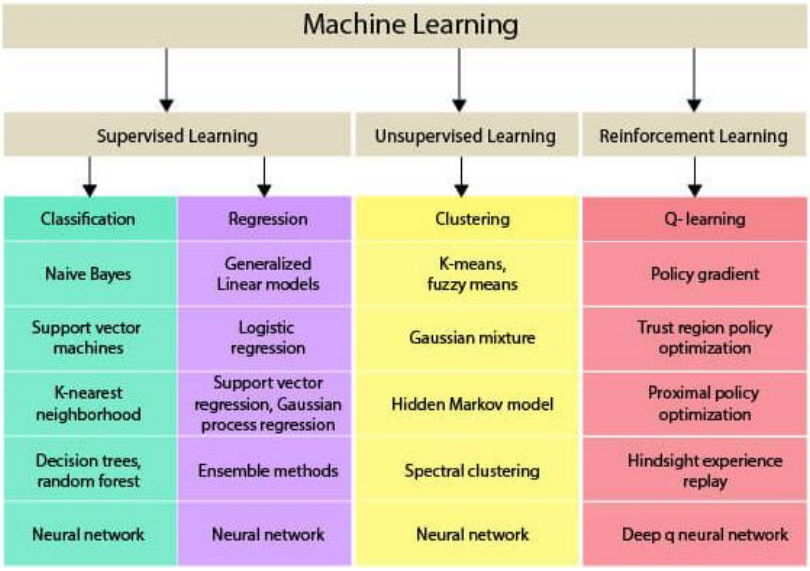

***Figure 4-2** ML categories* [135]

4.2.2 Model Training Considerations

Choosing the right algorithm from the many available in data science toolkits can be challenging, as multiple algorithms can solve the same problem by learning the relationship between input features

and the output variable. The performance of an algorithm can vary significantly with changes in model parameters. The model training process involves tuning hyperparameters, such as:

- Number of iterations for model training
- Fraction of training data (batch size) used in each iteration
- Learning rate (fraction of estimation error propagated to change model parameters)

The process of adjusting these hyperparameters to find the optimal model parameters is known as hyperparameter optimization. Additionally, selecting the optimal number and type of input features through feature engineering and feature selection is crucial for improving model accuracy.

While this section provides a basic overview and sample code for selected machine learning algorithms, a comprehensive understanding of each algorithm requires in-depth study. We encourage further exploration of each algorithm, its model parameters, and hyperparameters before application. Detailed parameter lists can be found in the official documentation of each machine learning library.

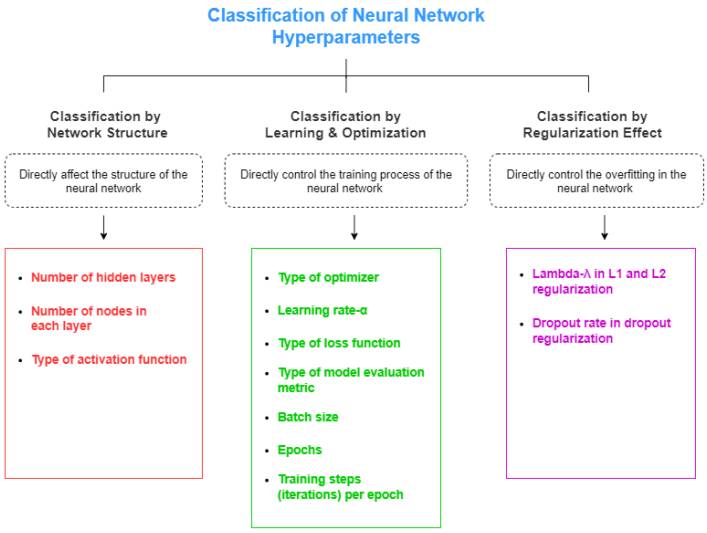

Figure 4-3 *ANN hyperparameters*[135]

Each machine learning algorithm has three primary components:

- ***Representation:*** Functions are represented numerically, symbolically, instance-based, or as probabilistic graph models.
- ***Optimization:*** Methods like gradient descent, dynamic programming, or evolutionary computation are used to improve algorithm performance.
- ***Evaluation:*** Models are evaluated using statistical metrics such as precision and recall for classification and RMSE, MSE or R2 for regression tasks.

4.2.3 Machine Learning Libraries

There are several prominent open-source machine learning libraries available in Python:

- **Scikit-learn**: Developed on top of NumPy, SciPy, and Matplotlib, Scikit-learn is widely used for implementing both supervised and unsupervised learning algorithms. It originated in 2007 as part of the Google Summer of Code project and offers a comprehensive Python interface.
- **TensorFlow**: Created by Google, TensorFlow is a highly popular library for numerical computations, particularly in machine learning. It supports a variety of machine learning tasks, including shallow and deep neural networks, using dataflow graphs with tensors (multidimensional arrays). TensorFlow is designed for parallel execution across multiple CPUs and GPUs and provides interfaces for Python, C++, and Java. This book focuses on TensorFlow 2.x release.
- **Keras**: Known for its user-friendly and modular design, Keras is an open-source high-level neural network library. It simplifies the development of neural network models but relies on a backend engine, primarily TensorFlow, for low-level computations.

Other notable libraries include Theano, PyTorch, OpenCV, and Apache Spark ML. Despite the availability of these libraries, TensorFlow is preferred for its extensive community support and comprehensive feature set.

4.2.4 Data Management and Preprocessing Strategies for Enhanced Decision-Making in Drilling Engineering

Data collection and storage are pivotal in data mining, particularly in drilling engineering. To gather pertinent and varied data, sensors and instruments on drilling rigs are utilized, capturing critical parameters like pressure and temperature. This data, derived from sensors, logs, cores, and real-time rig sensors, informs decision-making in drilling operations[136]. For effective analysis, structured database models are indispensable, ensuring data availability and efficient planning. Challenges such as data volume and structured extraction need addressing, underscoring the importance of optimized data warehouses. Maintaining data quality is imperative, requiring error handling, cleansing, and outlier removal, thus facilitating informed decision-making and optimization[136].

Preprocessing techniques are vital for model stability and accuracy. Rescaling input features and output variables, through methods like normalization and standardization, ensure consistent ranges. This is crucial for mitigating computational instability, especially in scenarios with varied feature range[136]s. Dataset splitting into training, validation, and test sets is pivotal to mitigate overfitting. The training data enables model parameter learning, while validation data aids in performance evaluation. [136]

Feature engineering in drilling data is paramount for model performance enhancement. Selecting pertinent features like depth and pressure, informed by domain expertise, is crucial. Feature transformation, such as normalization, ensures uniform scales for improved model performance. Creating new features through mathematical transformations or aggregations captures complex data relationships. Handling missing data, through techniques like imputation, ensures data completeness, crucial for accurate modeling[136].

In conclusion, effective data collection, storage, preprocessing, and feature engineering are pivotal for optimizing drilling operations and enhancing decision-making processes in drilling engineering. These practices, by ensuring data quality and model stability, facilitate informed decision-making and operational efficiency.

"Torture the data and it will confess to anything"

Ronald Coase .. British author and Economist

4.3 Fundamentals of Neural Networks

4.3.1 Overview and Concepts

A neural network is a type of machine learning model designed to emulate the decision-making process of the human brain. It operates by simulating how biological neurons collaborate to process information, identify patterns, evaluate options, and draw conclusions. The unique feature of neural networks lies in their structured approach to information processing. They excel in interpreting complex or ambiguous data, uncovering intricate patterns, and identifying trends that may evade human or traditional computational methods. Once trained, a neural network becomes proficient, akin to an "expert," in analyzing specific categories of information. It can effectively predict outcomes and address hypothetical scenarios based on its learned knowledge. This capability allows neural networks to offer insights and solutions to new problems that fall within the scope of their training.

"Neural networks are a bit like black boxes, and we don't fully understand what's going on inside them. But we know they work, and they work incredibly well." **Geoffrey Hinton**, a pioneer in deep learning,

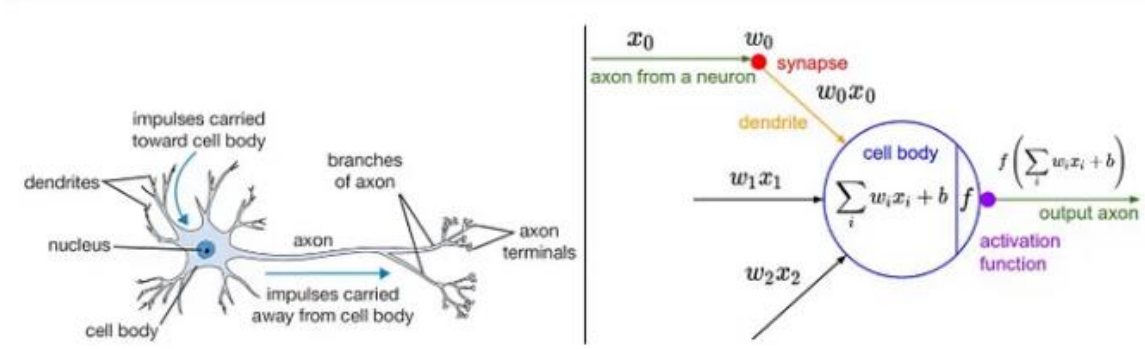

Figure 4-4 *Biological inspiration of ANNs*[137]

4.3.2 Basic structure and components of a neural network

Neural networks are structured with layers of nodes, or artificial neurons, including an input layer, hidden layers, and an output layer. Each neuron connects with others, possessing its own weights and threshold. If a neuron's output surpasses its threshold, it activates, transmitting data to the subsequent layer; otherwise, no data is forwarded.

These networks learn and refine their accuracy through training data, becoming potent tools in computer science and artificial intelligence. Once optimized, they swiftly classify and cluster data, dramatically speeding up tasks like speech or image recognition compared to manual human efforts. Google's search algorithm stands as one of the most famous neural network applications.

Often referred to as artificial neural networks (ANNs) or simulated neural networks (SNNs), they are a subset of machine learning and form the foundation of deep learning models.

- Neuron Processing in a Neural Network

In an artificial neural network, each neuron performs a series of operations on the input data it receives. Here is a step-by-step explanation of how a neuron processes data:

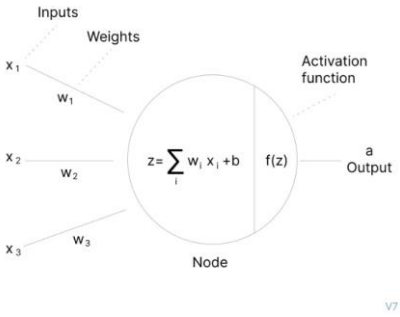

Figure 4-5 *Neuron processing criteria in a network*[137]

- ***Weighted Sum Calculation:*** Each neuron receives input data from the previous layer. These inputs are multiplied by corresponding weights, which represent the strength of the connections.
- ***Bias Addition:*** A bias term is added to the weighted sum. The bias allows the activation function to be shifted to the left or right, which can help the network learn more effectively.
- ***Activation Function:*** The resulting value is then passed through an activation function, which introduces non-linearity into the model. Common activation functions include the sigmoid, tanh, and ReLU (Rectified Linear Unit).

A single neuron by itself is relatively useless, but, when combined with hundreds or thousands (or many more) of other neurons, the interconnectivity produces relationships and results that frequently outperform any other machine learning methods.

To enhance the understanding of the process, see fig which incorporate the calculation mechanisms for various architectures, ranging from single-input single-output to multiple-input multiple-output.

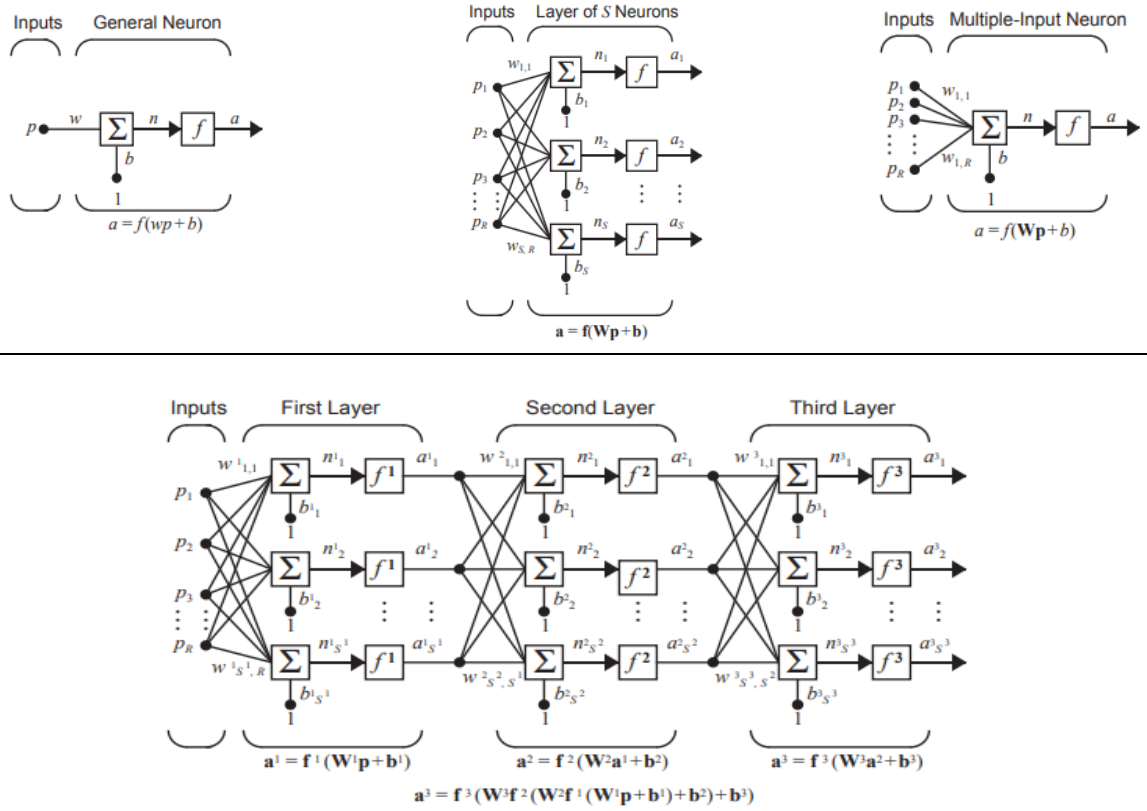

Figure 4-6 *Neural Network Calculation Process for multiple architectures* [138]

4.4 Fundamentals of Metaheuristic Optimization

4.4.1 Definition and explanation

optimization problems that are difficult to tackle using traditional methods. Unlike exact algorithms that guarantee finding the optimal solution, metaheuristics aim to find good enough solutions within a reasonable time frame by exploring the search space more flexibly. These algorithms are inspired by natural processes or social behaviors, such as genetic evolution, the foraging behavior of animals, and the collective intelligence of swarms.

Metaheuristics operate through iterative improvement, often incorporating mechanisms like randomness and local search to escape local optima and explore the global search space effectively. Common examples include Genetic Algorithms (GAs), Simulated Annealing (SA), Particle Swarm Optimization (PSO), and Ant Colony Optimization (ACO). These methods are characterized by their robustness and adaptability, making them suitable for a wide range of real-world problems, including those with complex landscapes, multiple objectives, and large-scale data. By balancing exploration and exploitation, metaheuristic optimizations provide powerful tools for achieving near-optimal solutions in challenging and dynamic environments.

4.4.2 Overview of Genetic Algorithms (GA)

4.4.2.1 Basic Principles

Genetic Algorithms (GAs) are optimization algorithms that draw inspiration from natural selection and genetics. They operate by evolving a population of candidate solutions through successive generations to solve both constrained and unconstrained optimization problems. GAs excel in tackling complex problems that conventional optimization methods find challenging.

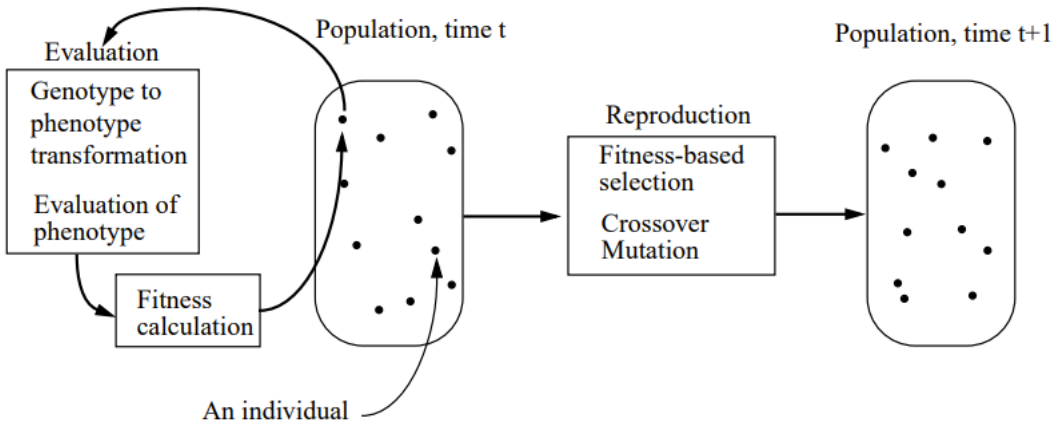

Figure 4-7 *Eas' principal* [139]

4.4.2.2 ***Key Components and Operators of Genetic Algorithms***

- Population Initialization

The process begins with a randomly generated population of candidate solutions, called chromosomes or individuals. Each chromosome represents a potential solution to the optimization problem and is typically encoded as a string of binary digits (bits), real numbers, or other representations suitable for the problem.

- Fitness Function

The fitness function evaluates each chromosome to determine how well it solves the problem. The fitness value guides the selection process, with higher fitness values indicating better solutions.

- Selection

The selection operator chooses individuals from the current population to create offspring for the next generation. The goal is to select fitter individuals more frequently to pass their genes to the next generation. Common selection methods include:

  - Roulette Wheel Selection: Individuals are selected with a probability proportional to their fitness.
  - Tournament Selection: A subset of individuals is chosen randomly, and the fittest among them is selected.
  - Rank Selection: Individuals are ranked based on fitness, and selection probability is based on this ranking.

- Crossover (Recombination)

The crossover operator combines the genetic information of two parent chromosomes to produce offspring. This operator mimics biological reproduction and promotes the exploration of new solutions. Common crossover techniques include:

  - Single-point Crossover: A single crossover point is chosen, and the segments of parent chromosomes beyond this point are swapped.
  - Two-point Crossover: Two crossover points are chosen, and the segments between these points are swapped.
  - Uniform Crossover: Each gene from the parents is independently chosen for the offspring with equal probability.

- Mutation

The mutation operator introduces random changes to individual genes in a chromosome to maintain genetic diversity and prevent premature convergence to local optima. Mutation ensures that the search space is thoroughly explored. Common mutation methods include:

- Bit Flip Mutation: A single bit in a binary chromosome is flipped (0 becomes 1, and vice versa).
- Gaussian Mutation: A small random value is added to a gene in a real-valued chromosome.
- Swap Mutation: Two genes in the chromosome are swapped.

4.5 Inverse Mapping

4.5.1 Definition and application

Inverse mapping, also known as inversion, refers to the process of determining input patterns that produce specific activations in the output nodes of a trained artificial neural network (ANN). The objective of this process is to identify one or more input patterns that result in a desired output, providing insight into the network's learned representations and decision-making processes[140].

One notable application of inverse mapping was demonstrated by King (1990)[141], who used it to understand an ANN trained on handwritten digit recognition. By inverting the network, he was able to visualize the typical representation of each digit according to the network. The success of this approach largely depends on the quality of the training data and the network's ability to generalize beyond the training examples.

4.5.2 Existing methods to Invert an ANN Mapping

- Gradient Descente techniques

Gradient descent is a widely used optimization technique that adjusts the parameters of a model iteratively to minimize a loss function. When applied to inversion of an ANN, the goal is to adjust the input variables (features) to match a desired output. In other words, instead of adjusting weights and biases (as done during training), gradient descent adjusts input values to achieve a specific output activation or pattern[139].

- Prototype extraction technique

Prototype extraction involves creating a new ANN that attempts to approximate the inverted mapping of the original ANN. Instead of directly adjusting inputs like in gradient descent, this method builds a separate network (referred to as the inverted or prototype network) trained to produce the inverse of the original network's outputs for given inputs[139].

4.5.3 Limitations and challenges

Both gradient descent and prototype extraction methods for inverting an Artificial Neural Network (ANN) mapping face the challenge of potentially getting stuck in local optima during their optimization processes[139]. Gradient descent, despite its effectiveness in adjusting input variables towards a desired output, relies heavily on the initial guess and the nature of the optimization landscape. If the input space is highly non-linear or contains multiple local minima, gradient descent may converge to a suboptimal solution instead of the global optimum. Similarly, prototype extraction, which involves training a separate network to approximate the inverse mapping, can also encounter local optima issues depending on the complexity of the original ANN's mapping and the representation of input-output relationships in the training dataset. Both methods require careful initialization, parameter tuning, and sometimes multiple iterations to navigate and escape local optima, ensuring that the inverted mappings accurately reflect the desired outputs across diverse input scenarios.

Evolutionary Algorithms (EAs), unlike methods such as gradient descent and prototype extraction, generally have less potential to get stuck in local optima. This advantage stems from their population-based approach, where multiple candidate solutions (individuals) evolve concurrently over successive generations. EAs maintain diversity within the population through mechanisms like mutation and crossover, allowing them to explore a broader search space effectively.

4.6 Inverse mapping with Eas

4.6.1 Core advantage Concepts

the population-based nature of EAs enables them to explore multiple regions of the solution space simultaneously, making them less prone to getting trapped in local optima compared to methods that rely on single-point searches or specific training objectives[140]. This characteristic makes EAs particularly well-suited for complex optimization problems where the landscape may contain numerous local optima, ensuring robust and effective exploration towards finding high-quality solutions.

4.6.2 Sharing, a method to introduce niches into the population

Despite the discussed above, the challenge of local optima persists in evolutionary algorithms (EAs), where populations often converge towards a single, potentially local, optimum. However, in scenarios where multiple equivalent solutions exist, there is a need to explore and discover more than just one optimal solution. This necessitates methods to diversify the population across the search space, enhancing the chances of uncovering diverse solutions. One effective strategy is niching, which involves partitioning the population into distinct niches. This approach encourages the EA to explore broader regions of the search space by fostering competition among individuals within each niche.

Niching can be implemented using techniques like sharing introduced by Goldberg (1986)[142], where similar individuals share resources, mimicking natural ecosystems where organisms compete for limited resources. This strategy ensures that densely populated niches are constrained in size, thereby reducing competition among similar individuals. By penalizing individuals that are too close to each other in genotypic space, sharing promotes the exploration of new and potentially more promising areas of the search space. As a result, niching with sharing in EAs enhances the algorithm's ability to discover multiple diverse solutions to complex optimization problems.

Conclusion

In conclusion, this chapter has explored the application of AI and machine learning techniques, including artificial neural networks (ANNs) and metaheuristic optimization methods, in drilling engineering. Looking ahead, integrating these technologies holds significant potential for advancing efficiency and safety in drilling operations. Continued research and innovation in AI-driven approaches are crucial for addressing challenges and unlocking new opportunities in the oil and gas industry.

Results and Discussion

CHAPTER *V*

Chapter 5. Results and Discution

Introduction

In this chapter, in order to achieve the objectives of our work, four stages are adopted. Firstly, we gather and monitor data, setting the foundation for further analysis. Next, we build predictive artificial neural network (ANN) models. These models predict both filtrate invasion volume and rheological behavior. Then, we use advanced techniques to reverse the filtrate invasion model combining it with the rheological ANN model. Finally, by merging these models, we achieve a balanced approach, revealing the best drilling mud compositions for desired filtrate properties and rheological characteristics. This systematic approach highlights both the precision of scientific study and the advancement in drilling fluid optimization.

5.1 Data Collection and Monitoring

In the initial phase of data collection, a robust repository of 5000 data points was meticulously assembled, each serving as a vital conduit into the intricate dynamics of nano-based drilling fluid behavior. The 5000 data points were judiciously curated from an extensive survey of relevant literature, thereby enriching our dataset with a diverse array of perspectives and empirical observations ***Gasser et al. (2022)***[28]

5.1.1 Data interpretation and visualization

Within this expansive dataset, seven distinct types of nanoparticles (NPs) emerged as pivotal elements, each characterized by unique combinations of size and concentration. These nanoparticles, ranging from 15 to 50 nanometers in size and concentrations from 0 to 7 weight percent, were meticulously selected to ensure the model's universality and applicability across diverse operational scenarios. This comprehensive range of nanoparticle attributes enables our model to transcend the confines of specificity, embracing the multifaceted nature of drilling fluid optimization with exceptional fidelity.

In addition to nanoparticle size and concentration, the dataset incorporates a variety of chemical compositions with different additives, further enhancing the model's robustness. Filtration properties under varying conditions of temperature and pressure were carefully considered, alongside measurements of density and solid content. Furthermore, the rheological properties of the nano-drilling mud, including yield point, plastic viscosity, apparent viscosity and gel strength were thoroughly examined. This holistic approach ensures that the model not only accurately reflects real-world conditions but also provides reliable guidance for optimizing drilling fluid performance across a wide array of operational parameters.

	***Table 5-1** Data description*	**Units**
DF Types	B-WBM| LSNDM| SP-WBM	/
N-PS	Types: (Al2O3| CuO| Fe2O3| MgO| SiO2| TiO2| ZnO)| Size| MW	***(wt***%) | nm | g/mol
Chemical composition	Bentonite| Barite| caustic soda| soda ash| PAC R| Calcium-Carbonate| XC polymer| KCl| Sodium-Cloride	(wt%)
Rheological properties	AV| PV| YP| GS	Cpo | (Lb/100ft2)
Filtration properties	Pressure| Temperature| Time| Filtrate	Psi | F° | s | ml
Others	Solid content| Density	***(***%) | PPg

5.1.2 Data Preprocessing and Enhancement

5.1.2.1 Enhancing Data Quality

we employed one hot encoding to transform categorical data, such as drilling fluid types and nanoparticle types, into numerical values. This process involves representing each category as a binary vector, wherein each category is assigned a unique numerical index. Subsequently, each index is converted into a binary vector where only one element is "hot" (represented by 1), while the rest remain "cold" (represented by 0).

Each drilling fluid type is assigned a binary vector, with a 1 indicating the presence of that particular fluid type and 0s elsewhere. Similarly, nanoparticle concentrations are encoded as binary vectors, with the concentration value indicating the np's concentration and 0s elsewhere. This transformation not only facilitates the numerical processing of categorical data but also preserves the inherent relationships between different categories, enabling more robust model training and analysis.

Moreover, prior to model development, a rigorous data filtration process was undertaken to eliminate noise and ensure the integrity and reliability of our dataset. By meticulously filtering out noisy data points, we aimed to enhance the signal-to-noise ratio, thereby bolstering the accuracy and efficacy of our subsequent analyses and model predictions.

5.1.2.2 Standardization and Scaling Techniques for Data Optimization

Table 5-2 provides a comprehensive depiction of the statistical distribution of our dataset, encompassing both input parameters and the target parameter, which is the volume of filtrate.

To ensure optimal performance and convergence during the training process, we adopted the practice of normalization, which involves scaling the input and target parameters to a standardized range. for all the models considered in this study same technique has been taken.

For the inputs parameters this normalization was executed meticulously using the Standard-Scaler function from the renowned scikit-learn library which standardizes features by removing the mean and scaling them to unit variance. In other words, it transforms the data to have a mean of 0 and a standard deviation of 1. It does this by. Employing *Eq 5-1* separately for each parameter.

Table 5-2 *statistical description of the output parameters*

Parameter	mean	std	Min	25%	50%	75%	max
Filtrate (ml)	8.473	7.671	0.1	2.5	7.5	9	90
AV (C-Po)	16.546	13.443	7	8	20	35	119
PV (C-Po)	18.667	15.877	6	10	30	44	115
YP	9.554	8.661	8	5	8	15	82
GS10S	15.444	14.453	5	6	8	20	38
GS10M	17.665	16.786	8	9	21	35	76

$$X\_normalized = \ (X - mean(X))/std(X)\ ) \quad 5\text{-}1$$

On the other hand, the target parameter was transformed using *Eq 5-2* to expedite and enhance the efficiency of the training process.

$$Y\_normalized = \ln(Y + 1) \quad 5\text{-}2$$

The output is then given as

$$\text{Output-S} = \sum_{j=1}^{N_L} W_j^{(L)} f\left(\sum_{i=1}^{N_{L-1}} W_{ji}^{(L-1)} f\left(\cdots f\left(\sum_{k=1}^{N_1} W_{ik}^{(1)} X_k + b_i^{(1)}\right) + b_i^{(2)} \cdots\right) + b_j^{(L-1)}\right) + b^{(L)} \quad 5\text{-}3$$

Descaling the output would give the desired predicted parameter and that is done by applying *Eq. 5-4* :

$$Output = exp(S - Output) - 1 \quad 5\text{-}4$$

With: ***L***: Number of layers in the neural network, ***Nl***: Number of neurons in layer l. ***X***: Input vector with M features. W_l: Weight matrix for layer (l), *F* activation function.

This standardization process not only enhances the model numerical stability but also accelerates the training process by promoting more efficient convergence.

As shown in ***figure 5.1***. Before Scaling, the data distribution unfolds as a sprawling landscape, characterized by a wide dispersion and punctuated by numerous outliers. This heterogeneity within the dataset poses formidable challenges to the ANN, as the presence of outliers may engender spurious correlations and confound the model's learning process. Moreover, the risk of overfitting looms large, wherein the ANN may excessively tailor its predictions to accommodate these outliers, thereby compromising its capacity to generalize to unseen data.

However, scaling the data brings significant improvements, as shown in the After Scaling depiction. The data becomes more compact and consistent, with fewer outliers. This consolidation creates a more uniform dataset, enhancing the ANN's ability to detect meaningful patterns amidst the noise. By reducing the impact of outliers, the scaled data improves the ANN's accuracy and reliability, leading to better predictions.

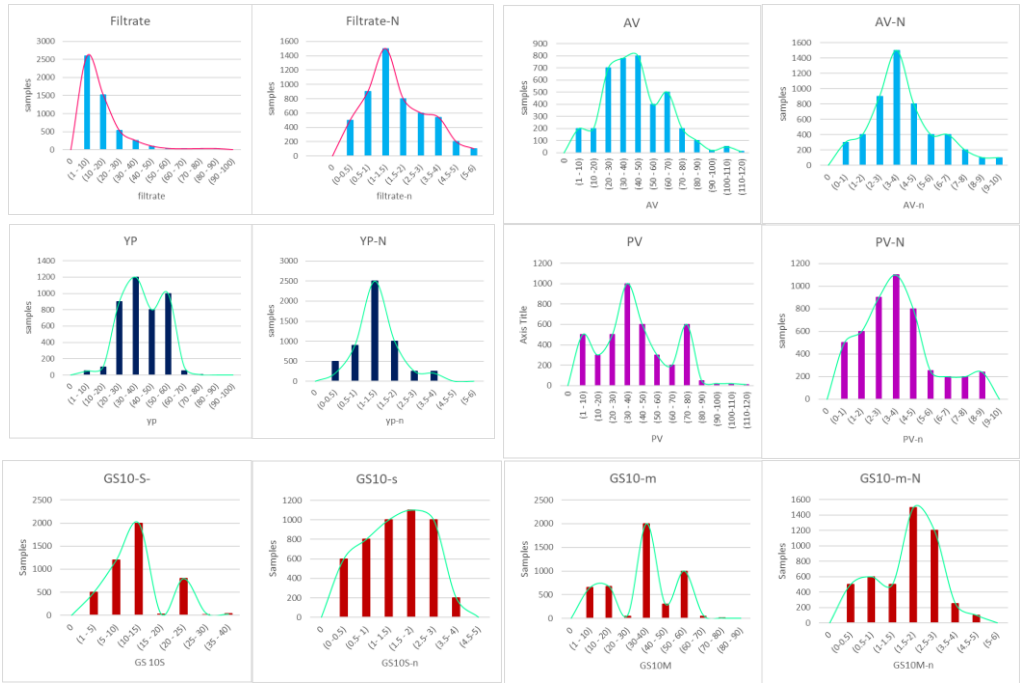

Figure 5-1 *Pre and Post scaling distribution of the output data*

5.1.2.3 ***Splitting dataset***

Furthermore, to foster robust model generalization and performance assessment, our dataset was partitioned randomly into two distinct subsets: a training dataset comprising 70% of the total data and a test or validation dataset comprising the remaining 30%. This partitioning strategy ensures that our model is trained on a diverse array of instances while retaining a separate pool of data for independent validation. Such delineation mitigates the risk of overfitting and provides a reliable benchmark for evaluating the model's performance on unseen data.

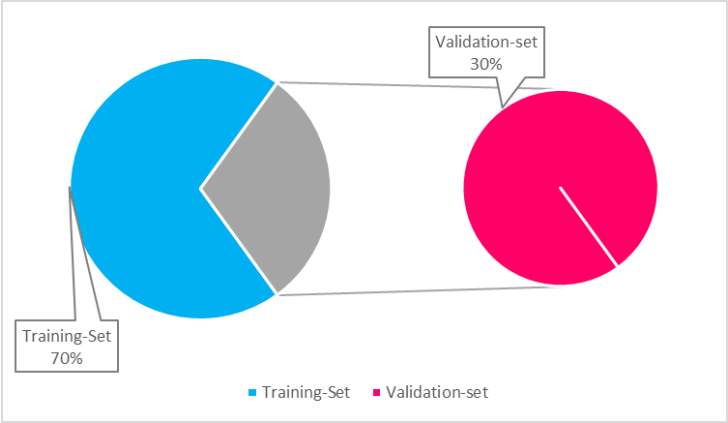

Figure 5-2 *Training and validation sets: Random Splitting*

5.1.2.4 ***Model Architecture and Hyperparameter Tuning***

A Python script was developed to optimize the hyperparameters of Artificial Neural Network (ANN) models using Keras Tuner. The script utilizes a systematic approach to find the optimal configuration from many given parameters as summarized in Table 5-3 parameters used for . By defining a model-building function within the tuner, each combination is evaluated based on its (MSE) and (R^2) performance metric, ensuring that the chosen hyperparameters optimize model accuracy and generalization. This approach not only streamlines the optimization process but also enhances the ANN's ability to achieve superior performance across different datasets and tasks.

Table 5-3 parameters used for the tuning phase

Training functions	SGD | RMS-prop | Adam | Adam-W | Ada-delta | Ada-grad | Ada-max | Ada-factor | Na-dam | FTRL | Lion | Loss Scale | Optimizer|
Transfer functions	Relu | sigmoid | soft-plus | soft-sign | tanh | Selu | Elu | exponential | Leaky_Relu | Relu-6 | Silu |
Number of hidden layers	1:5
Number of neurons in each layer	1:1000
Learning rate	10^{-1} – 10^{-4}
Batch size	16, 32, 64, 28

The flowchart in Figure 5-3 was used to build all the prediction models including the mud filtration, the apparent viscosity, the yield point and the gel strength models.

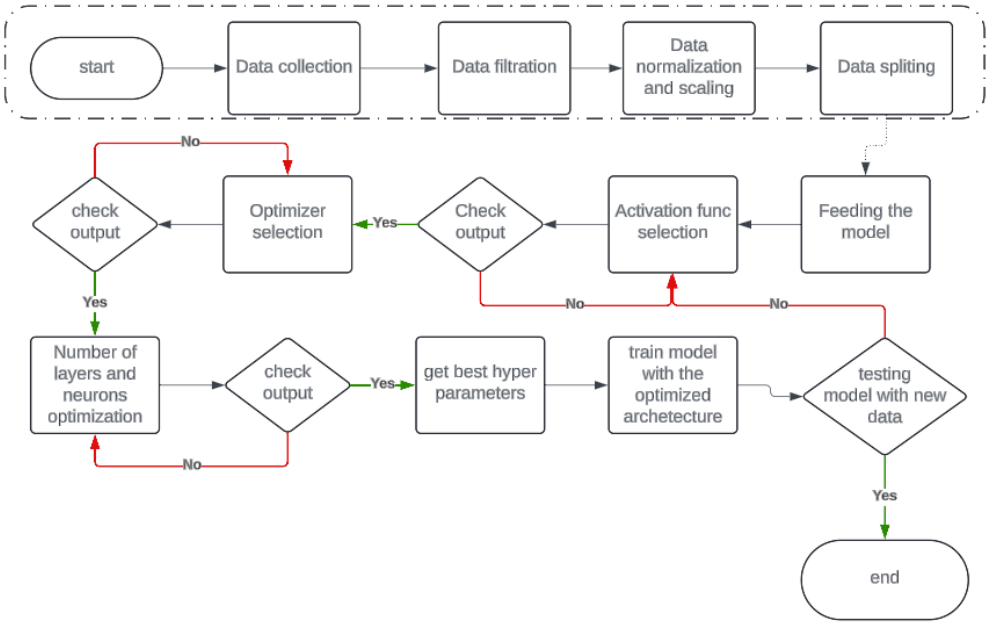

Figure 5-3 *Flow chart used to build the prediction models*

5.2 Drilling-mud Filtration model (M-FLT)

5.2.1 Training and validating

The best-hyper-parameters for the M-FLT are shown in Table 5-4 those parameters were used to train the model. The forward pass through this ANN with two hidden layers and (tanh) as an activation function is given in Eq 5-5. Figure 5-4 shows the evaluation, the tuning phase of the ANN model resulted in an optimal architecture consisting of two hidden layers, each with 75 neurons. This configuration was determined to be the most effective in minimizing the mean squared error (MSE) and maximizing the (R2) during tuning. The activation function chosen for both layers is the hyperbolic tangent (tanh) function. The use of this activation function helps in capturing complex, non-linear relationships within the data, contributing to the overall robustness and performance of the neural network.

Table 5-4 *Tuning results: best hyperparameters for M-FLT model*

Training functions	Adam
Transfer functions	Tanh
Number of hidden layers	2
Number of neurons in each layer	75
Performance goal (Mse and R2)	Mse=Min possible and R2 = Max possible (stop after 10 epochs with no improvement)
Learning rate and batch size	0.0028 / 64
Number of inputs	***27: DF type,*** *N*-PS (type, size and MW), Chemical composition, Filtration conditions (P, T and t), Solid content, Density
Number of outputs	1 (filtrate volume in ml)
Network type	F-F-B-P
Number of training simples	3500
Number of Validation simples	1500

$$\text{Filtrate-P} = \exp\left(\sum_{j=1}^{75} W_j^{(3)} \tanh\left(\sum_{i=1}^{75} W_{ji}^{(2)} \tanh\left(\sum_{k=1}^{M} W_{ik}^{(1)} X_k + b_i^{(1)}\right) + b_j^{(2)}\right) + b^{(3)}\right) - 1 \quad \text{5-5}$$

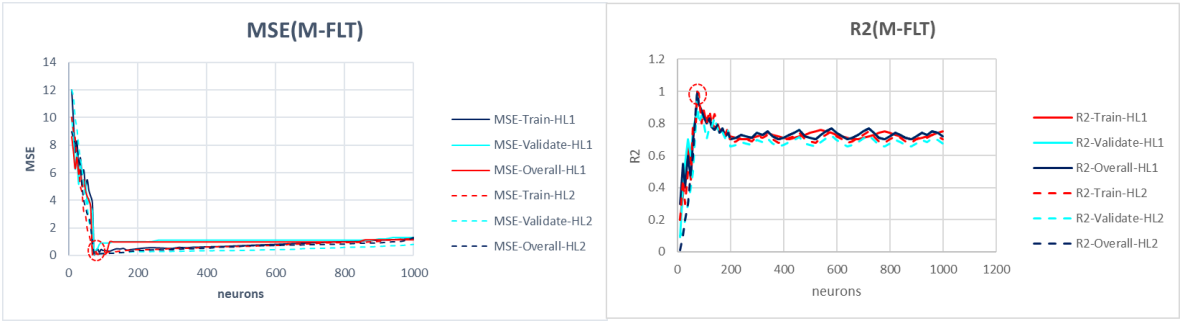

Figure 5-4 *MSE and R2: Tuning layers and number of neurons for M-FLT model*

5.2.2 Accuracy and performance evaluation

The model demonstrated an excellent accuracy across all training, testing, and overall datasets. This indicates the robustness of the ANN in capturing the complex relationships between input features and mud filtrate invasion. Through meticulous analysis, the predicted values were juxtaposed against the actual values. Figure 5-5 offers a comprehensive assessment of the ANN's efficiency across all datasets. It is evident that the model's predictions closely align with the actual observations. The M-FLT model consistently predicts filtrate volumes with good accuracy across varying dataset sizes, as evidenced by the substantial overlap of predicted (red) and actual values (blue). Few discrepancies can be observed but the model can handle large datasets very well. This visual validation underscores the reliability of the ANN in making accurate predictions.

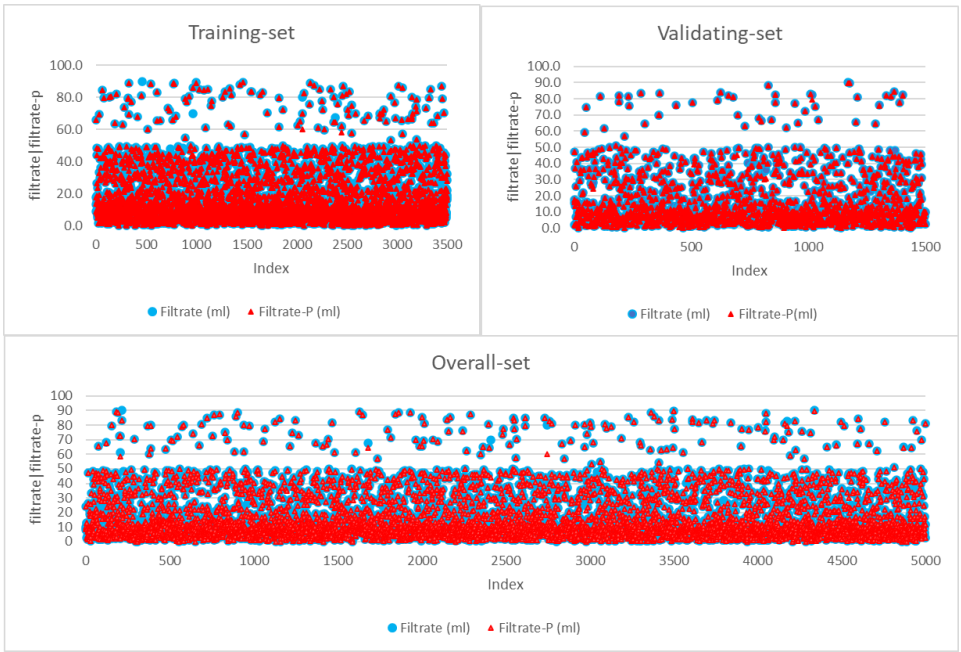

Figure 5-5 *M-FLT Model Predictions vs. Actual Filtrate Volumes: Training, Testing, and Overall Results*

Figure 5-6 illustrates the scatter plot of the ANN predicted results, where it is shown that the data points ideally converge near the line of the unit slope (red), denoting a perfect alignment between the ANN predictions and the actual targets. Also, the dashed blue regression line closely aligns with the red line, indicating a strong correlation and suggesting that the M-FLT model predicts filtrate volumes with high accuracy. The clustering of points around the regression line further confirms the model's robust predictive performance. This alignment underscores the model's proficiency in extrapolating from training data to accurately predict filtration volume across diverse scenarios.

Moreover, we assessed the relative deviation (RD) of the predicted data from the actual data, plotting it against the actual data values, as depicted in Figure 5-7 **(right)**. RD serves for gauging the disparity between predicted and actual data, offering valuable insights into their proximity. Notably, the maximum RD values was 12, while the minimum RD value was -8 for the overall data leading to an average RD of 1.5. Additionally, Figure 5-7 (**left)** illustrates the ratio between predicted and actual values. The max ratio was calculated to be 1.159 and the minimum to be 0.795, culminating in an overall average ratio of 1.002 across the overall dataset. These figures further prove the reliability of the M-FLT model.

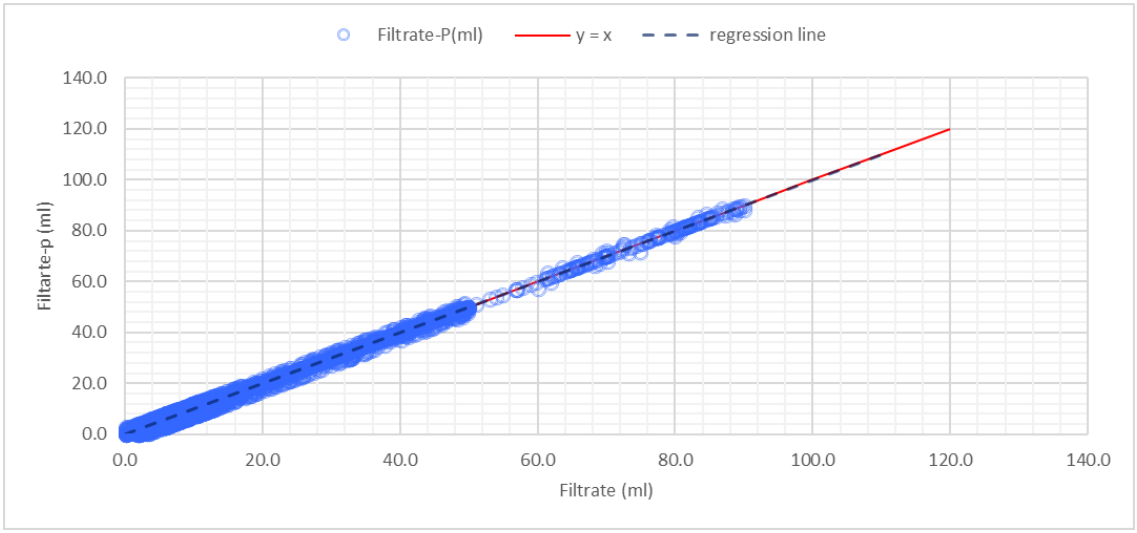

Figure 5-6 *Regression Analysis of the M-FLT Model Predictions vs. Actual Filtrate Volumes overall-set*

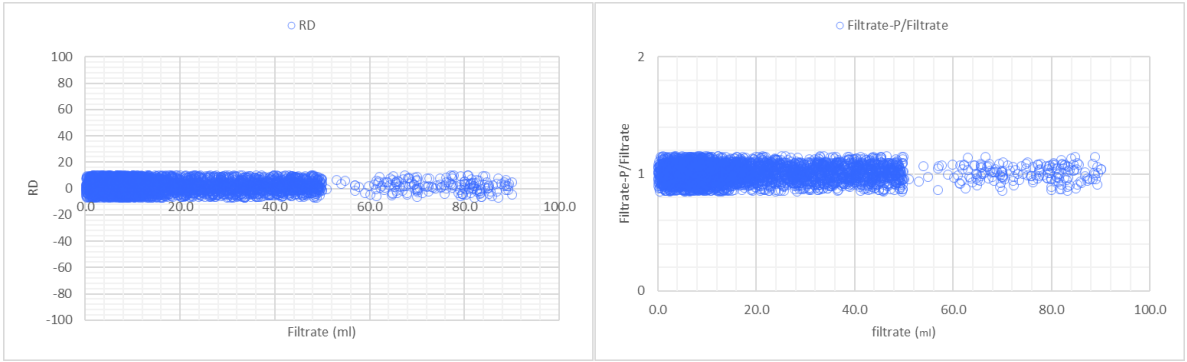

Figure 5-7 *Assessed relative deviation RD (right) and ratio between predicted and actual values (left)*

5.2.3 Evaluation metrics analysis

The M-FLT model's performance is evaluated using different metrics such as R2, MSE, RMSE, MAPE, and MAE as summarized in ***Figure 5-8***. The R^2 value of 0.996 suggests that 99.6% of the variance in actual filtrate volumes is explained by the model's predictions, demonstrating a strong correlation. The mean squared error (MSE) is very low, with a value of 0.095, indicating minimal average squared differences between predicted and actual values. The root mean squared error (RMSE) of 0.308 reflects the model's high precision. Additionally, the mean absolute percentage error (MAPE) of 0.015 highlights the model's accuracy in terms of relative error (1.5%). The mean absolute error (MAE) of 0.121 further indicates good accuracy in absolute terms. Overall, these metrics collectively show that the M-FLT model provides highly accurate and precise predictions of filtrate volumes, with minor areas for potential improvement.

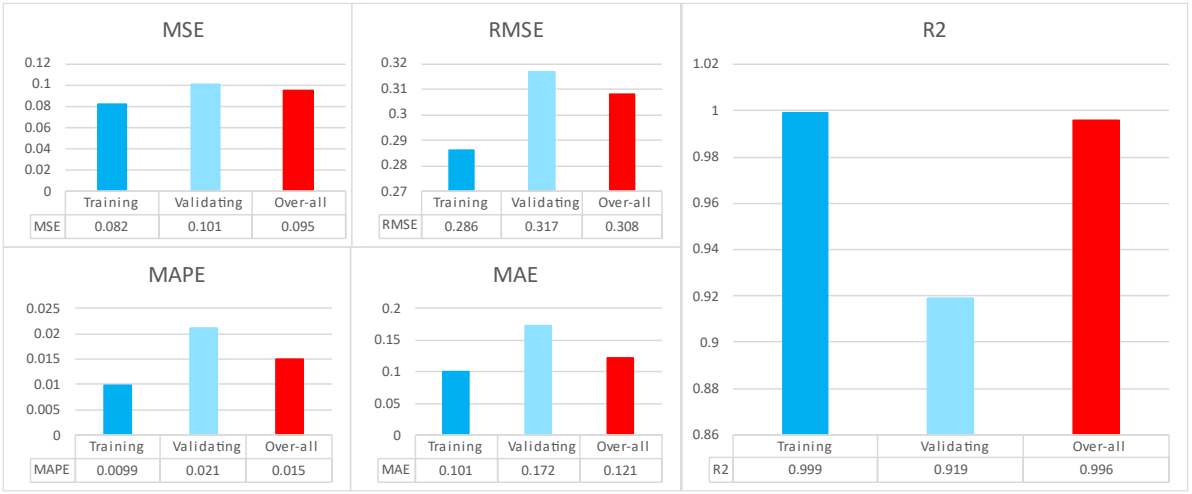

Figure 5-8 *Metrics assessment for the M-FLT model*

5.2.4 Cross-Validation and Comparative Analysis

5.2.4.1 Model validation

The bar chart in Figure 5-9 compares the performance of the M-FLT model with ***Aleksander Lekomtsev et al.(2022) PSO-LSSVM and ELM*** [27], ***Alireza Golsefatan & Shahbazi (2019)*** [26], and ***Gasser et al. (2022)*** [143] models in predicting filtrate volumes. Our M-FLT model exhibits a strong correlation with actual values, with an R^2 of 0.996, and outperforms other models with the lowest MAPE of 0.015, indicating superior accuracy. Its RMSE of 0.308 signifies high precision, while the MSE of 0.095 reflects minimal average squared differences between predicted and actual values compared to other models. Overall, the M-FLT model demonstrates competitive performance across all metrics, particularly excelling in accuracy, showcasing its effectiveness in filtrate volume prediction.

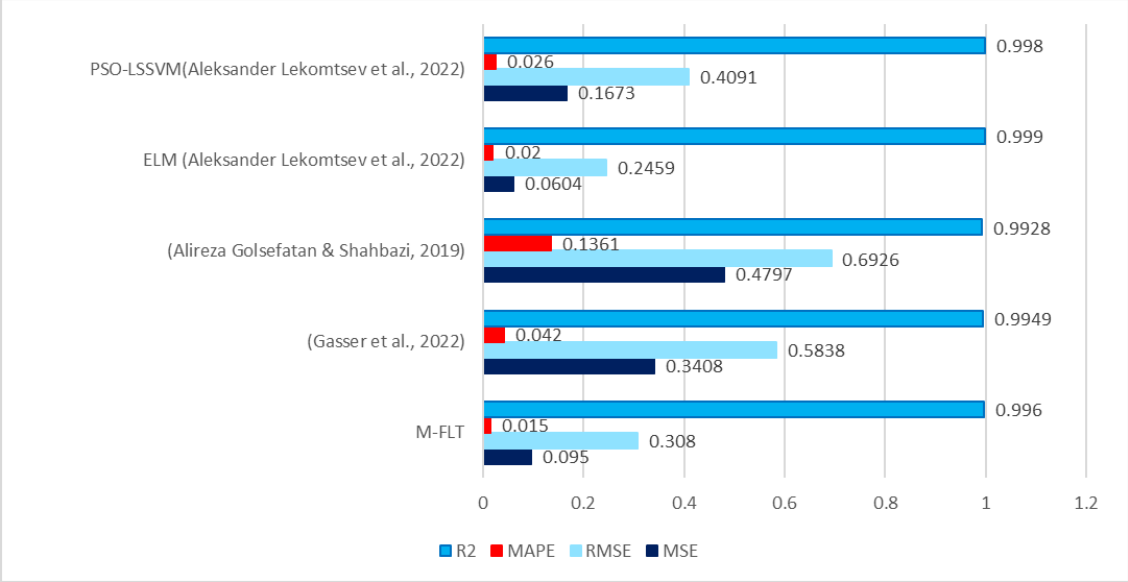

Figure 5-9 *Comparison of the developed Model (M-FLT) with Other Models in literature for Filtrate Volume Prediction*

.In addition, the data from (Alireza Golsefatan & Shahbazi, 2019) [26] used by (Aleksander Lekomtsev et al., 2022) [27] is utilized as a testing data-set for the previously developed model. This data set contains 1003 datapoints of a SP based mud. The results are shown below in Figure 5-10. The M-FLT model outperforms all other models as the metrics values indicate.

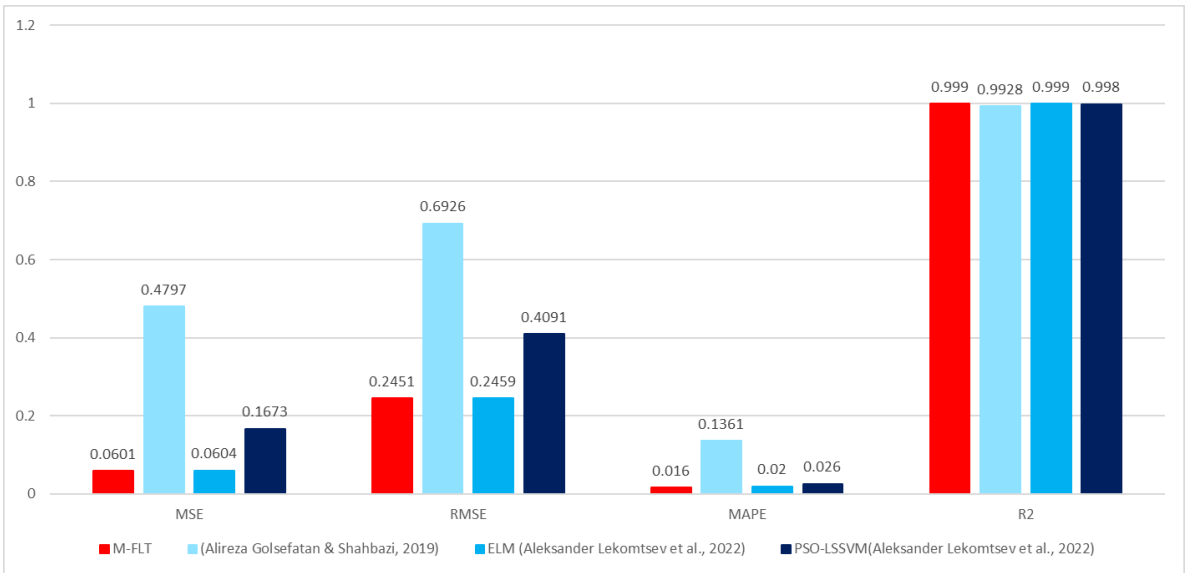

Figure 5-10 *Evaluation and comparison of the M-FLT model across various metrics using (Alireza Golsefatan & Shahbazi, 2019) data.*

5.2.4.2 *Consistency between Experimental and Modeled Temperature and concentrations: Alignment of Modeled and Experimental Temperature Impact on Nano Particle Mud Filtration Volume*

Likewise, experimental data from ***(Amirhossein Parizad et al., 2018)*** [144] was fed into our model for both a KCl-base mud and an SiO2-KCl-base mud , simulating the temperature-induced changes in mud filtration volume and concentration dynamics. By utilizing the input parameters from the experimental study, we aimed to replicate the experimental conditions and observe how well our model could predict the filtration volumes.

Model results in alignment with experimental results are shown in Figure 5-11. The consistency between the modeled and experimental results highlights the robustness and accuracy of our predictive model in capturing the temperature-induced variations in mud filtration volume and concentration dynamics. This close agreement underscores the model's reliability and its potential for real-world applications in predicting mud behavior under varying temperature and composition conditions.

Table 5-5 *different temperature values used for the experiments (**in fig.5-11 low center**) **[144]***

Temp 1	Temp 2	Temp 3	Temp 4
107 F	109.4F	149 F	199.4 F

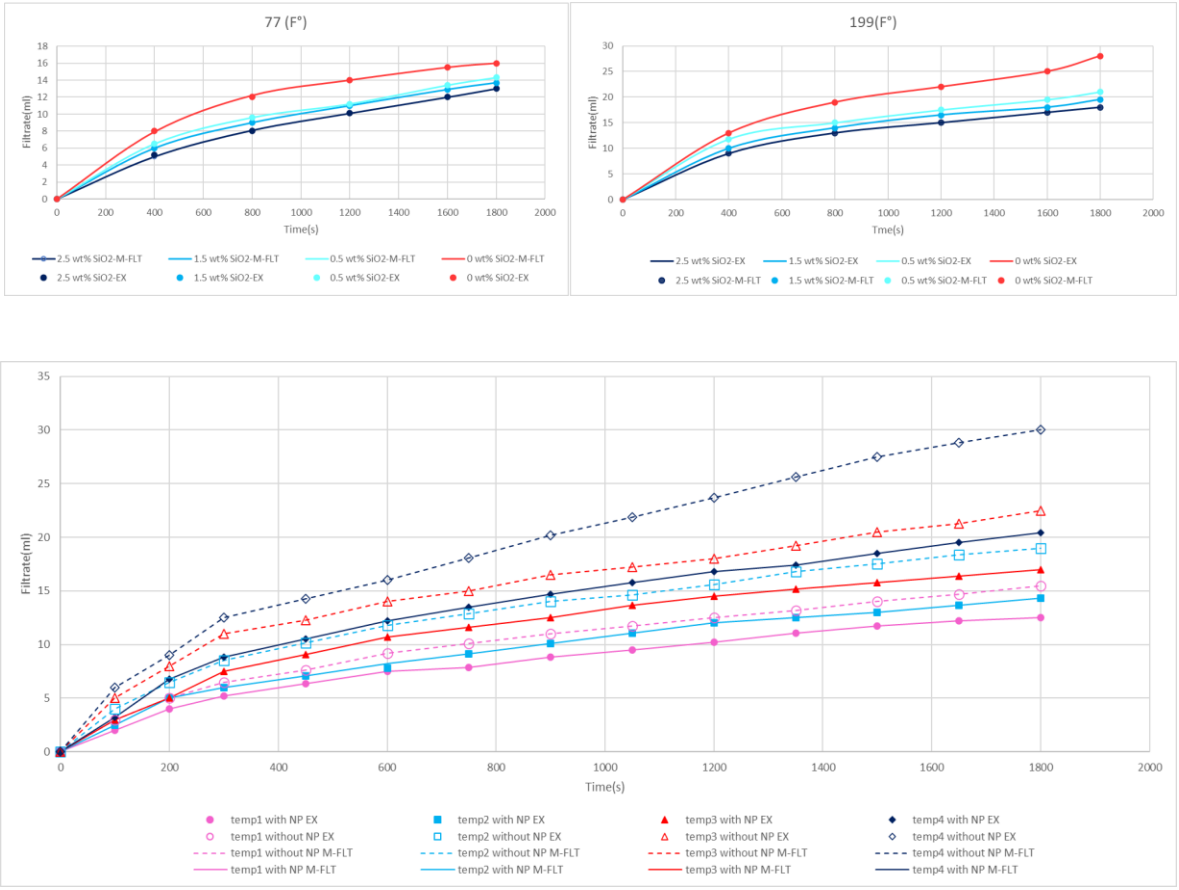

Figure 5-11 *Alignment of the M-FLT model results with the experimental results across different temperatures taken from **(Amirhossein Parizad et al., 2018)***

5.2.5 Sensitivity analysis

5.2.5.1 Comparative Analysis of Temperature Effects on Filtration Dynamics: Free Mud vs. Nanoparticle-Based Mud Variants

In this section, we delve into the impact of temperature on filtration dynamics, comparing the responses of free mud (B-WBM) and various nanoparticle-based mud all 7 variants (0.5w%). By systematically varying the temperature from 10°F to 500°F, we aim to elucidate how different nanoparticle compositions influence filtration volume and temperature dynamics in comparison to free mud.

In order to accomplish this task, an algorithm, specifically engineered to meticulously adjust all inputs to desired values taken from one datapoint of the dataset while systematically varying the temperature within a defined range of 10 to 500 degrees, was used. The rationale behind this meticulous approach was to ensure comprehensive coverage of potential scenarios and outcomes within the model.

The results are illustrated in Figure 5-12. The comparative analysis revealed distinct responses of nanoparticle-based mud variants and free mud to temperature variations. Remarkably, we observed that the filtration volumes for nanoparticle-based mud variants exhibited unique trends compared to free mud that shows the highest filtration volume. Some nanoparticles demonstrated enhanced filtration volume retention at higher temperatures, while others displayed different patterns. This suggests that the composition of nanoparticles significantly influences mud behavior under varying temperature conditions. The results can be summarized in the following points:

- SiO2, Al2O3, and TiO2 show the lowest increase in filtration volume with increasing temperature, indicating a positive correlation between temperature and filtration reducing efficiency.
- CuO, Fe2O3, MgO, and ZnO initially follow a similar trend as the temperature increases, but beyond a certain point, their filtration volumes plateau to closely even match the free mud, resembling the behavior of the free mud, after certain temperature those np's re-get their affects but not as good as first.
- Free mud exhibits a gradual increase in filtration volume with temperature, albeit the highest filtration volume.

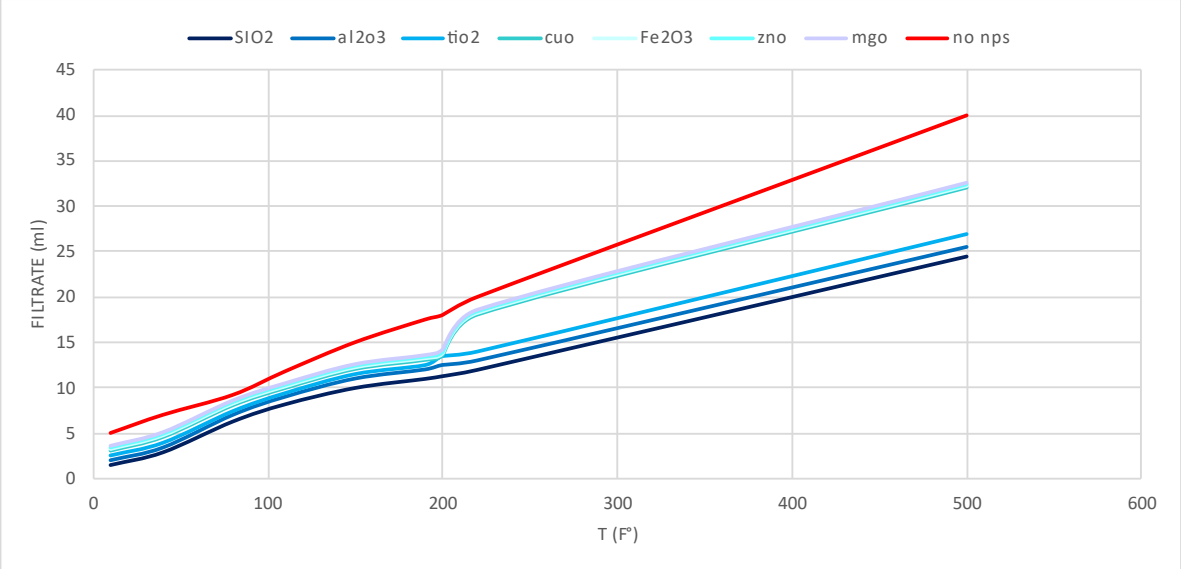

Figure 5-12 *sensitivity analysis: behavior of filtrate volume across various T and NPS types modeled results*

NB:

Several literature articles have demonstrated the significance of temperature on nanoparticles in drilling mud, particularly focusing on SiO2 and Al2O3 and their efficacy in enhancing performance at elevated temperatures (as explained in ***Chap.3***). However, there's a scarcity of studies encompassing other nanoparticle types. The results of the model presented above Figure 5-12 offer a broad perspective on nanoparticle behavior across different temperatures, highlighting the superior performance of certain nanoparticles. While the model yields promising results as already seen in sections above, further experimental validation still be necessary to confirm this superiority**.**

5.2.5.2 The Impact of Nanoparticle Concentration on Filtration Dynamics in Nanoparticle-Based Mud Variants

In this section, the same previous script was used, however, we systematically varied the concentration of nanoparticles (0 to 7 w%) while keeping all other input parameters fixed at a 100(F°). This approach allowed us to isolate the effects of nanoparticle concentration on filtration dynamics without confounding factors. All the various nanoparticles exhibit similar behavior (all the lines are on top of each other). As well as, we notice that higher concentrations of NPs results in reduced filtrate volumes (Figure 5-13).

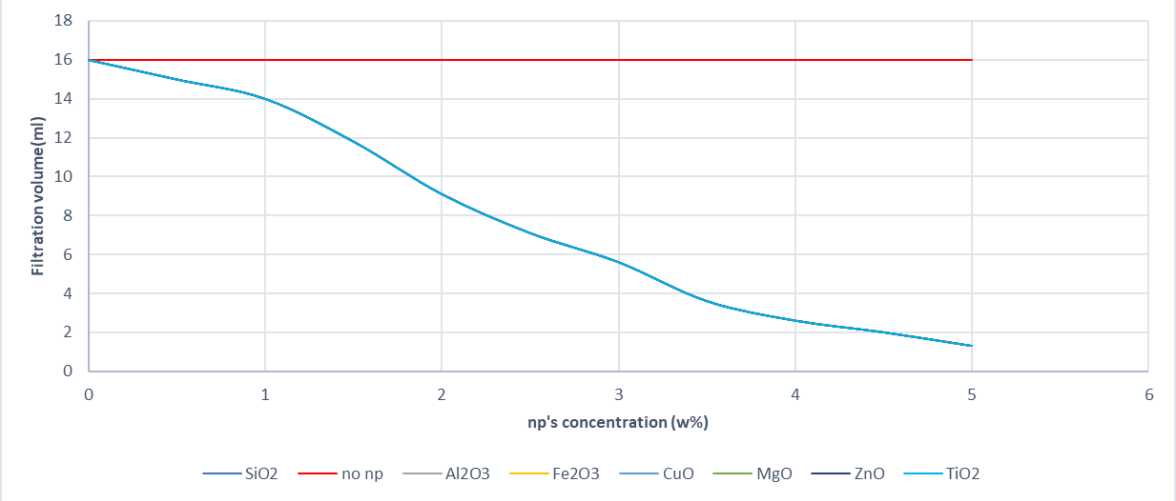

Figure 5-13 *Effect of concentration of nanoparticles on mud filtration M-FLT results*

NB:

Keeping the solid percentage constant while varying the concentration might not accurately reflect real-world conditions, as typically, changing the concentration would affect the solid percentage. However, conducting the sensitivity analysis in this manner can still provide valuable insights into the behavior of the system under controlled variables. It simplifies the analysis and allows for a focused examination of the effect of concentration changes independently, even if it doesn't perfectly mimic practical scenarios. For more comprehensive results, additional analyses considering variable solid percentages would be beneficial.

5.3 Rheological del (M-RH)

5.3.1 Apparent viscosity model (M-AV)

5.3.1.1 Training and validating

The best-hyper-parameters for the M-AV are shown in. These parameters were used to train

the model through this ANN with one hidden layer and soft-sign activation function as expressed in 5-6. Figure 5-7 shows the tuning phase of the ANN model resulted in an optimal architecture consisting of one hidden layer with 57 neurons. This configuration was determined to be the most effective in minimizing the mean squared error (MSE) and maximizing the (R2) during tuning. The use of softsign activation function helps in capturing complex, non-linear relationships within the data, contributing to the overall robustness and performance of the neural network.

Table 5-6 Tuning best hyperparameters M-AV model

Training functions	SGD
Transfer functions	Softsign
Number of hidden layers	1
Number of neurons in each layer	57
Performance goal	***Mse=Min possible and R2 = Max possible (stop after 10 epochs with no improvement)***
Learning rate and batch size	***0.0014 / 64***
Number of inputs	24 (NPs (Types size and MW) DF types| Chemical composition| Density and Solid content)
Number of outputs	***1 (Apparent Viscosity CPo)***
Network type	***F-F-B-P***
Number of training simples	3500
Number of testing simples	1500

$$\text{AV-P} = \exp\left(\sum_{i=1}^{57} W_i^{(2)}\ \text{Softsign}\left(\sum_{k=1}^{M} W_{ik}^{(1)} X_k + b_i^{(1)}\right) + b^{(2)}\right) - 1 \qquad 5\text{-}6$$

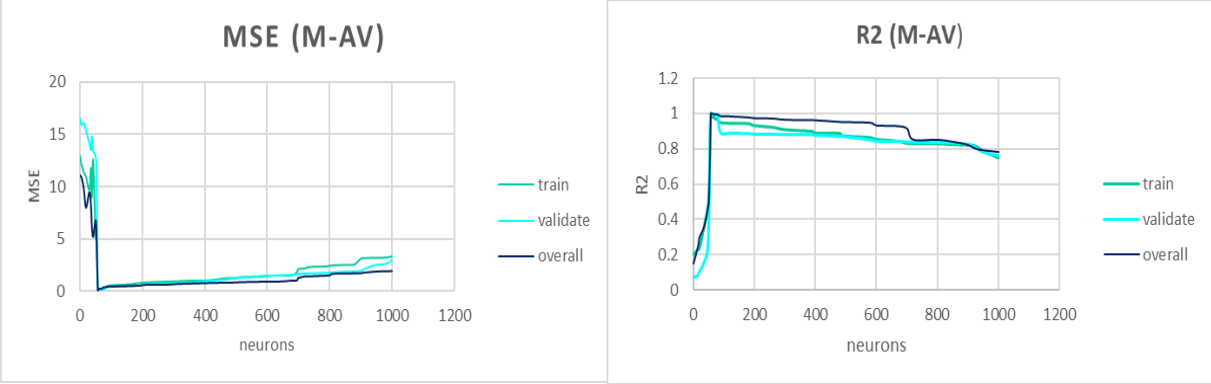

Figure 5-14 *Hyperparameter Tuning Results for M-AV Model*

5.3.1.2 Accuracy and performance evaluation

The model exhibited good accuracy across all datasets, demonstrating the ANN's robustness in capturing complex relationships between input features and mud filtrate invasion. Figure 5-15 shows

good agreement between predicted and actual values of AV, with few discrepancies, underscoring the ANN's effectiveness and reliability in making accurate predictions across varying dataset sizes.

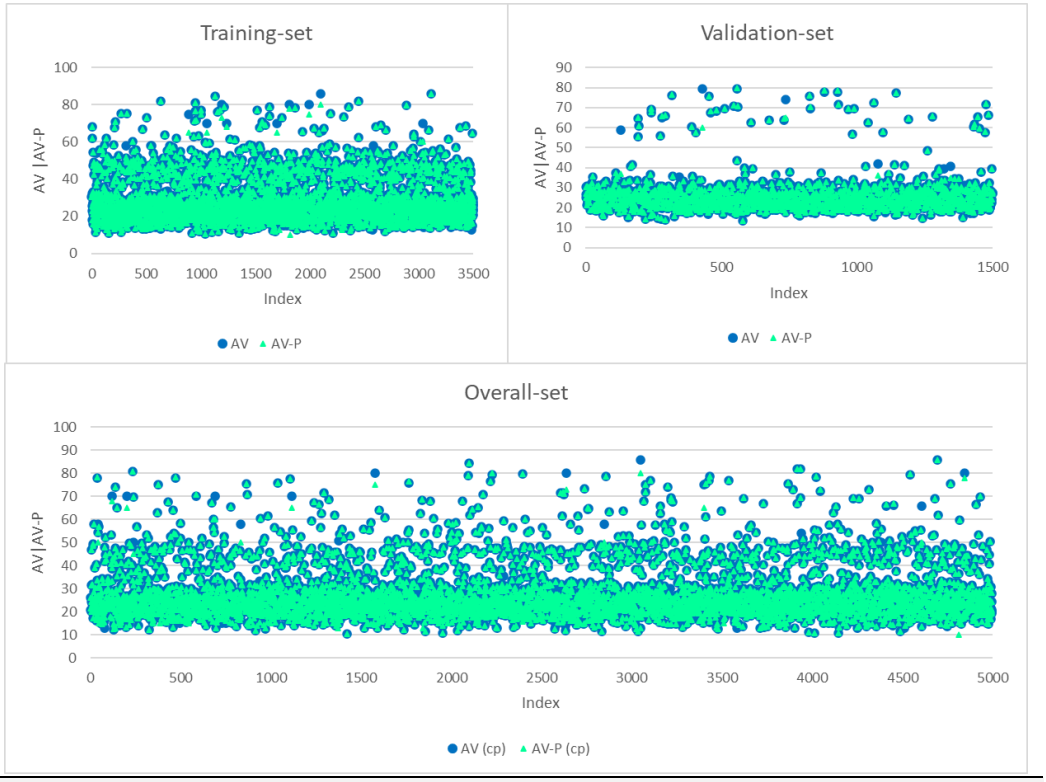

Figure 5-15 *M-AV Model Predictions vs. Actual apparent viscosity: Training, Testing, and Overall Results*

Figure 5-16 demonstrates the ideal fit premise, with data points converging near the red unit slope line, indicating strong alignment between ANN predictions and actual targets. This agreement signifies high accuracy in predicting AV by the M-AV model.

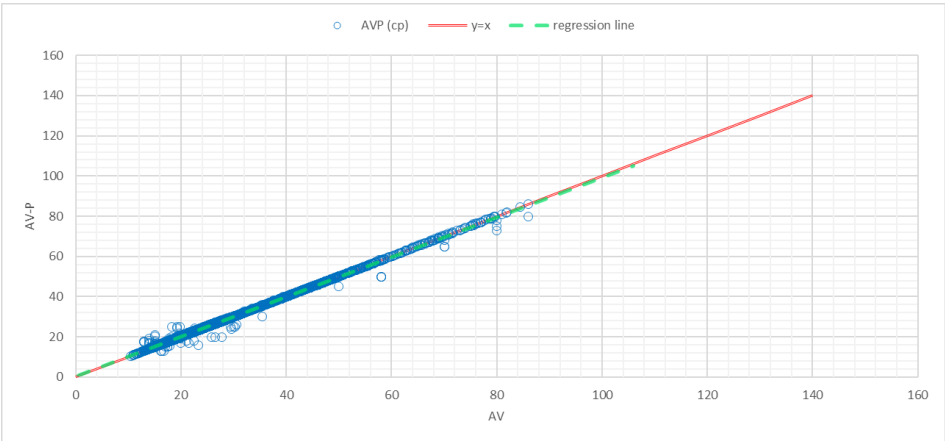

Figure 5-16 *Regression Analysis of the M-AV Model Predictions vs. Actual Apparent viscosity values*

We also evaluated the relative deviation (RD) of the predicted data from the actual data and plotted it against the actual values, as shown in Figure 5-17. Figure 5-17***(right)*** displays the ratio of predicted to actual values, with a maximum ratio of 1.421 and a minimum of 0.665, leading to an overall average ratio of 1.001. These metrics further confirm the reliability of the M-AV model.

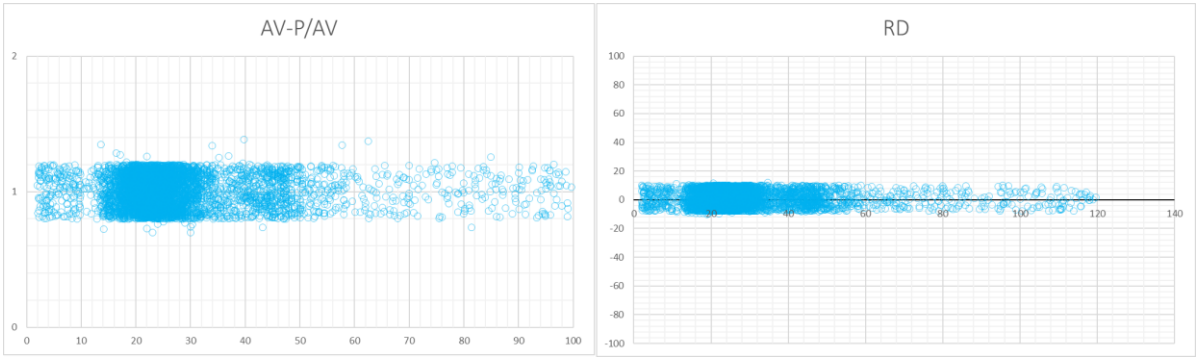

Figure 5-17 *Assessed relative deviation RD and ratio between predicted and actual values M-AV model*

5.3.1.3 ***Evaluation metrics analysis***

Based on the values of different key metrics, as illustrated in Figure 5-18, the M-AV model excels in predicting the apparent viscosity. The high R^2 value (R2=0.999), and the low mean squared error (MSE) of 0.082 shows small differences between predicted and actual values, while the root mean squared error (RMSE) of 0.286 underscores its high precision. The mean absolute percentage error (MAPE) of 0.013 reflects a relative error of just 1.3%, demonstrating significant accuracy. Additionally, the mean absolute error (MAE) of 0.126 confirms the model's good absolute accuracy. Collectively, these metrics reveal that the M-AV model offers highly precise and accurate predictions of filtrate volumes, with only minor areas for potential enhancement.

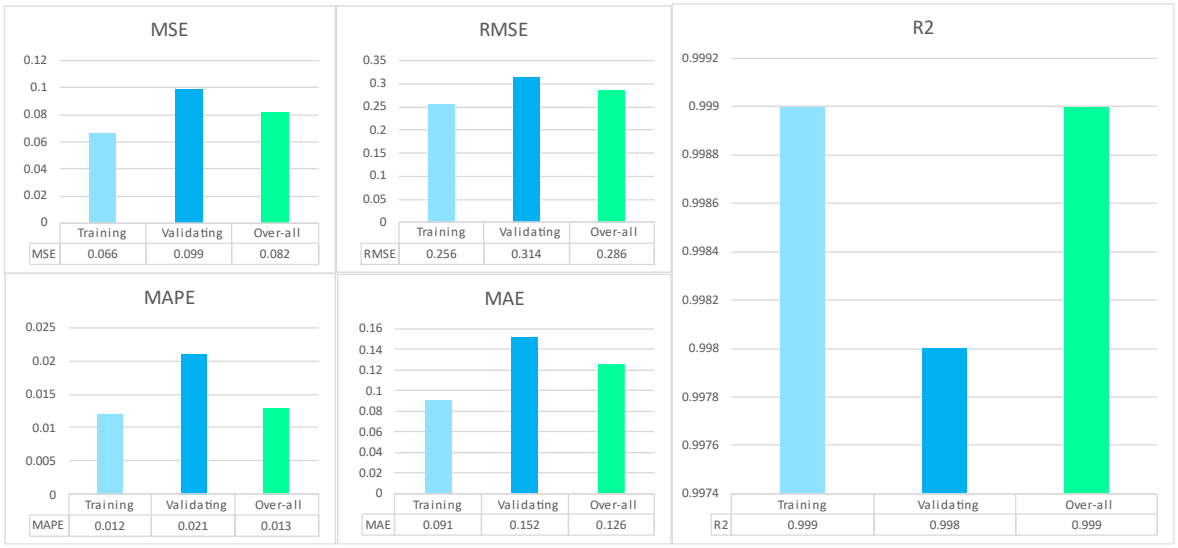

Figure 5-18 *Metrics values of the M-AV model*

5.3.1.4 ***Model Validation and Comparative Analysis***

M-AV model was compared against others models from literature: ***Pitt's***[145], ***Almahdawi's***[146]**,** ***Gowida et al. (2020)*** [147], ***Al-Khdheeawi & Doaa Saleh Mahdi (2019)***[148], ***Alsabaa et al (2020)***[149]**, ANFIS-AV-DIRECT** and **ANFIS-AV-Q600**. The results are presented in Figure 5-19. As shown, our model outperforms others models with a MAPE of 0.013 and R^2 of 0.99.

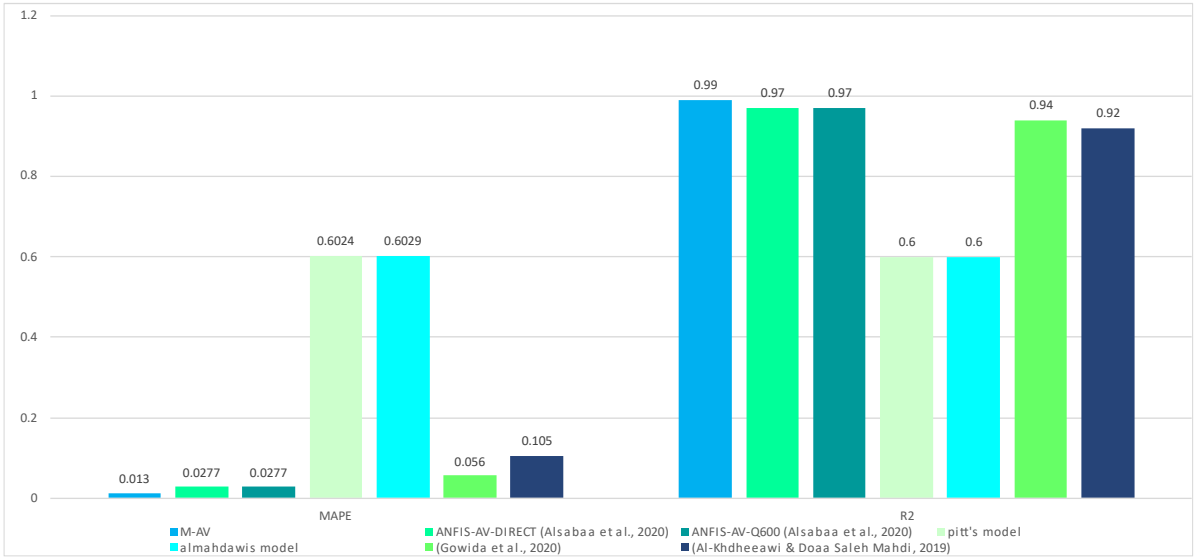

Figure 5-19 *Comparison of MAPE and R2 values of (M-AV) Model with Other Models from literature for Filtrate Volume Prediction*

5.3.2 Plastic viscosity model (M-PV)

5.3.2.1 Training and validating

The best hyper-parameters for the M-PV are shown in ***Table 5-7***. These parameters were used to train the model through this ANN. Figure 5-20 shows the tuning phase of the ANN model resulted in an optimal architecture consisting of one hidden layer, with 197 neurons. The activation function chosen for both layers is the softsign function. This configuration was determined to be the most effective in minimizing the mean squared error (MSE) and maximizing the (R2) during tuning.

Table 5-7 *tuning best hyperparameters M-PV*

Training functions	SGD
Transfer functions	Softsign
Number of hidden layers	1
Number of neurons in each layer	197
Performance goal	Mse=Min possible and R2 = Max possible (stop after 10 epochs with no improvement)
Learning rate and batch size	0.0023 / 64
Number of inputs	24 (NPs (Types size and MW) DF types| Chemical composition| Density and Solid content)
Number of outputs	1 (Plastic viscosity CPo)
Network type	F-F-B-P
Number of training simples	3500
Number of testing simples	1500

$$\text{PV-P} = \exp\left(\sum_{i=1}^{197} W_i^{(2)}\ \text{Softsign}\left(\sum_{k=1}^{M} W_{ik}^{(1)} X_k \quad + b_i^{(1)}\right) + b^{(2)}\right) - 1 \qquad 5\text{-}7$$

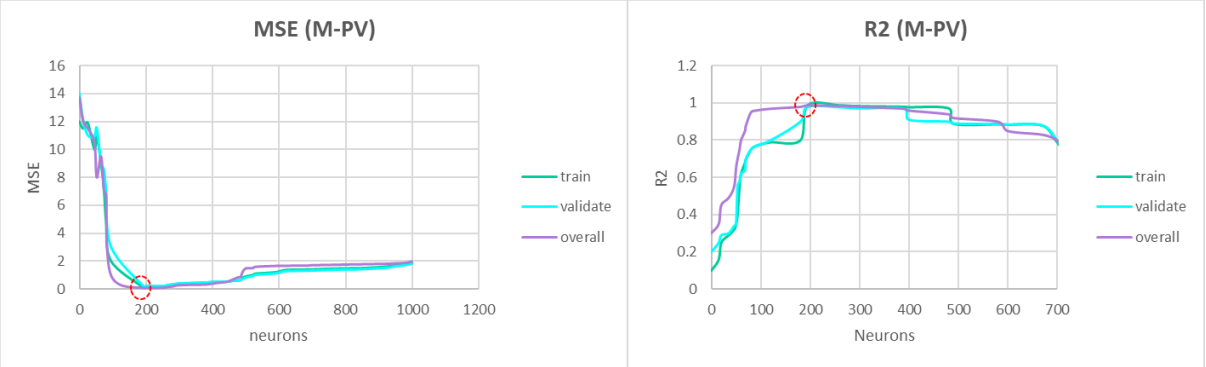

Figure 5-20 *Hyperparameter Tuning Results for M-PV Model*

5.3.2.2 ***Accuracy and performance evaluation***

The model demonstrated high accuracy for all datasets. As shown in Figure 5-21, there is a good agreement between predicted values (green) and actual values (purple), with minimal discrepancies. This highlights the ANN's effectiveness and reliability in making accurate predictions, regardless of dataset size.

Figure 5-21 *M-PV Model Predictions vs. Actual Filtrate Volumes: Training, Testing, and Overall Results*

Figure 5-22 illustrates the ideal fit premise, where data points cluster near the y=x line, indicating a strong alignment between ANN predictions and actual targets. The close alignment of the dashed green regression line with the red line signifies the M-PV model's high accuracy in predicting PV.

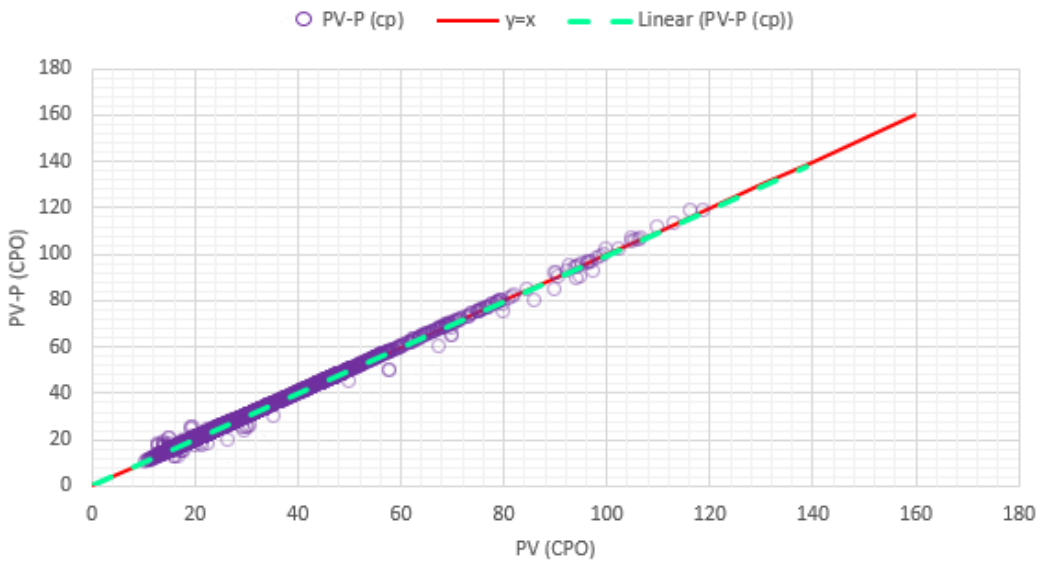

Figure 5-22 *Regression Analysis of the M-PV Model Predictions vs. Actual Filtrate Volumes*

We also assessed the relative deviation (RD) of the predicted data from the actual data and plotted it against the actual values, as shown in Figure 5-23 ***(right).*** The maximum, the minimum, and the average RD were 14.356, -6.246, and 2, respectively. Figure 5-23 ***(left)*** shows the ratio of predicted to actual values, with a maximum ratio of 1.444, a minimum of 0.771, and an overall average ratio of 1.002. These metrics further validate the reliability of the M-PV model.

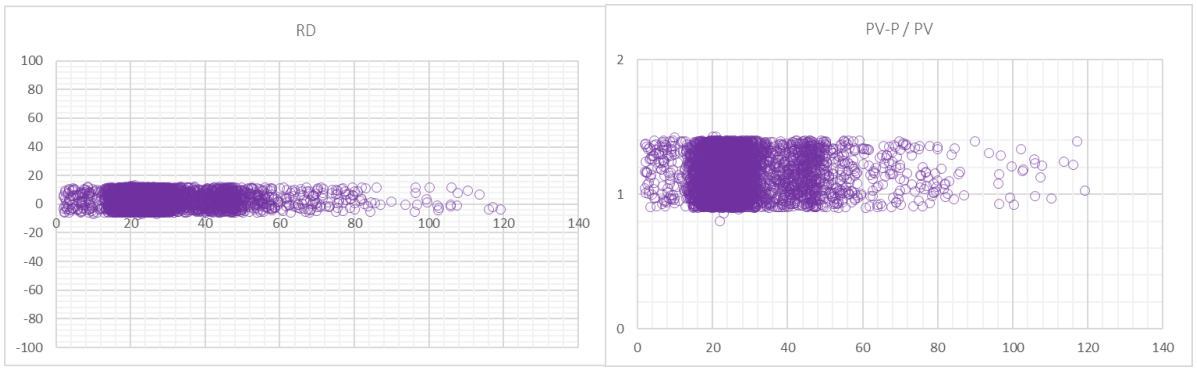

Figure 5-23 *Assessed relative deviation RD (right) and ratio between predicted and actual values (left) FOR THE M-PV model*

5.3.2.3 ***Evaluation metrics analysis***

As sown in ***Figure 5-24*** the M-PV model demonstrates exceptional proficiency in predicting the plastic viscosity, supported by several key metrics. With an R^2 value of 0.97, it accounts for 97% of the variance in actual plastic viscosity, indicating a robust correlation. The model exhibits a low mean squared error (MSE) of 0.09, signifying minimal average squared differences between predicted and

actual values, while the root mean squared error (RMSE) of 0.3 underscores its high precision. The mean absolute percentage error (MAPE) of 0.02 reflects a relative error of only 2%, highlighting its significant accuracy. Furthermore, the mean absolute error (MAE) of 0.251 confirms the model's excellent absolute accuracy. Together, these metrics demonstrate that the M-PV model provides highly precise and accurate predictions of filtrate volumes, with minor areas for potential enhancement.

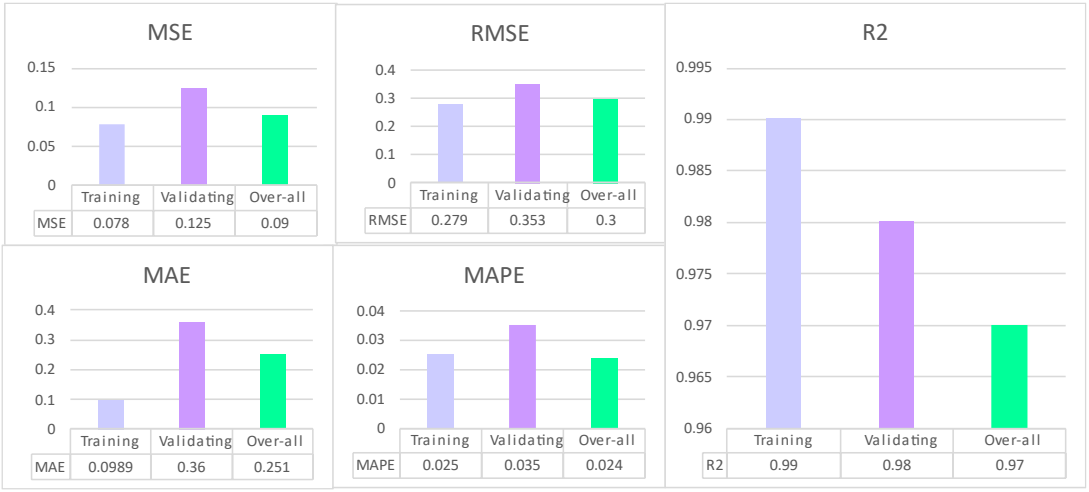

Figure 5-24 *Metrics assessment for the M-PV model*

5.3.2.4 *Cross-Validation and Comparative Analysis: Alignment with other literature models*

Based on the provided metrics illustrated in Figure 5-25, **M-PV** seems to be the best-performing model, followed closely by **ANFIS-PV-DIRECT**, while the other two models, **ANFIS-PV-Q600-300** and **(Gowida et al., 2020)**, are slightly less accurate.

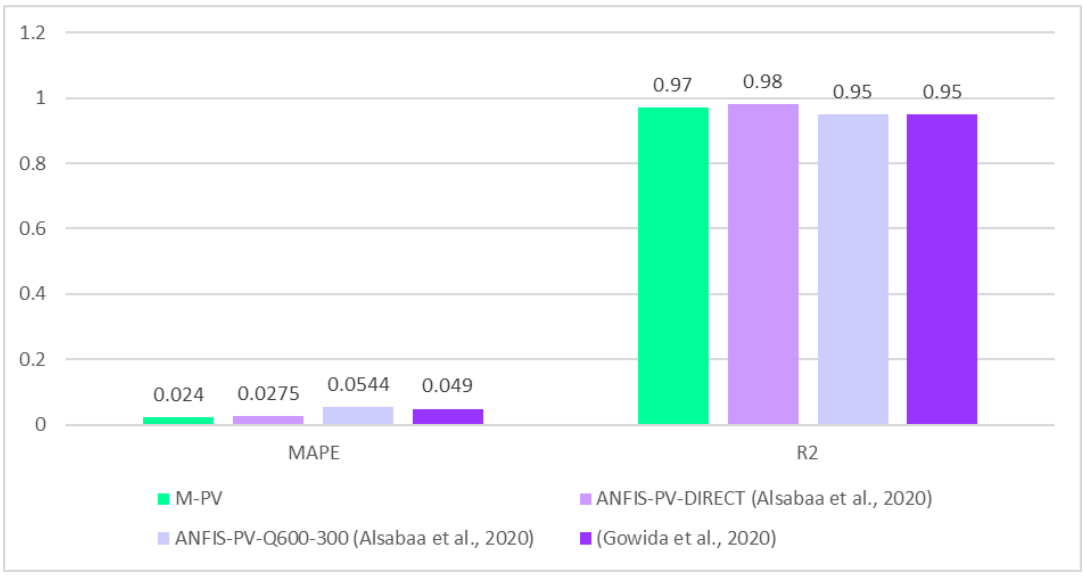

Figure 5-25 *Comparison of Model (M-PV) with Other Models in literature for Filtrate Volume Prediction*

5.3.3 Yield point model (M-YP)

5.3.3.1 Training and validating

The best-hyper-parameters for the M-YP are shown in *Table 5-8*. These parameters were used to train the model through this ANN with 2 hidden layers and tanh activation function (Eq. 5-8). Figure 5-26 shows the evaluation, the tuning phase of the ANN model which resulted in an optimal architecture consisting of two hidden layers, each with 195 and 310 neurons respectively. The activation function chosen for both layers is the hyperbolic tangent (tanh) function. This configuration was determined to be the most effective in minimizing the mean squared error (MSE) and maximizing the (R2) during tuning. The use of tanh activation functions helps in capturing complex, non-linear relationships within the data, contributing to the overall robustness and performance of the neural network.

***Table 5-8** tuning best hyperparameters M-YP*

Training functions	Adam
Transfer functions	tanh
Number of hidden layers	2
Number of neurons in each layer	195 / 310
Performance goal	Mse=Min possible and R2 = Max possible (stop after 10 epochs with no improvement)
Learning rate and batch size	0.0018 / 64
Number of inputs	24 (NPs (Types size and MW) DF types| Chemical composition| Density and Solid content)
Number of outputs	1 (yield point (lb/100 ft²))
Network type	F-F-B-P
Number of training simples	3500
Number of testing simples	1500

$$\text{YP-P} = \exp\left(\sum_{j=1}^{310} W_j^{(3)} \tanh\left(\sum_{i=1}^{195} W_{ji}^{(2)} \tanh\left(\sum_{k=1}^{M} W_{ik}^{(1)} X_k + b_i^{(1)}\right) + b_j^{(2)}\right) + b^{(3)}\right) - 1 \qquad 5\text{-}8$$

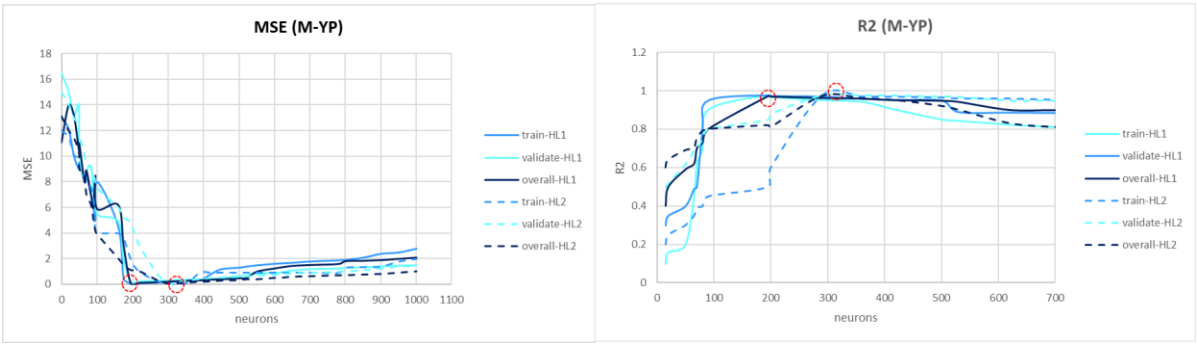

***Figure 5-26** Hyperparameter Tuning Results for M-YP Model*

5.3.3.2 ***Accuracy and performance evaluation***

The model achieved remarkable accuracy across all datasets. Figure 5-27 illustrates a strong correlation between the predicted values (green) and the actual values (purple), with only minor differences.

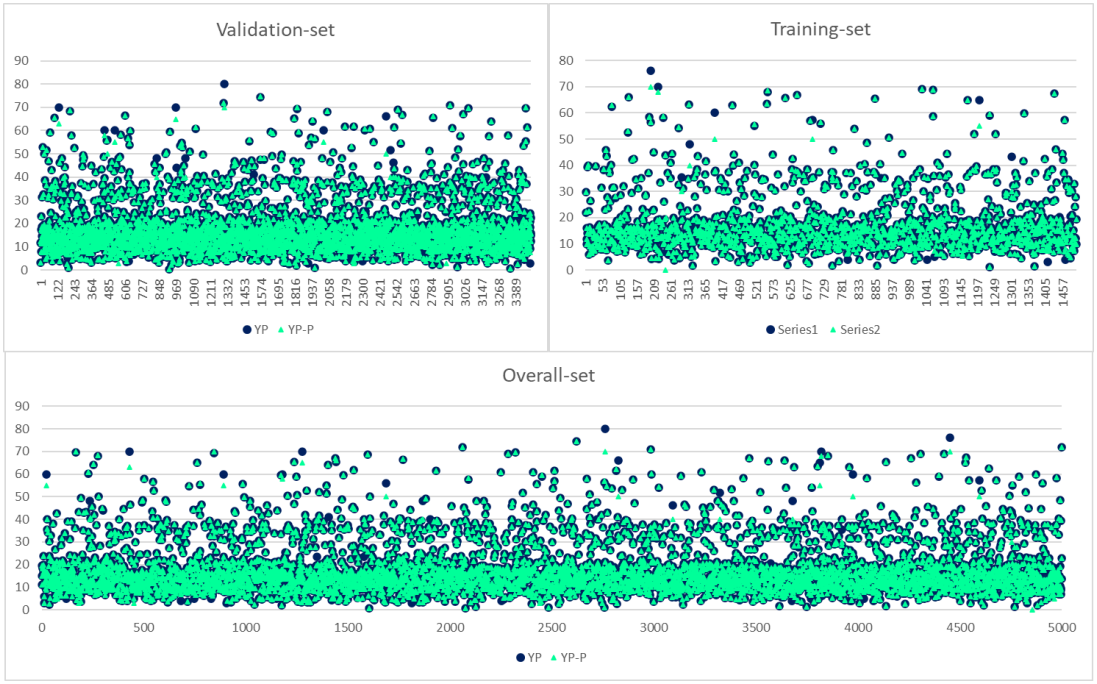

Figure 5-27 *M-YP Model Predictions vs. Actual Yield point: Training, Testing, and Overall Results*

Figure 5-28 illustrates the scatter plot of the results with data points converging near the y=x line, indicating a strong correspondence between ANN predictions and actual targets. The close match between the dashed green regression line and the red line highlights the M-YP model's high accuracy in predicting YP.

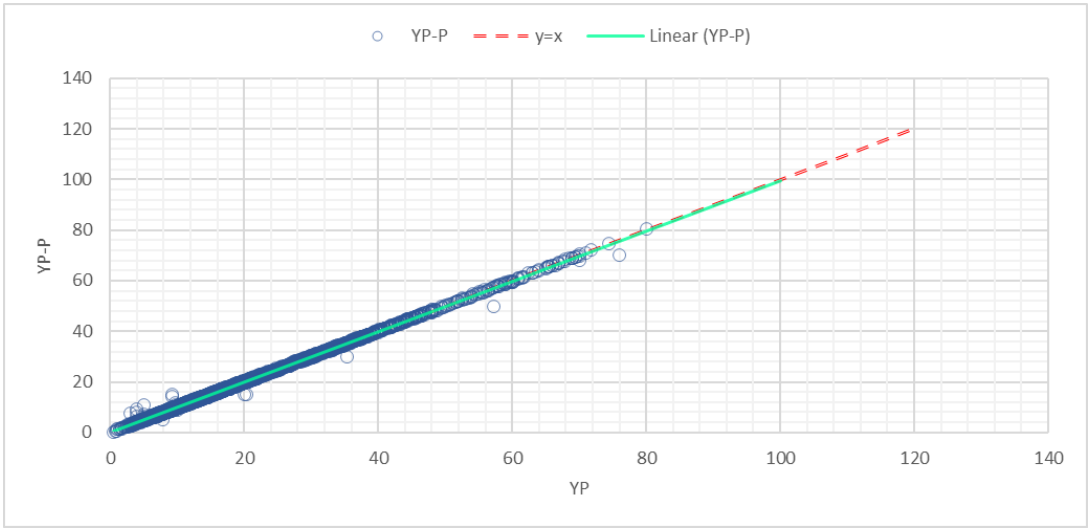

Figure 5-28 *Scatter plot of the M-YP Model Predictions vs. Actual Filtrate Volumes*

We also evaluated the relative deviation (RD) of the predicted data from the actual data and plotted it against the actual values, as shown in Figure 5-29 ***(left).*** The RD values ranged from a maximum of 12.121 to a minimum of -9.156, with an average RD of 2. Figure 5-29 ***(right)*** illustrates the ratio of predicted to actual values, revealing a maximum ratio of 1.523, a minimum of 0.825, and an overall average ratio of 1.0015. These metrics further confirm the reliability of the M-YP model.

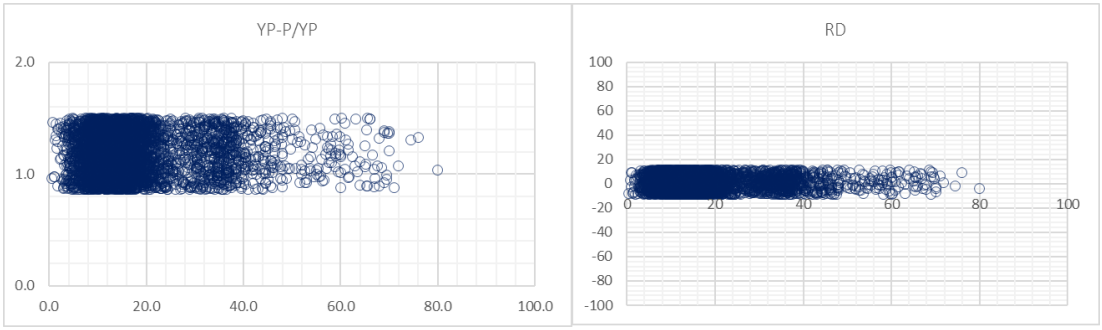

Figure 5-29 *Assessed relative deviation RD (right) and ratio between predicted and actual values (left) for the M-YP model*

5.3.3.3 ***Evaluation metrics analysis***

Various metrics were used to assess the reliability of results as summarized in Figure 5-30. As shown, the M-YP model offers highly precise and accurate predictions of yield point, with only minor areas for potential enhancement.

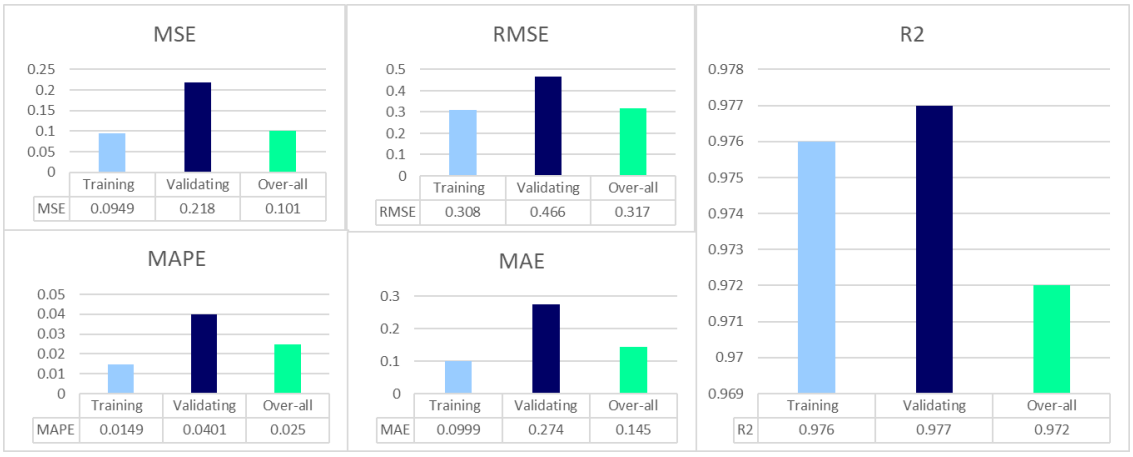

Figure 5-30 *Metrics assessment for the M-YP model*

5.3.3.4 ***Cross-Validation and Comparative Analysis: Alignment with other literature models***

As depicted in Figure 5-31, M-YP exhibits the lowest MAPE (0.0149) and highest R2 (0.972), indicating superior accuracy. ***ANFIS-YP-DIRECT*** follows with a slightly higher MAPE (0.0278) and a respectable R2 (0.96). Meanwhile, the model by ***Gowida et al.*** shows higher MAPE (0.0295) and lower R2 (0.94), indicating less accuracy and fit. Overall, M-YP outperforms the others in both metrics.

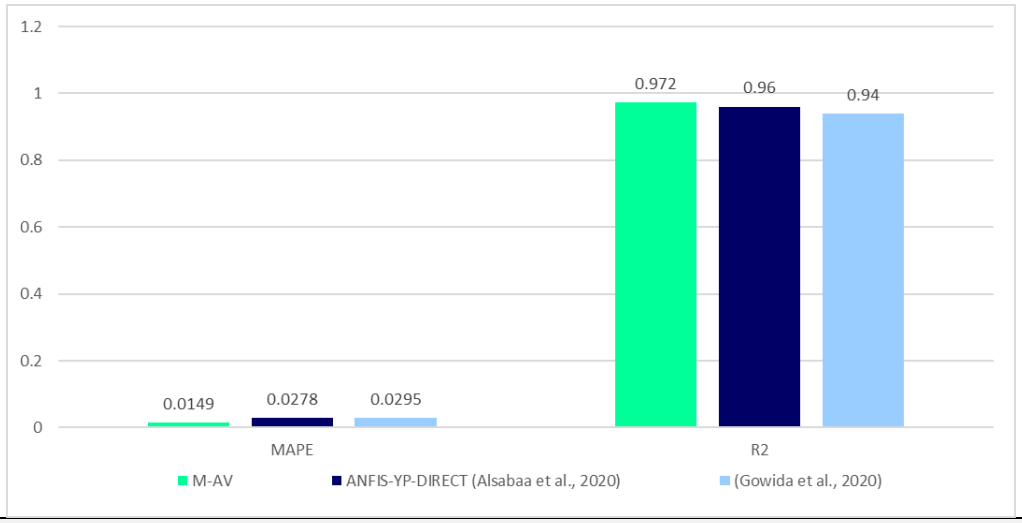

Figure 5-31 *Comparison of Model (M-YP) with Other Models in literature for Filtrate Volume Prediction*

5.3.4 Gel strength model (M-GS)

5.3.4.1 Training and validating

The best-hyper-parameters for the M-YP are shown in **Table 5-9**. These parameters were used to train the model through this ANN with 3 hidden layers. Figure 5-32 shows the tuning phase of the ANN model resulted in an optimal architecture consisting of three hidden layers, each with 100, 240 and 498 neurons respectively. The activation function chosen for both layers is the hyperbolic tangent (tanh) function. This configuration was determined to be the most effective in minimizing the mean squared error (MSE) and maximizing the (R2) during tuning. The use of tanh activation functions helps in capturing complex, non-linear relationships within the data, contributing to the overall robustness and performance of the neural network.

Table 5-9 tuning best hyperparameters M-GS

Training functions	Adam
Transfer functions	tanh
Number of hidden layers	3
Number of neurons in each layer	100 / 240 / 498
Performance goal	Mse=Min possible and R2 = Max possible (stop after 10 epochs with no improvement)
Learning rate and batch size	0.0021 / 64
Number of inputs	24(NPs (Types size and MW) DF types| Chemical composition| Density and Solid content)
Number of outputs	2 (GS10S / GS10M in lb/100ft^2)
Network type	F-F-B-P
Number of training simples	3500
Number of testing simples	1500

$$GS = \exp\left(\sum_{j=1}^{498} W_j^{(4)} \tanh\left(\sum_{l=1}^{240} W_{jl}^{(3)} \tanh\left(\sum_{i=1}^{100} W_{li}^{(2)} \tanh\left(\sum_{k=1}^{M} W_{ik}^{(1)} X_k + b_i^{(1)}\right) + b_l^{(2)}\right) + b_j^{(3)}\right) + b^{(4)}\right) - 1 \qquad 5\text{-}9$$

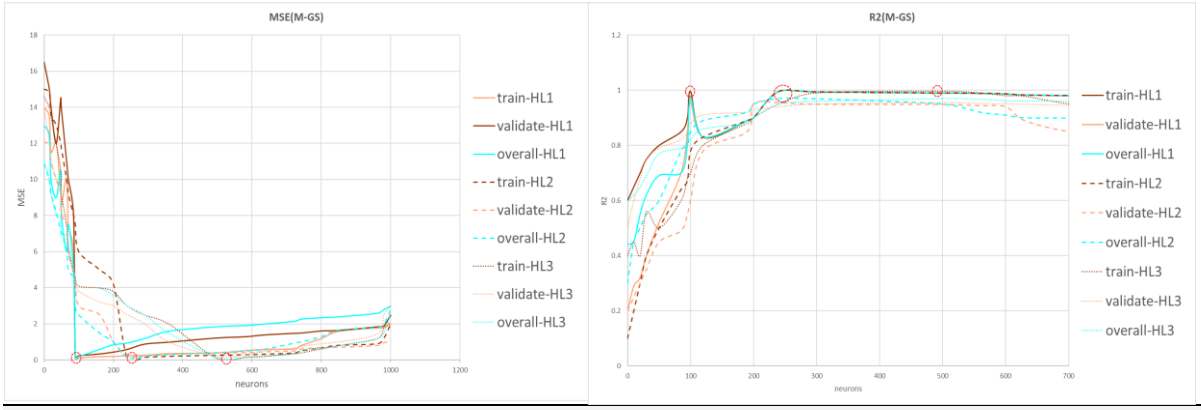

Figure 5-32 *Best hyperparameters tuning for model M-GS*

5.3.4.2 Accuracy and performance evaluation

The model achieved remarkable accuracy across over all. Figure 5-33 illustrates a strong correlation between the predicted values (green) and the actual values (purple), with only minor differences.

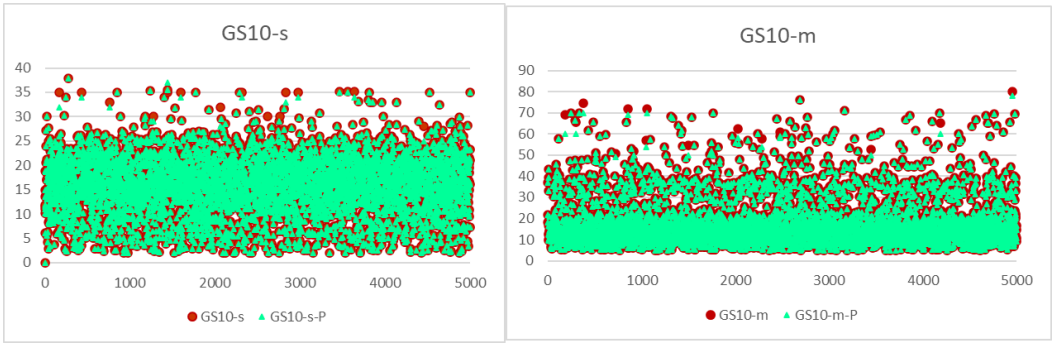

Figure 5-33 *M-GS Model Predictions vs. Actual Gel Strength: Overall Results*

Figure 5-34 illustrates the scatter plot, with data points converging near the y=x line, indicating a strong correspondence between ANN predictions and actual targets. The close match between the dashed green regression line and the red line highlights the M-GS model's high accuracy in predicting GS.

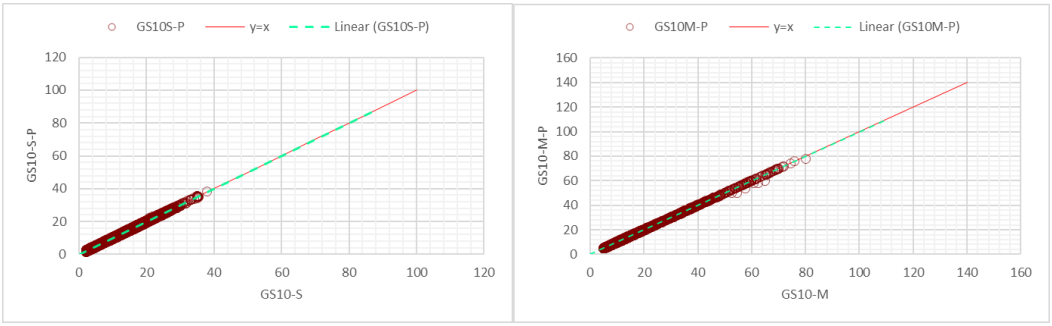

Figure 5-34 *Scatter plot of M-GS Model Predictions vs. Actual GS*

We also evaluated the relative deviation (RD) of the predicted data from the actual data and plotted it against the actual values, as shown in Figure 5-35 (***left).*** The RD values ranged from a maximum of 13.111 to a minimum of 9,786, with an average RD of 1.5. Figure 5-35 ***(right)*** illustrates the ratio of predicted to actual values, revealing a maximum ratio of 1.789, a minimum of 0.777, and an overall average ratio of 1.002. These metrics further confirm the reliability of the M-GS model.

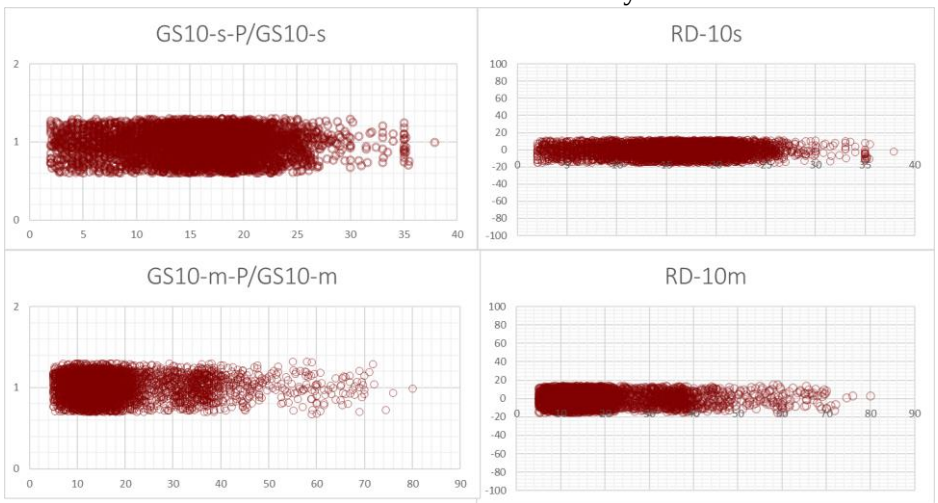

Figure 5-35 *M-GS Model Predictions vs. Actual GS: RD and Ratio*

5.3.4.3 ***Evaluation metrics analysis***

Various metrics are summarized in Figure 5-30. As shown, the M-GS model offers highly precise and accurate predictions of gel strength. The performance metrics were evaluated by taking the sum of the two-output metrics and dividing by 2. This approach ensures that the final metric value is an average of the two individual output metrics, providing a balanced assessment of the model's performance.

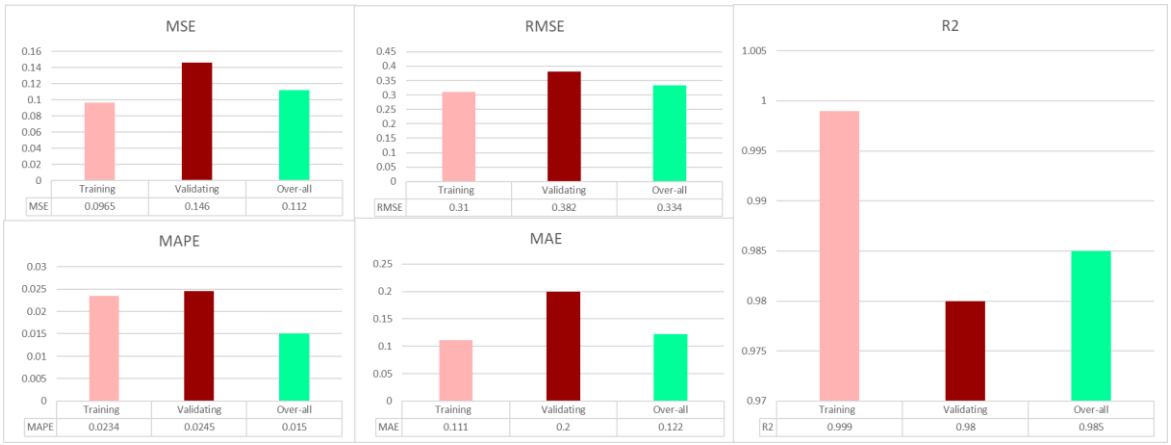

Figure 5-36 *Metrics assessment for the M-GS model*

5.3.5 combining the sub-models: Building a combined M-RH model

So now, we have four artificial neural network (ANN) models **(M-AV| M-PV| M-YP| M-GS)**, each designed to perform different tasks but using the same input parameters. Our goal is to combine these four models into a single unified model M-RH that can simultaneously generate four distinct outputs, corresponding to each of the original models.

To achieve this, a python script was created to implement the following steps:

- Create a Shared Input Layer:

We designed a single input layer that receives the input parameters. This input layer will be common to all four models.

- Distribute Inputs to Individual Models:

The shared input layer will distribute the input data to the individual network structures of the four original ANN models. This means each model will receive the same input data but process it independently according to its unique architecture and purpose.

- Generate Outputs:

Each of the four ANN models will process the input data and produce its specific output. Thus, we will have four distinct outputs (AV, PV,YP, and GS), each corresponding to one of the original models.

By integrating these models in this manner, we maintain the individual functionalities of each ANN while leveraging a shared input mechanism. This approach allows for efficient processing and simultaneous generation of multiple outputs from the same set of input parameters.

5.3.5.1 ***Consistency between Experimental and Modeled Rheology: Alignment of Modeled and Experimental RH parameters***

The M-RH model was tested by experimental data from ***Sabah et al***.[150] and ***Alsaba et al***. [151]. The results shown in Figure 5-37& Figure 5-38demonstrates a good alignment between the predicted

and actual values. This indicates that the model effectively captures the underlying patterns in the data and performs well in real-world scenarios. The high degree of accuracy and consistency observed in the predictions validates the robustness and reliability of the ANN model, making it a valuable tool for future predictive tasks.

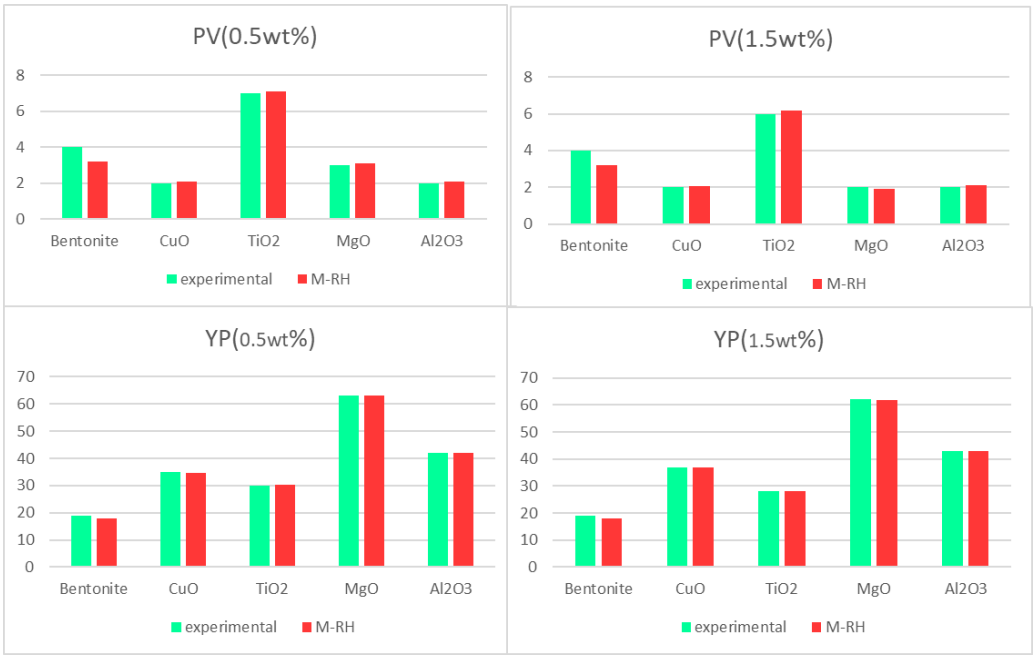

Figure 5-37 *Comparison of M-RH model results and experimental results from* ***Alsaba et al.*** [151]

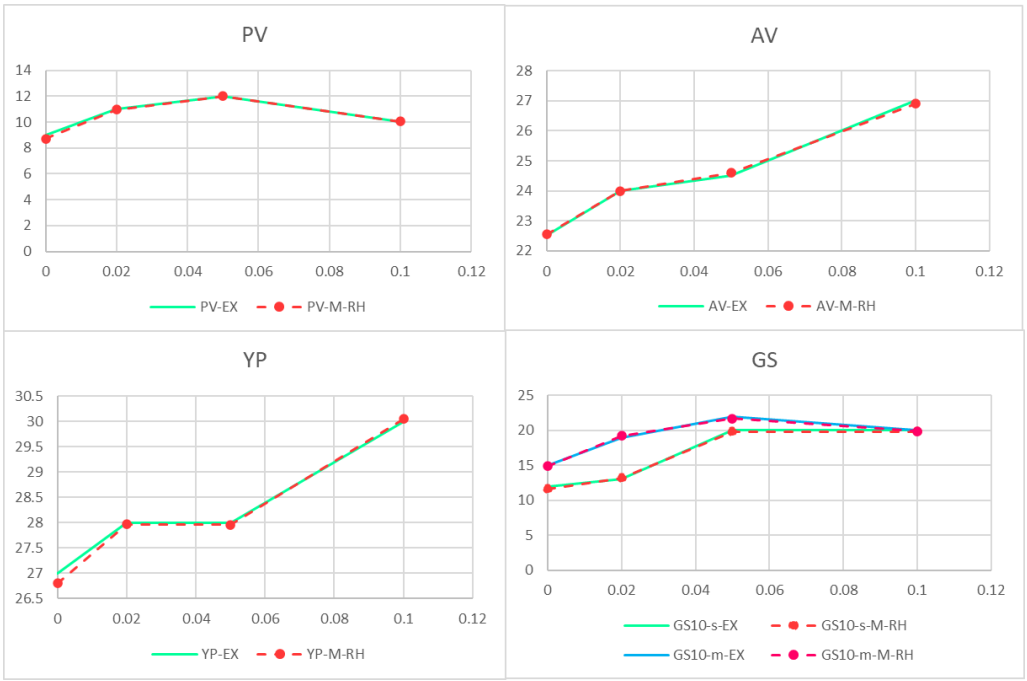

Figure 5-38 *Comparison of the M-RH model results and experimental results from* ***Sabah et al.***[150]

5.4 Building up the hybrid model (M-HYBRID)

5.4.1 The Main Concept

The hybrid model (HYBRID-M) concept leverages two primary components to optimize fluid loss processes. Firstly, it involves inverting the initial predictive model (M-FLT), which forecasts filtrate volume using optimization techniques, particularly evolutionary algorithms. Secondly, it incorporates the (M-RH) model as a secondary, surrogate model. This surrogate model aids in refining the input search space during optimization.

By specifying desired values for rheological properties such as plastic viscosity, apparent viscosity, yield point, and gel strength, the hybrid model efficiently searches for the optimal composition. This composition aims to either achieve a user-specified filtrate volume or minimize the filtrate output.

In essence, the hybrid model combines predictive accuracy with efficient optimization, enabling precise control over the filtration process. It facilitates achieving targeted filtrate volumes or minimizing them based on specified rheological parameters. This approach provides a robust framework for optimizing composition selection, thereby enhancing operational efficiency in fluid loss management.

5.4.2 Setting up the EA

5.4.2.1 Defining the search space

Before employing the Evolutionary Algorithm (EA), it is crucial to establish the range of values for each input parameter (concentrations of NPs and Additives). This can be determined based on the output of the (M-RH) model, which indicates the specific concentrations required to achieve the desired rheological properties. For instance, if the user aims to achieve specific rheological properties to elicit certain behaviors, such as low plastic viscosity for enhanced fluid flow, the ranges of each parameter should reflect this objective. For that, the user might specify a range for plastic viscosity parameter from 10 cPo to 50 cPo for instance. This range indicates that compositions (concentrations of NPs and Additives) that results in solutions with plastic viscosity values within this range are preferable, as they contribute to the desired behavior. Table 5-10 outlines the controllable parameters to be specified by the user.

Table 5-10 *setting up the environment for the genetic algorithm*

NPs size (nm)	NPs MW (g/mol)	T(s)	P (Psi)	T (F°)	Solid (%)	Density (ppg)	AV (cPo)	PV (cPo)	YP (lb/100ft^2)	GS10s (lb/100ft^2)	GS10m (lb/100ft^2)
fixed	fixed	fixed	fixed	fixed	fixed	fixed	Fixed or range	Fixed or range	Fixed or range	Fixed or range	Fixed or range

For the rest of the parameters (chemical composition), The user can specify the concentrations of various components in the chemical composition. For example, the user can set the concentration of Bentonite or Barite, NaCl, …. or even the NPs concentration as desired. The components that are not desired to be part of the composition should be set to zero. If the user does not specify a concentration for any component (empty) those are considered as values to be determined (unknowns).

5.4.2.2 Defining The Fitness Function

For the objective or the fitness function in Ea's terms, the user is allowed to choose between the two possibilities:

1. Max-F

In this case, the fitness function calculates the disparity between the user-specified target and the predicted output derived from the initial model (M-FLT). The objective is to minimize this disparity. For instance, if the user aims for a specific filtrate volume, the fitness function evaluates how close the predicted value aligns with this target. The closer the prediction to the user's goal, the higher the fitness score.

This fitness function is utilized when the user desires a composition resulting in a specific filtrate value. This is particularly crucial for tasks such as drilling in specific formations where precise control over filtrate is necessary. The function ensures convergence towards the user-specified filtrate value. For example, if the user aims for a filtrate volume of 6 milliliters, the function adjusts the composition accordingly.

$$F = Max_F = \frac{1}{\left(\text{flt}_{predicted} - \text{flt}_{desired}\right)^2 + \epsilon} \quad 5\text{-}10$$

2. Min-F

On the other hand, the Min-F function results in compositions that serves the purpose of minimizing filtration, to the lowest extent feasible.

In this scenario, the fitness function directly assesses the predicted filtrate volume from the model. The aim remains consistent: to minimize the fitness function. Regardless of the specific target value, the focus is on driving the predicted filtrate volume towards its lowest possible extent.

$$F = Min_F = \text{flt}_{predicted} = Filtrate - P \quad 5\text{-}11$$

5.4.3 Encoding method

The choice of encoding method to represent solutions within the evolutionary algorithm significantly impacts its performance. Various encoding schemes such as binary, real-valued, or permutation were considered to offer distinct advantages and trade-offs. In the context of minimizing model complexity and considering the inherent nature of the model, employing a real-valued encoding proves advantageous.

Real-valued encoding allows for a direct representation of continuous parameters, aligning seamlessly with the input requirements of many models. Unlike binary encoding, which necessitates discretization and potentially introduces loss of precision, real-valued encoding maintains the integrity of parameter values in their natural continuous form. This fidelity to the model's intrinsic characteristics promotes smoother convergence and facilitates more precise optimization.

5.4.4 Hyper-Parameters for RGA

Table 5-11 *Tuning hyperparameters for the RGA*

Population Size	***Num of generations***	***Cross-over operator***	***Mutation operator***	***Selection operator***
0-1000	0-1000	LCO| SBX | BLX | FR| UNDX	UM | NUM |GM| PM|RM	RWS |SUS |TS RBS | SSS

5.4.5 Sharing properties

- Setting up a distance function

A Euclidean function is used to calculate the distance between the individuals of the population

$$d = \sqrt{\sum_{i=1}^{n} (x_{i2} - x_{i1})^2} \quad 5\text{-}12$$

Where n represents the number of dimensions, and xi1 and xi2 are the coordinates of the two points in the i-th dimension.

- Setting up a sharing function

$$S(d) = \frac{d_{max} - d}{d_{\max}} \quad 5\text{-}13$$

where d-max is the maximum Euclidean distance between a chromosome pair given the current problem, this gives a simple triangular sharing function s(d) resulting in s(d) between 0 and 1 Selection of parents is based on the shared fitness values.

- Apply sharing to the fitness

$$F_s = \frac{F}{\sum S(d(x_{i1}, x_{i2}))} \quad 5\text{-}14$$

5.4.6 Price filtering

Upon applying the sharing method in the evolutionary algorithm, the outcome can indeed vary. It may yield multiple solutions or converge to a single solution, contingent upon factors such as the diversity of the initial population and the specific problem being addressed. In scenarios where multiple solutions are generated, a post-processing step, such as a price check, becomes essential to select the most economically viable composition.

$$P_t = \sum_{n=1}^{N} (c_n \cdot density \cdot p_n) \quad 5\text{-}15$$

With cn and pn the price and the concentration as a fraction (/100) of the component respectively .

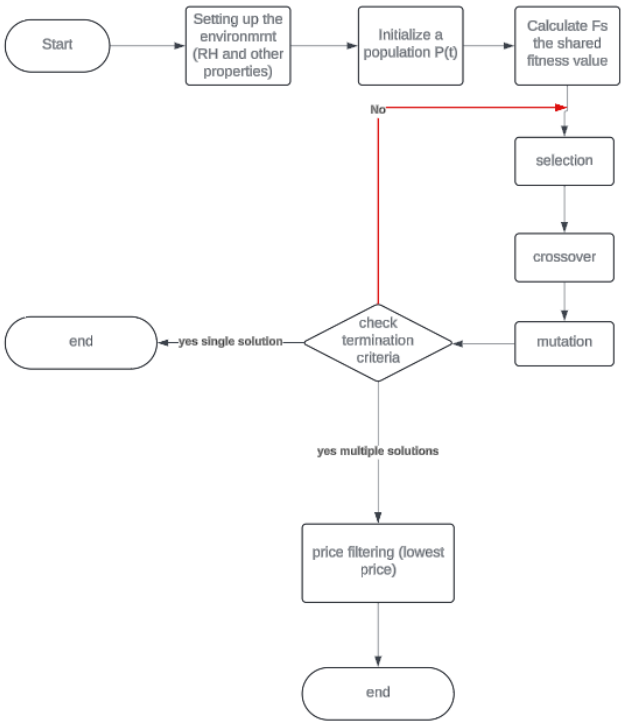

Figure 5-39 *Flow chart for the RGA used in inversion*

5.4.7 Deeper view: Trying some scenarios

To better understand the whole concept and the functioning of the model, three scenarios were executed:

5.4.7.1 *1st Scenario*

In this scenario we used the first fitness function max-f for a desired filtrate volume of 6 (ml)

- Setting up the environment

In this segment, we aimed for a lightweight DF with moderate viscosity and gel strength. It can offer effective cuttings transport and suspension while minimizing the risk of formation damage and maintaining good flow properties. This balance makes it suitable for various drilling conditions, especially those involving low-pressure formations.

Table 5-12 *setting up the environment for the genetic algorithm*

NPs size	*NPs MW (g/mol)*	*T(s)*	*P(Psi)*	*T(F°)*	*Solid (%)*	*Density (ppg)*	*AV (CPo)*	*PV (CPo)*	*YP (Lb/100ft²)*	*GS10s (Lb/100ft²)*	*GS10m (Lb/100ft²)*
30	60.0843	300	100	100	12	9	20 -30	10 -20	10 - 20	2 - 5	4 - 10

Table 5-13 *chemical composition for the first scenario*

Bentonite	Barite	SiO2	XC POLYMER	NaCl	Others
7%	3%	X	Y	Z	0%

- ***Tuning results***

Table 5-14 *Tuning results for the first scenario*

Population Size	Num of generations	Cross-over operator	Mutation operator	Selection operator
150	95	SBX With ηc = 15	RM	RWS

The fitness vs generations plot in Figure 5-40 represents the evolution of the genetic algorithm's performance using sharing. Initially, there is an increase in the maximum, mean, and minimum fitness values, indicating quick identification and exploitation of beneficial traits. After some fluctuations between generations 30 and 90, the fitness values stabilize, suggesting the algorithm has found high-quality solutions and is maintaining them. The stability of the maximum fitness and the minor fluctuations in mean and minimum fitness indicate that sharing helps maintain a diverse set of good solutions and supports the presence of multiple niches. This diversity prevents premature quick convergence to a single solution and ensures thorough exploration of the search space.

While Figure 5-44 shows the distance vs generations and illustrates the changes in diversity within the population throughout the genetic algorithm's run. Initially, there is high diversity, as shown by the high maximum and mean distances between individuals. This diversity decreases slowly as the algorithm progresses, indicating convergence towards similar high-quality solutions. After generation 100, the distances stabilize, with the minimum distance remaining low and the mean distance leveling off, while the maximum distance slightly increases. This pattern suggests that the population has clustered around a few distinct niches. The use of sharing has controlled the convergence rate, maintaining sufficient diversity to explore different areas of the search space and prevent premature convergence, ensuring the algorithm can find multiple high-quality solutions.

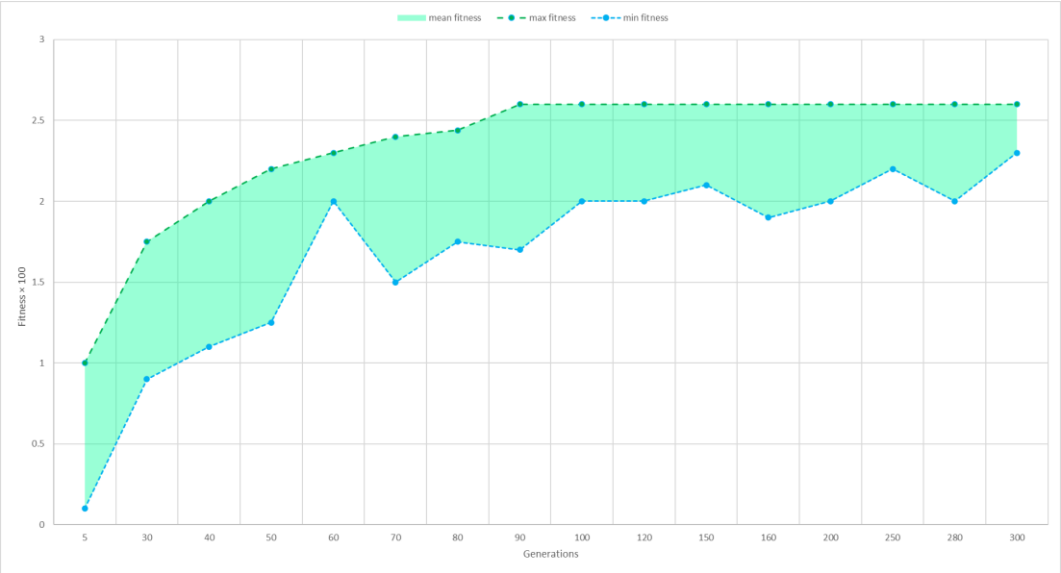

Figure 5-40 *Fitness values over generation for the first scenario*

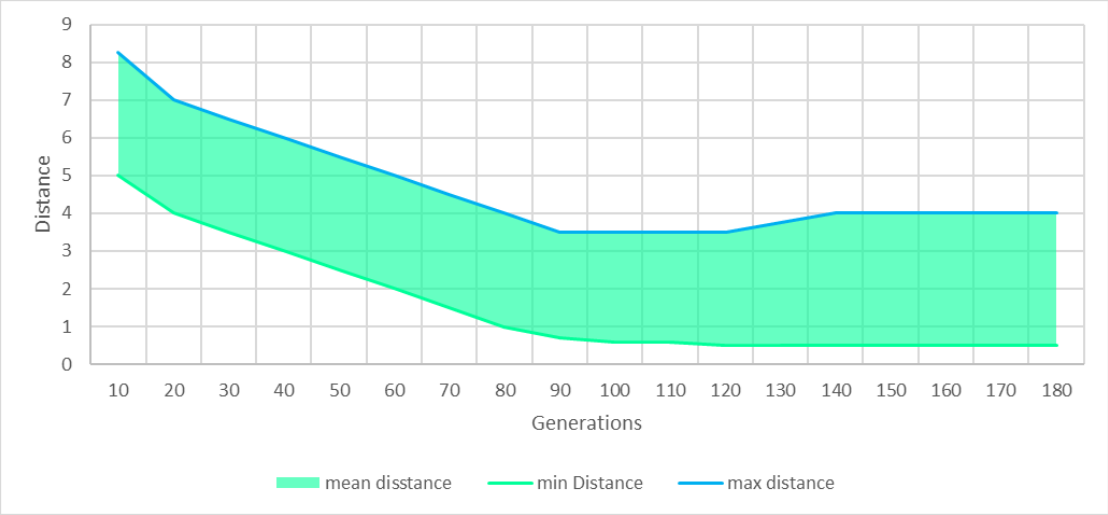

Figure 5-41 *Distance between individuals vs generations for the first scenario*

- Results and discussion

Figure 5-45 helps visualizing the progress of the genetic algorithm (GA) over multiple generations, showing how the population evolves over time. The images likely represent a 3D fitness landscape with different generations of individuals plotted on it.

Initial Population (upper left):

- The initial population is scattered across the fitness landscape.
- Individuals are represented as points with varying fitness values (indicated by height).
- This distribution is typically random, ensuring diverse genetic material for the evolutionary process.

20^{th} and 45^{th} Generation (upper and lower right):

- By the 20^{th} generation, you can see that the population has started to cluster around certain areas of the fitness landscape.
- Sharing functions are likely at play, which penalizes individuals that are too close to each other, promoting the formation of niches which is more evolved in generation 45th.

- Niching helps maintain diversity in the population by preventing individuals from converging too quickly on a single peak.

Final Generation (lower left):

- The final generation shows a more refined distribution with clear niches around the peaks of the fitness landscape.
- These niches represent different solutions or "species" that have been maintained due to the sharing mechanism (2 solutions were maintained).
- The presence of multiple peaks indicates that the algorithm has explored various regions of the fitness landscape and identified multiple high-fitness solutions.

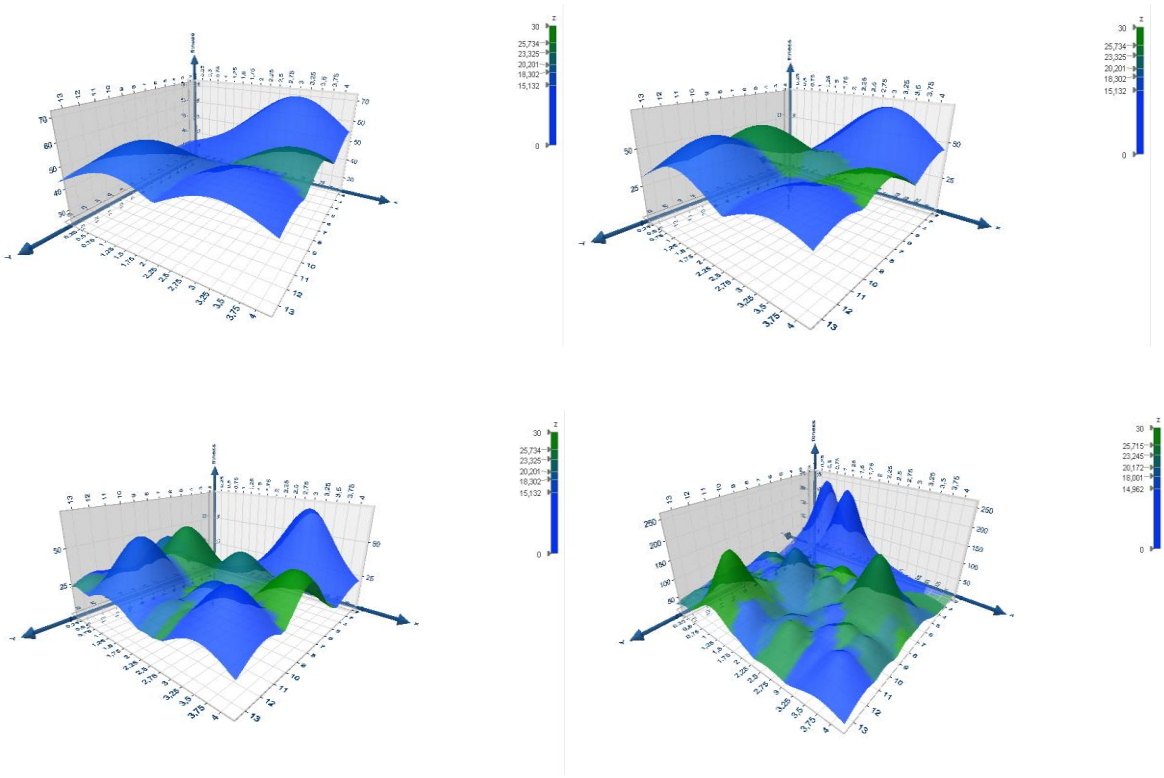

Figure 5-42 *Results and Fitness evolution over generations for the first scenario (initial, 20th 45th and final generations, respectively)*

As discussed previously, in case of multiple solutions as in this case, a price check is needed to select the most economically viable composition. As shown in Table 5-15, solution 1 is the most economically favorable solution. Thus, we choose the first composition.

Table 5-15 *Compositions for the first scenario*

composition	Bentonite	Barite	SiO2	XC POLYMER	NaCl	Others	Price DA/bbl
1	7%	3%	1.2%	0.27%	2%	0%	1279.008
2	7%	3%	0.3%	0.7%	3%	0%	2736.0585

5.4.7.2 *2nd Scenario*

In this scenario we also used the first fitness function Max-F for a desired filtrate volume of 5 (ml) but with a heavier drilling fluid with different desired composition and properties

- Setting up the environment

Table 5-16 *setting up the environment for the genetic algorithm for the second scenario*

NPs size (nm)	*NPs MW (g/mol)*	*T(s)*	*P(Psi)*	*T(F°)*	*Solid (%)*	*Density (ppg)*	*AV (CPo)*	*PV (CPo)*	*YP (Lb/100ft²)*	*GS10s (Lb/100ft²)*	*GS10m (Lb/100ft²)*
50	101.96	300	200	300	12	10	35 -50	25 -40	25 - 30	5 - 10	15 -20

Table 5-17 *Desired chemical composition for the second scenario*

Bentonite	Barite	Al2O3	Pac R	NaOH	Others
7%	3%	X	Y	Z	0%

- Tuning results

Table 5-18 *Tuning results for the second scenario*

Population Size	Num of generations	Cross-over operator	Mutation operator	Selection operator
165	220	BLX with $\alpha = 0.543$	NUM	RWS

In Figure 5-43, The fitness vs generations plot for the genetic algorithm with sharing illustrates the progression of the population's fitness over time. Initially, the mean, minimum, and maximum fitness values are relatively low, reflecting the early stages of exploration and variation within the population. As generations progress, there is a notable increase in all fitness measures, indicating that the population is evolving towards better solutions. By generation 120, the fitness values begin to stabilize, with the mean fitness showing a consistent upward trend and the minimum fitness converging more closely to the mean fitness. The maximum fitness also plateaus, suggesting that the algorithm has identified several high-quality solutions. The stabilization of these fitness values around generation 220 indicates that the population has effectively converged, with the sharing mechanism successfully maintaining multiple high-fitness niches. This ensures that the population does not overly converge on a single solution, promoting a diverse set of optimal or near-optimal solutions within the search space.

The distance vs generations plot in Figure 5-44 for the genetic algorithm with sharing demonstrates the changes in population diversity throughout the evolutionary process. Initially, there is high diversity, indicated by the high maximum and mean distances between individuals. This diversity decreases steadily, as shown by the declining mean and maximum distances until around generation 220. At this point, the minimum distance reaches a very low value and remains there, indicating that some individuals have converged to very similar solutions. From generation 220 onwards, the mean and maximum distances stabilize, although the maximum distance experiences minor fluctuations. This suggests that while the population has converged to several distinct niches (maintained by sharing), a sufficient level of diversity persists to prevent premature convergence and to allow the algorithm to explore different areas of the search space effectively. This balance ensures the algorithm's robustness and ability to find multiple high-quality solutions.

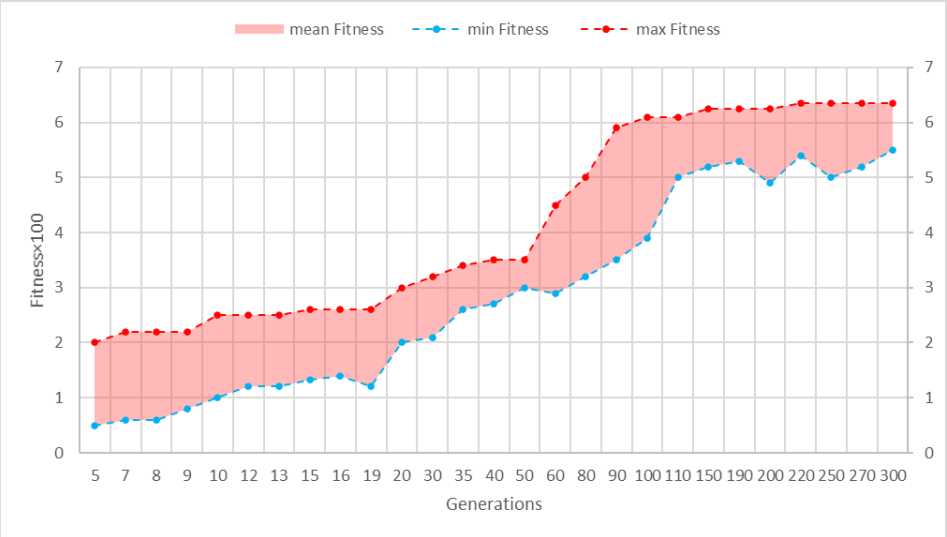

Figure 5-43 *Fitness values over generation for the second scenario*

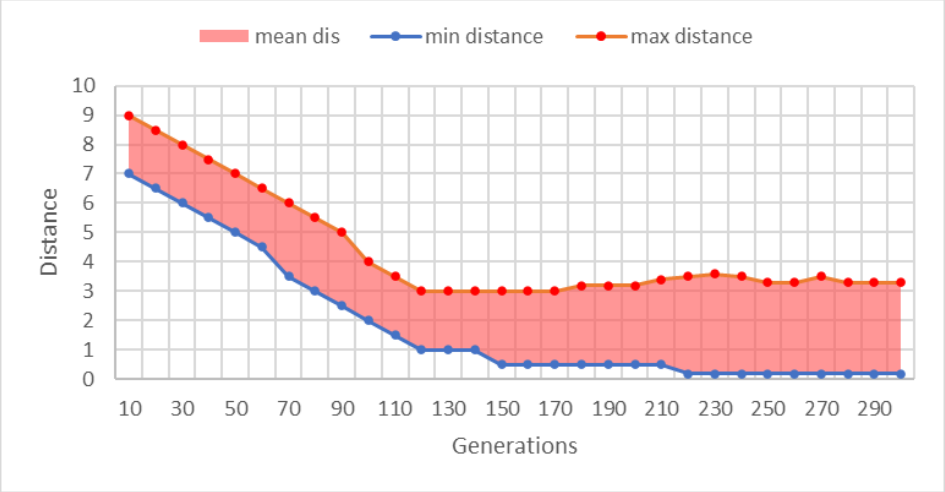

Figure 5-44 *Distance between individuals vs generations for the second scenario*

- Results and discussion

The progression of the population's fitness over the generations displayed in Figure 5-45 provides a detailed look at how the genetic algorithm with sharing improves the overall fitness of the population.

Initial Population (higher right):

- The initial fitness values are relatively low, with a mean fitness starting below 1, indicating that the population is initially exploring the fitness landscape.
- The wide range between the minimum and maximum fitness values shows a diverse population with varying levels of solution quality.

Early Generations (5-70) (higher left)

- During the early generations, the mean fitness increases rapidly, reflecting significant improvements in the population's average solution quality.

- Both the minimum and maximum fitness values also rise, indicating that even the worst-performing individuals are improving, while the best individuals are reaching higher fitness peaks.
- This rapid improvement phase demonstrates the effective exploration and exploitation balance achieved by the genetic algorithm.

Mid Generations (70-150) (lower left):

- In the mid generations, the rate of fitness improvement slows down, but the mean fitness continues to climb steadily.
- The minimum fitness starts to stabilize, while the maximum fitness reaches a plateau, indicating that the algorithm is honing in on high-quality solutions.
- The narrowing gap between minimum and maximum fitness values suggests that the population is becoming more homogeneous in terms of fitness, but diversity is still maintained by the sharing mechanism.

Late Generations (150-300) (lower right):

- In the later generations, the max and mean fitness stabilizes, indicating that the population has reached a point where significant improvements are less frequent.
- The minimum fitness shows a slight increase, suggesting that diversity is still being refined.
- The stability in the fitness values implies that the algorithm has effectively converged, with multiple high-fitness niches being preserved thanks to the sharing mechanism.

The presence of multiple high-fitness peaks at generation 220 confirms that the genetic algorithm with sharing has successfully identified and maintained diverse optimal solutions within the fitness landscape.

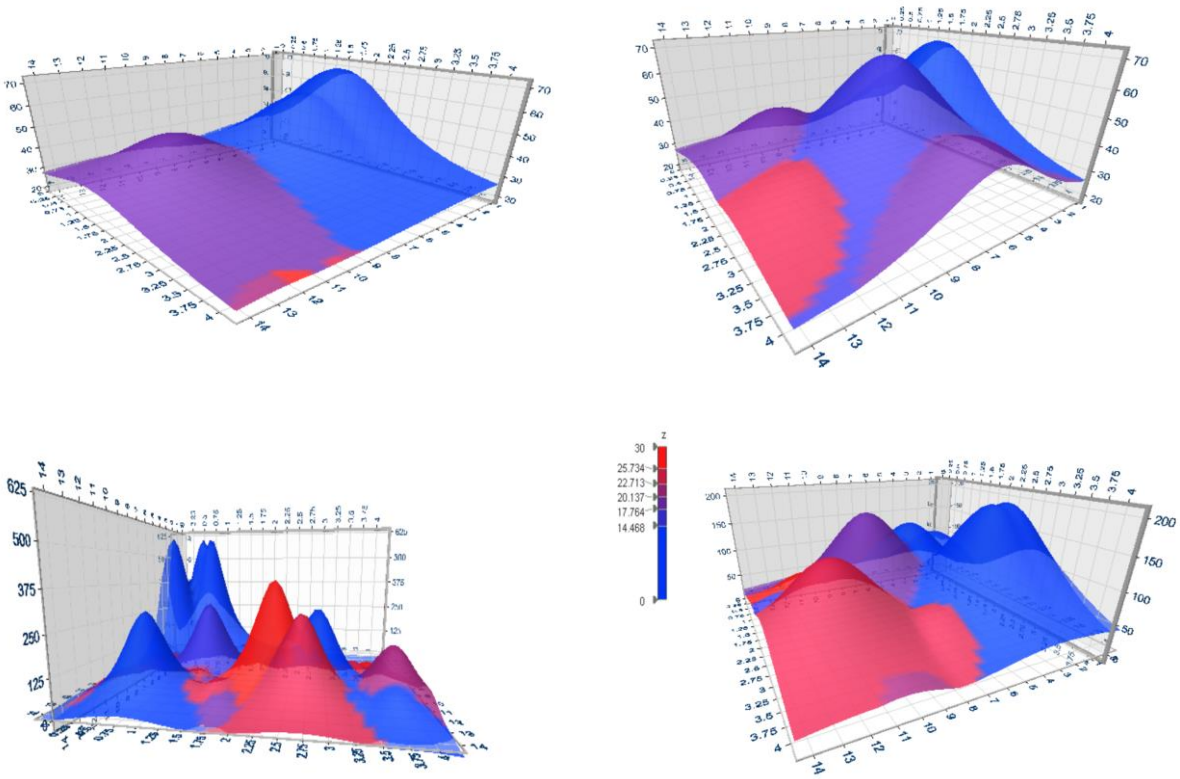

Figure 5-45 *Results and Fitness evolution over generations for the second scenario (initial,60th ,150th and final generations respectively)*

Since, multiple solutions are found, price filtering is used to choose the best solution. *Table 5-19* revealed that composition 3 is the most economical thus preferable composition.

Table 5-19 *Results for the second scenario*

composition	Bentonite	Barite	Al2O3	PAC R	NaOH	Others	Price (DA/ bbl)
1	7%	3%	0%	1.8%	0.5%	0%	3530.5662
2	7%	3%	0.7%	0.7%	0.5%	0%	2084.6028
3	7%	3%	0.5%	0.4%	0.4%	0%	1443.2418

5.4.7.3 *3rd Scenario*

In this scenario, we utilized the second fitness function min-f to minimize the filtration volume for a specified composition. We did not initialize any components; instead, we directly set the desired components to be used.

- Setting up the environment

Same constraints for 2nd scenario were taking but with different more enriched composition.

Table 5-20 *setting up the environment for the genetic algorithm for the third scenario*

NPs size	NPs MW (g/mol)	T (s)	P (Psi)	T (F°)	Solid (%)	Density (ppg)	AV (cPo)	PV (CPo)	YP(lb/100ft^2)	GS10s(lb/100ft^2)	GS10m(lb/100ft^2)
30	81,38	300	200	300	12	10	35 -50	25 -40	25 - 30	5 - 10	15 - 20

Table 5-21 *Desired composition for the third scenario*

Bentonite	Barite	ZnO	KCl	NaCl	PAC R	Others
X	Y	Z	W	L	M	0%

- Tuning results

Table 5-22 *Tuning results for the third scenario*

Population Size	Num of generations	Cross-over operator	Mutation operator	Selection operator
500	660	SBX with η= 15 FR with d = 0.22	RM	RWS

The genetic algorithm with sharing using (***Fmin)*** fitness function, as depicted in Figure 5-46 and Figure 5-47, demonstrates effective convergence towards 7 optimal solutions. Over the generations, the mean, minimum, and maximum fitness values consistently decrease, indicating progressive improvement in the population's solutions. The steady decline in the mean fitness suggests a continual optimization process, while the reduction in minimum fitness values shows the algorithm's ability to identify increasingly better solutions. Concurrently, the distance metrics reveal a decrease in both mean and minimum distances between individuals, signifying that the population is becoming more similar and converging. However, the maximum distance's slower decrease suggests the algorithm maintains its diversity, preventing premature convergence to local optima. Overall, these trends confirm the

algorithm's efficiency in exploring the solution space while ensuring a diverse population, ultimately leading to robust and optimal outcomes.

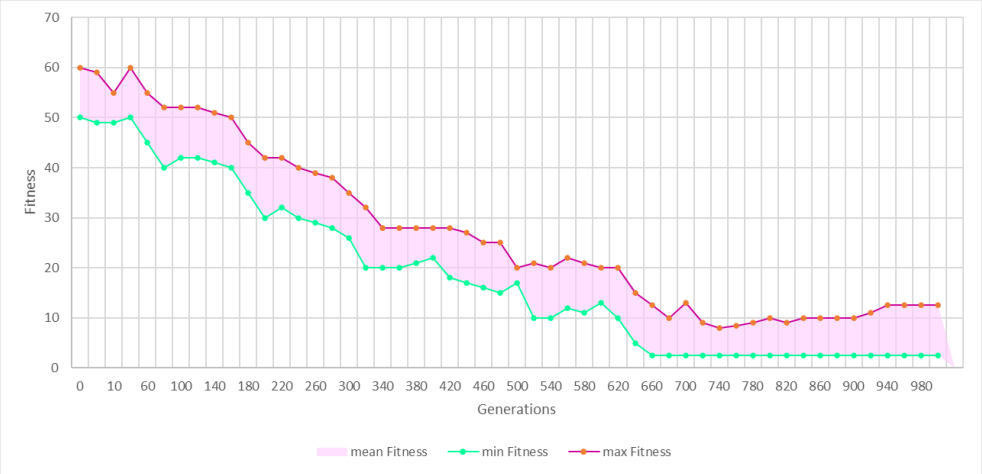

Figure 5-46 *Fitness values over generation for the third scenario*

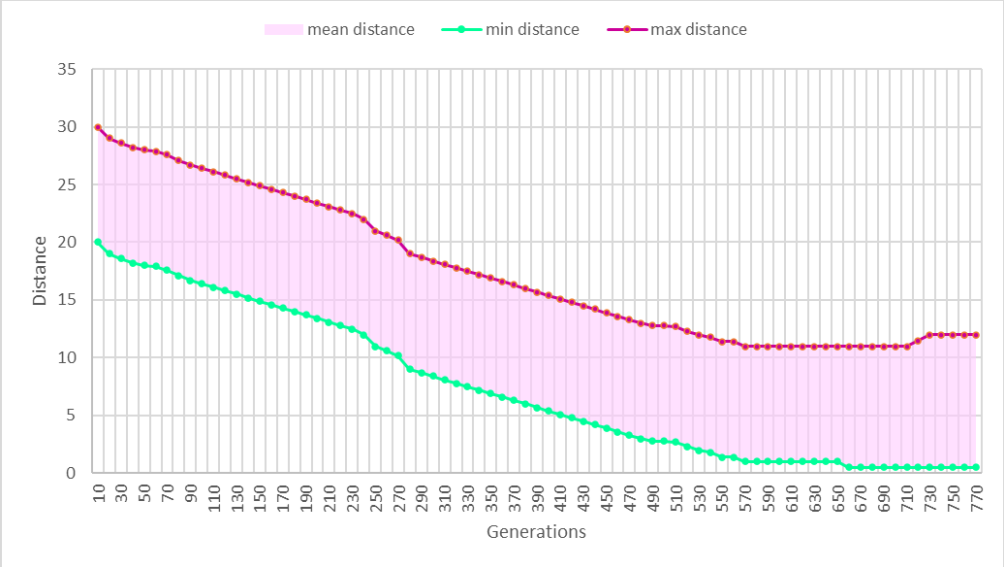

Figure 5-47 *Distance between individuals vs generations for the third scenario*

The model successfully identified several potential solutions with varying compositions and prices. Table 5-23 summarizes the compositions and corresponding prices of the solutions found by the algorithm. Among these, Composition 1 was selected as the ideal choice based on price filtering.

Table 5-23 Resulted compositions for the 3rd Scenario

Composition	Bentonite (%)	Barite (%)	ZnO (%)	KCl (%)	NaCl (%)	PAC R (%)	Others (%)	Price (DA/bbl)
1	6.2	4	0.2	2	2	0.1	0	1351.57344
2	5.6	5	0.3	2.5	1.5	0.2	0	1873.44112
3	6.7	3	0.4	1.5	2	0.4	0	1859.12034

4	4.5	6	0.3	3	1	0.2	0	2055.2511
5	5.3	4.9	0.2	1.5	2.5	0.3	0	1640.92026
6	5	5	0.4	2	1.7	0.1	0	1562.484
7	8	4	0.33	2.6	2	0.25	0	2048.4219

Conclusions

The integration of artificial intelligence (AI) and nanotechnology in drilling engineering, as demonstrated in this thesis, offers promising advancements for optimizing drilling mud properties. Through the development and validation of several predictive models using artificial neural networks (ANNs) and genetic algorithms (GAs) for building the final hybrid INN, this research has established a foundation for enhancing drilling operations. The results obtained from the models, trained on laboratory data, showcase their effectiveness and potential for real-world applications.

- ***Filtrate Model (M-FLT)***

The filtrate volume prediction model, achieved an impressive performance. The model's training results exhibited an average mean squared error (MSE) of 0.095, a mean absolute percentage error (MAPE) of 0.015, and an R^2 of 0.096. When tested with unseen test data, the model showed good agreement, yielding an MSE of 0.0601, a MAPE of 0.016, and an R^2 of 0.999. The high alignment with laboratory experimental results underscores the model's accuracy and reliability in predicting filtrate volumes.

- ***Rheological Properties Models (M-RH)***

Apparent Viscosity Model (M-AV):

- ✓ This model utilized one hidden layer with a soft sign activation function.
- ✓ It achieved an MSE of 0.082, a MAPE of 0.013, and an R^2 of 0.999.
- ✓ These results indicate exceptional performance and high predictive accuracy.

Plastic Viscosity Model (M-PV):

- ✓ Constructed with one hidden layer and tanh activation, this model achieved an MSE of 0.09, a MAPE of 0.024, and an R^2 of 0.97.
- ✓ It outperformed many existing models in the literature, demonstrating its superior predictive capability.

Yield Point Model (M-YP):

- ✓ Utilizing two hidden layers with tanh activation functions, this model produced an MSE of 0.101, an R^2 of 0.972, and a MAPE of 0.025.
- ✓ These metrics confirm the model's strong performance in predicting yield points.

Gel Strength Model (M-GS):

- ✓ This model, with three hidden layers and tanh activation, achieved an MSE of 0.112, a MAPE of 0.015, and an R^2 of 0.985.
- ✓ The results reflect the model's high accuracy and alignment with experimental data.

The combined rheological (M-Rh) model, which integrates the four sub-models for apparent viscosity, plastic viscosity, yield point, and gel strength, also demonstrated high accuracy and strong agreement with real experimental data. This integrated model is particularly valuable for predicting comprehensive rheological properties of drilling muds.

- ***The Hybrid Inverse Model***

The hybrid inverse model, which employs genetic algorithms to optimize mud composition based on desired filtrate volumes and rheological properties, produced excellent results across three scenarios:

Scenario 1:

- ✓ The maximum fitness value was 256, indicating a small error value.
- ✓ The solution converged to the optimal design, selected based on price, with a cost of 127,900.8 DA/bbl.

Scenario 2:

- ✓ The maximum fitness value was approximately 600, indicating an even smaller error value than Scenario 1.
- ✓ The solution converged to the optimal design, chosen based on price, with a cost of 144,324.18 DA/bbl.

Scenario 3:

- ✓ Utilizing the F-min fitness function, the model achieved an enhanced filtration volume of 2.52 ml.
- ✓ The solution converged to seven variant solutions, with the optimal design selected based on the minimum price criterion at 135,157.344 DA/bbl.

General Conclusion

The journey from Edwin Drake's first oil well in Pennsylvania, in 1859 to the sophisticated drilling operations of today highlights the relentless pursuit of innovation in the oil and gas industry. This thesis has explored the transformative impact of integrating nanotechnology and artificial intelligence (AI) into drilling fluids, demonstrating their potential to revolutionize drilling operations.

The initial goal of this research was to identify the optimal concentration of nanoparticles to achieve desired filtration properties at high temperatures. The resulting models have proven to be much more versatile. They are capable of designing a complete drilling mud composition tailored to various conditions set by the user. The AI-driven approach, combined with nanotechnology, allows adjustments and optimization, ensuring optimal performance and efficiency. The main results can be summarized in the following points:

- ✓ The filtrate volume prediction model, with its impressive performance metrics, demonstrated high alignment with laboratory experiments.
- ✓ The rheological properties models for apparent viscosity, plastic viscosity, yield point, and gel strength also showed exceptional predictive capabilities, outperforming many existing models in the literature. The combined rheological model further validated the effectiveness of this approach.
- ✓ The hybrid inverse model, employing genetic algorithms, produced excellent results across multiple scenarios, optimizing mud compositions based on desired outcomes and economic considerations.
- ✓ This innovative approach highlights the potential of AI to revolutionize drilling operations by continuously monitoring and adjusting drilling fluid properties in real-time.

The spirit of innovation and the need of sophisticated drilling technologies drive the oil and gas industry forward. The integration of nanotechnology and AI represents a paradigm shift, addressing longstanding challenges and offering solutions that are more efficient, cost-effective, and environmentally friendly.

The story of drilling fluids is a testament to human ingenuity and the relentless pursuit of improvement. By combining the unique properties of nanoparticles with the analytical power of AI, we are setting new standards for innovation in the industry. The future of drilling holds endless possibilities, promising to be more sustainable, efficient, and transformative than ever before.

Aspects and Future Work

One of the primary limitations of the current study is its reliance on laboratory data. While laboratory conditions provide a controlled environment for initial model development and validation, they do not fully capture the complexities and variability of real-world drilling operations. To bridge this gap, future work should focus on using the same idea but with incorporating real-time data from actual drilling sites. This includes:

Real Filtration Invasion Data: Collecting and integrating data on actual filtration rates and invasion depths in various rock formations encountered during drilling operations. This would enhance the accuracy and applicability of the model in predicting filtration performance under diverse field conditions.

Real lithology and Rock Properties: Incorporating a wide range of rock properties, such as porosity, permeability, and mechanical strength, to better understand how different geological formations interact with the drilling mud. This information is crucial for tailoring mud compositions to specific drilling scenarios.

Real Fluid Dynamics and rheological properties: Gathering data on the actual flow behavior of drilling fluids in the wellbore, considering factors like pressure, temperature, and flow rates. This will enable the development of more sophisticated models that can predict and optimize mud performance in dynamic drilling environments.

Integrating with Logging Data and Real-Time Adjustments: To fully realize the potential of this AI-driven approach, future models should be designed to integrate seamlessly with logging tools and real-time data acquisition systems. This integration would enable continuous monitoring and adjustment of drilling mud properties during drilling operations in real time. Key advancements could include:

- ✓ ***Automated Mud Composition Adjustments:*** Developing algorithms that can automatically adjust the composition of the drilling mud in real-time based on sensor data and predictive model outputs. This would ensure optimal performance and minimize issues such as mud loss, formation damage, and wellbore instability.
- ✓ ***Feedback Loops for Continuous Improvement:*** Implementing feedback loops that continuously update the AI models with new data from ongoing drilling operations. This iterative approach would enhance the models' predictive accuracy and adaptability over time.
- ✓ ***User-Friendly Interfaces:*** Creating user-friendly interfaces that allow drilling engineers to input desired filtration and rheological properties and receive immediate recommendations for mud composition adjustments. This would simplify the decision-making process and improve operational efficiency.

References

[1] C. Zamora-Ledezma, C. Narváez Muñoz, V. Guerrero, E. Medina Dagger, and L. Meseguer-Olmo, "Nanofluid Formulations Based on Two-Dimensional Nanoparticles, Their Performance, and Potential Application as Water-Based Drilling Fluids," *ACS Omega*, vol. 7, p. 20457−20476, Jun. 2022, doi: 10.1021/acsomega.2c02082.

[2] M. L. Barrett, "ABSTRACT: Drilling Mud: A 20th Century History," 2011, Accessed: Jun. 03, 2024. [Online]. Available: https://archives.datapages.com/data/phi/v12_2011/barrett_abs.htm

[3] G. Cheraghian, "Nanoparticles in drilling fluid: A review of the state-of-the-art," *J. Mater. Res. Technol.*, vol. 13, pp. 737–753, Jul. 2021, doi: 10.1016/j.jmrt.2021.04.089.

[4] Z. Vryzas and V. Kelessidis, "Nano-Based Drilling Fluids: A Review," *Energies*, vol. 10, p. 540, Apr. 2017, doi: 10.3390/en10040540.

[5] R. Lee, "Nanomaterial production," Bioeconomy.XYZ. Accessed: Jun. 03, 2024. [Online]. Available: https://medium.com/bioeconomy-xyz/nanomaterial-production-35da92726ec7

[6] "nanoparticles in drilling fluid.pptx," SlideShare. Accessed: Jun. 03, 2024. [Online]. Available: https://www.slideshare.net/slideshow/nanoparticles-in-drilling-fluidpptx/257389965

[7] R. Taghdimi, B. Kaffashi, M. R. Rasaei, M.-S. Dabiri, and A. Hemmati-Sarapardeh, "Formulating a novel drilling mud using bio-polymers, nanoparticles, and SDS and investigating its rheological behavior, interfacial tension, and formation damage," *Sci. Rep.*, vol. 13, p. 12080, Jul. 2023, doi: 10.1038/s41598-023-39257-5.

[8] A. Kanjirakat, A. Carvero, R. Sadr, and M. Amani, *INFLUENCE OF CNT-NANOPARTICLES IN THE FILTRATE CHARACTERISTICS AND FILTER CAKE FORMATION OF A WATER-BASED DRILLING FLUID*. 2020, p. 252. doi: 10.1615/TFEC2020.env.032112.

[9] "The effect of nanoparticles additives on filtration properties of drilling muds with microparticles - IOPscience." Accessed: Jun. 03, 2024. [Online]. Available: https://iopscience.iop.org/article/10.1088/1742-6596/1105/1/012127

[10] O. Mahmoud and H. A. Nasr-El-Din, "Formation-Damage Assessment and Filter-Cake Characterization of Ca-Bentonite Fluids Enhanced with Nanoparticles," *SPE Drill. Complet.*, vol. 36, no. 01, pp. 75–87, Mar. 2021, doi: 10.2118/191155-PA.

[11] A. Utomo, N. J. Alderman, G. A. Padron, and G. Ozcan-Taskin, "Effects of particle concentration and dispersion rheology on the breakup of nanoparticle clusters through ultrasonication," Jan. 2023, doi: 10.1016/j.cherd.2023.01.041'].

[12] C. Martin, A. Nourian, M. Babaie, and G. G. Nasr, "Environmental, health and safety assessment of nanoparticle application in drilling mud – Review," *Geoenergy Sci. Eng.*, vol. 226, Apr. 2023, Accessed: Jun. 03, 2024. [Online]. Available: https://eprints.whiterose.ac.uk/203133/

[13] "[PDF] Application Of Artificial Intelligence Methods In Drilling System Design And Operations: A Review Of The State Of The Art | Semantic Scholar." Accessed: Jun. 05, 2024. [Online]. Available: https://www.semanticscholar.org/paper/Application-Of-Artificial-Intelligence-Methods-In-A-Bello-Holzmann/088850c07e3d592d5b7ad333d4d337ed8fea69dc

[14] H. Yang, G. Shang, X. Li, and Y. Feng, "Application of Artificial Intelligence in Drilling and Completion," 2023. doi: 10.5772/intechopen.112298.

[15] "AI in Oil and Gas Market Size, Share | CAGR of 11.3%," Market.us. Accessed: Jun. 05, 2024. [Online]. Available: https://market.us/report/ai-in-oil-and-gas-market/

[16] "Generative AI in Oil and Gas Market Size and Forecast 2032," MarketResearch.biz. Accessed: Jun. 05, 2024. [Online]. Available: https://marketresearch.biz/report/generative-ai-in-oil-and-gas-market/

[17] B. Beaubouef, “Artificial intelligence applications promise improved drilling efficiency,” Offshore. Accessed: Jun. 05, 2024. [Online]. Available: https://www.offshore-mag.com/drilling-completion/article/14301447/artificial-intelligence-applications-promise-improved-drilling-efficiency

[18] “How AI is Changing The Drilling Industry.” Accessed: Jun. 05, 2024. [Online]. Available: https://www.linkedin.com/pulse/how-ai-changing-drilling-industry-wwt-international

[19] G. Energy, “AI mostly used for predictive maintenance in oil and gas, as per GlobalData poll,” Offshore Technology. Accessed: Jun. 05, 2024. [Online]. Available: https://www.offshore-technology.com/analyst-comment/ai-oil-and-gas-industry/

[20] “How Artificial Intelligence Will Benefit Drilling,” JPT. Accessed: Jun. 05, 2024. [Online]. Available: https://jpt.spe.org/how-artificial-intelligence-will-benefit-drilling

[21] T. Oguntade, T. Ojo, E. Efajemue, B. Oni, and J. Idaka, “Application of ANN in Predicting Water Based Mud Rheology and Filtration Properties,” presented at the SPE Nigeria Annual International Conference and Exhibition, OnePetro, Aug. 2020. doi: 10.2118/203720-MS.

[22] A. Alsabaa, H. Gamal, S. Elkatatny, and A. Abdulraheem, “New correlations for better monitoring the all-oil mud rheology by employing artificial neural networks,” *Flow Meas. Instrum.*, vol. 78, p. 101914, Apr. 2021, doi: 10.1016/j.flowmeasinst.2021.101914.

[23] K. Al-Azani, S. Elkatatny, A. Abdulraheem, and D. Al-Shehri, “Real Time Prediction of the Rheological Properties of Oil-Based Drilling Fluids Using Artificial Neural Networks,” Apr. 2018. doi: 10.2118/192199-MS.

[24] S. Elkatatny and Z. Tariq, “Real Time Prediction of Drilling Fluid Rheological Properties Using Artificial Neural Networks Visible Mathematical Model (White Box),” *J. Pet. Sci. Eng.*, vol. 146, Aug. 2016, doi: 10.1016/j.petrol.2016.08.021.

[25] “Recent Advances and Challenges of the Application of Artificial Intelligence to Predict Wellbore Instabilities during Drilling Operations | SPE Drilling & Completion | OnePetro.” Accessed: Jun. 05, 2024. [Online]. Available: https://onepetro.org/DC/article-abstract/38/04/645/520772/Recent-Advances-and-Challenges-of-the-Application?redirectedFrom=fulltext

[26] “A comprehensive modeling in predicting the effect of various nanoparticles on filtration volume of water-based drilling fluids.” Accessed: Jun. 01, 2024. [Online]. Available: https://www.researchgate.net/publication/335752455_A_comprehensive_modeling_in_predicting_the_effect_of_various_nanoparticles_on_filtration_volume_of_water-based_drilling_fluids

[27] “On the prediction of filtration volume of drilling fluids containing different types of nanoparticles by ELM and PSO-LSSVM based models - ScienceDirect.” Accessed: Jun. 01, 2024. [Online]. Available: https://www.sciencedirect.com/science/article/pii/S2405656121000274?ref=pdf_download&fr=RR-2&rr=88cf1c09cf7d2820

[28] M. Gasser, A. Naguib, M. Abdelhafiz, S. Elnekhaily, and O. Mahmoud, “Artificial Neural Network Model to Predict Filtrate Invasion of Nanoparticle-Based Drilling Fluids,” *Trends Sci.*, vol. 20, no. 5, Art. no. 5, Mar. 2023, doi: 10.48048/tis.2023.6736.

[29] “An Experiment-Based Study of Formation Damage Using a Microetching Model Displacement Method.” Accessed: Jun. 05, 2024. [Online]. Available: https://www.researchgate.net/publication/358600263_An_Experiment-Based_Study_of_Formation_Damage_Using_a_Microetching_Model_Displacement_Method

[30] C. Pedrosa, A. Saasen, and J. D. Ytrehus, “Fundamentals and Physical Principles for Drilled Cuttings Transport—Cuttings Bed Sedimentation and Erosion,” *Energies*, vol. 14, no. 3, Art. no. 3, Jan. 2021, doi: 10.3390/en14030545.

[31] “Drilling Mud Laboratory,” SlideShare. Accessed: Jun. 06, 2024. [Online]. Available: https://www.slideshare.net/slideshow/drilling-mud-laboratory/35592771

[32] “Functions of drilling fluid,” PetroWiki. Accessed: Jun. 05, 2024. [Online]. Available: https://petrowiki.spe.org/Functions_of_drilling_fluid

[33] “Xanthan Suspensions | Resolute Oil.” Accessed: Jun. 06, 2024. [Online]. Available: https://resoluteoil.com/applications/oil-and-gas/xanthan-suspensions/

[34] “Examining the current of drilling mud in a power section of the screw down-hole motor.” Accessed: Jun. 06, 2024. [Online]. Available: https://www.researchgate.net/publication/324844849_Examining_the_current_of_drilling_mud_in_a_power_section_of_the_screw_down-hole_motor

[35] A. Khalil and M. Adnan, “Effect of Mud Rheology on Cuttings’ Transport in Drilling Operations,” *IOP Conf. Ser. Mater. Sci. Eng.*, vol. 671, p. 012067, Jan. 2020, doi: 10.1088/1757-899X/671/1/012067.

[36] J. Wu, R. Wang, R. Zhang, and F. Sun, “Propagation model with multi-boundary conditions for periodic mud pressure wave in long wellbore,” *Appl. Math. Model.*, vol. 39, May 2015, doi: 10.1016/j.apm.2015.04.030.

[37] K. Abou Alfa, R. Harkouss, J. Khatib, K. Abou Alfa, K. Harkouss, and R. Khatib, “SIDERITE AS A WEIGHTING MATERIAL IN DRILLING MUD,” *BAU J. - Sci. Technol.*, vol. 1, Jan. 2019, doi: 10.54729/2959-331X.1002.

[38] “(PDF) The impact of different concentrations of viscosifiers on rheological properties of invert emulsion mud,” ResearchGate. Accessed: Jun. 13, 2024. [Online]. Available: https://www.researchgate.net/publication/326158430_The_impact_of_different_concentrations_of_viscosifiers_on_rheological_properties_of_invert_emulsion_mud

[39] J. Nwaiche, *Selection and Application of Drilling Fluids*. 2015. doi: 10.13140/RG.2.1.3243.4722.

[40] “Drilling muds - ScienceDirect.” Accessed: Jun. 13, 2024. [Online]. Available: https://www.sciencedirect.com/science/article/abs/pii/B9780323854382000013

[41] R. Farhan Hussain, A. Mokhtari, A. Ghalambor, and M. Amini Salehi, “Chapter 2 - Smart upstream sector: Smartness in upstream sector of the oil and gas industry,” in *IoT for Smart Operations in the Oil and Gas Industry*, R. Farhan Hussain, A. Mokhtari, A. Ghalambor, and M. Amini Salehi, Eds., Gulf Professional Publishing, 2023, pp. 19–56. doi: 10.1016/B978-0-32-391151-1.00011-3.

[42] G. DeBruijn and S. M. Whitton, “Chapter Five - Fluids,” in *Applied Well Cementing Engineering*, G. Liu, Ed., Gulf Professional Publishing, 2021, pp. 163–251. doi: 10.1016/B978-0-12-821956-0.00012-2.

[43] “Tipos de Flujo y Modelos Reológicos en el Lodo – Perfoblogger.” Accessed: Jun. 14, 2024. [Online]. Available: https://perfoblogger.wordpress.com/2020/09/05/tipos-de-flujo-y-modelos-reologicos-en-el-lodo/

[44] “Drilling Fluid Properties.” Accessed: Jun. 14, 2024. [Online]. Available: https://www.drillingformulas.com/drilling-fluid-properties/

[45] “Non-Newtonian Fluids - FluidFlow | FluidFlow.” Accessed: Jun. 14, 2024. [Online]. Available: https://blog.fluidflowinfo.com/non-newtonian-fluids

[46] C. K. Ferguson and J. A. Klotz, “Filtration From Mud During Drilling,” *J. Pet. Technol.*, vol. 6, no. 02, pp. 30–43, Feb. 1954, doi: 10.2118/289-G.

[47] M. Khodja, “Les fluides de forage : étude des performances et considérations environnementales,” Jan. 2008.

[48] "The SLB Energy Glossary | Energy Glossary." Accessed: Jun. 14, 2024. [Online]. Available: https://glossary.slb.com/

[49] M. Khalid and W. Pao, *Investigating the Effect of Fluid and Formation Parameters on Mud Cake Thickness, Filtration Velocity and Invasion Depth*. 2014. doi: 10.13140/RG.2.2.31455.25768.

[50] M. Magzoub, S. Salehi, I. Hussein, and M. Nasser, "Investigation of Filter Cake Evolution in Carbonate Formation Using Polymer-Based Drilling Fluid," *ACS Omega*, vol. XXXX, Feb. 2021, doi: 10.1021/acsomega.0c05802.

[51] B. Bennion, "Formation Damage-The Impairment of the Invisible, By the Inevitable And Uncontrollable, Resulting In an Indeterminate Reduction of the Unquantifiable!," *J. Can. Pet. Technol.*, vol. 38, no. 02, Feb. 1999, doi: 10.2118/99-02-DA.

[52] "Wll logging," SlideShare. Accessed: Jun. 14, 2024. [Online]. Available: https://www.slideshare.net/slideshow/wll-logging-67229527/67229527

[53] J. Zhang, "Effects of Porosity and Permeability on Invasion Depth During Drilling Mud-filtrate Invading into a Reservoir Dynamically," presented at the 7th International Conference on Education, Management, Information and Mechanical Engineering (EMIM 2017), Atlantis Press, Apr. 2017, pp. 203–206. doi: 10.2991/emim-17.2017.44.

[54] Q. Li *et al.*, "Effect of reservoir characteristics and chemicals on filtration property of water-based drilling fluid in unconventional reservoir and mechanism disclosure," *Environ. Sci. Pollut. Res.*, vol. 30, no. 19, pp. 55034–55043, Apr. 2023, doi: 10.1007/s11356-023-26279-9.

[55] R. and Innovation, "Temperature-Dependent Properties of Drilling Fluid: A Comparative Study of the Effect of…," Medium. Accessed: Jun. 14, 2024. [Online]. Available: https://medium.com/@rnispe2023/temperature-dependent-properties-of-drilling-fluid-a-comparative-study-of-the-effect-of-99967536d842

[56] "Filtrate Control - an overview | ScienceDirect Topics." Accessed: Jun. 20, 2024. [Online]. Available: https://www.sciencedirect.com/topics/engineering/filtrate-control

[57] S. Rehan, "Nanotechnology's Potential to Resolve Drill-Fluid Problems in Oil and Gas Industry," AZoNano. Accessed: May 18, 2024. [Online]. Available: https://www.azonano.com/news.aspx?newsID=38693

[58] "Nanotechnology for the oil and gas industry – an overview of recent progress." Accessed: May 18, 2024. [Online]. Available: https://www.degruyter.com/document/doi/10.1515/ntrev-2018-0061/html?lang=en

[59] "Nanotechnology Research and Development in Upstream Oil and Gas - Boul - 2020 - Energy Technology - Wiley Online Library." Accessed: May 18, 2024. [Online]. Available: https://onlinelibrary.wiley.com/doi/full/10.1002/ente.201901216

[60] K. A. Altammar, "A review on nanoparticles: characteristics, synthesis, applications, and challenges," *Front. Microbiol.*, vol. 14, 2023, doi: 10.3389/fmicb.2023.1155622.

[61] "Nanomaterials: a review of synthesis methods, properties, recent progress, and challenges - Materials Advances (RSC Publishing) DOI:10.1039/D0MA00807A." Accessed: Jun. 19, 2024. [Online]. Available: https://pubs.rsc.org/en/content/articlehtml/2021/ma/d0ma00807a

[62] "(PDF) Nanoparticles: Structure, Properties, Preparation and Behaviour in Environmental Media." Accessed: Jun. 19, 2024. [Online]. Available: https://www.researchgate.net/publication/5394035_Nanoparticles_Structure_Properties_Preparation_and_Behaviour_in_Environmental_Media?enrichId=rgreq-11003a0e8e593d24f8772e79428126e4-XXX&enrichSource=Y292ZXJQYWdlOzUzOTQwMzU7QVM6MTE1NDM3NzIzNDU5NTg0QDE0MDQ1MzM5MDY4MzU%3D&el=1_x_3&_esc=publicationCoverPdf

[63] L. McDowell-Boyer, J. Hunt, and N. Sitar, “Particle Transport Through Porous Media,” *Water Resour. Res. - WATER RESOUR RES*, vol. 22, pp. 1901–1921, Dec. 1986, doi: 10.1029/WR022i013p01901.

[64] “Transport of nanoparticles in porous media and associated environmental impact: A review. - ScienceDirect.” Accessed: Jun. 19, 2024. [Online]. Available: https://www.sciencedirect.com/science/article/pii/S2307187724000063

[65] J. Foroozesh and S. Kumar, “Nanoparticles behaviors in porous media: Application to enhanced oil recovery,” *J. Mol. Liq.*, vol. 316, p. 113876, Oct. 2020, doi: 10.1016/j.molliq.2020.113876.

[66] “iwasaki 1937 some nites on sand filtration - Recherche Google.” Accessed: Jun. 19, 2024. [Online]. Available: https://www.google.com/search?q=iwasaki+1937+some+nites+on+sand+filtration&oq=IWA&gs_lcrp=EgZjaHJvbWUqBggBEEUYOzIGCAAQRRg5MgYIARBFGDsyBggCEEUYQTIGCAMQRRhBMgYIBBBFGEEyBggFEC4YQNIBCDI0MjNqMGo0qAIAsAIB&sourceid=chrome&ie=UTF-8

[67] Yao K-M, “Influence of suspended particle size on the transport aspect of water filtration.,” 1968.

[68] Yao K-M Habbibian MT, O’Melia CR, “Water and wastewater filtration: concepts and applications.,” 1971.

[69] R. Rajagopalan and C. Tien, “Trajectory Analysis of Deep Bed Filtration Using Sphere-in-Cell Porous Media Model,” *AIChE J.*, vol. 22, pp. 523–533, May 1976, doi: 10.1002/aic.690220316.

[70] Stumm W, Morgan JJ, “Aquatic chemistry. Chemical equilibria and rates in natural waters,” 1996.

[71] Ruckenstein E, Prieve DC, “Rate of deposition of Brownian particles under action of London and double-layer forces.,” 1973.

[72] “A comprehensive review of nanoparticles applications in the oil and gas industry | Journal of Petroleum Exploration and Production Technology.” Accessed: May 18, 2024. [Online]. Available: https://link.springer.com/article/10.1007/s13202-019-00825-z

[73] A. Sircar, K. Rayavarapu, N. Bist, K. Yadav, and S. Singh, “Applications of nanoparticles in enhanced oil recovery,” *Pet. Res.*, vol. 7, no. 1, pp. 77–90, Mar. 2022, doi: 10.1016/j.ptlrs.2021.08.004.

[74] “Impact of Nanotechnology on Enhanced Oil Recovery: A Mini-Review | Industrial & Engineering Chemistry Research.” Accessed: May 18, 2024. [Online]. Available: https://pubs.acs.org/doi/10.1021/acs.iecr.9b03693

[75] “Nanotechnology Impact on Chemical-Enhanced Oil Recovery: A Review and Bibliometric Analysis of Recent Developments | ACS Omega.” Accessed: May 18, 2024. [Online]. Available: https://pubs.acs.org/doi/10.1021/acsomega.3c06206

[76] “Experimental and field applications of nanotechnology for enhanced oil recovery purposes: A review - ScienceDirect.” Accessed: May 18, 2024. [Online]. Available: https://www.sciencedirect.com/science/article/abs/pii/S0016236122015174?via%3Dihub

[77] “Nanomaterials | Free Full-Text | Nanoparticles in Chemical EOR: A Review on Flooding Tests.” Accessed: May 18, 2024. [Online]. Available: https://www.mdpi.com/2079-4991/12/23/4142

[78] B. Peng *et al.*, “A review of nanomaterials for nanofluid enhanced oil recovery,” *RSC Adv.*, vol. 7, no. 51, pp. 32246–32254, Jun. 2017, doi: 10.1039/C7RA05592G.

[79] L. Hendraningrat and O. Torsæter, “Effects of the Initial Rock Wettability on Silica-Based Nanofluid-Enhanced Oil Recovery Processes at Reservoir Temperatures,” *Energy Fuels*, vol. 28, no. 10, pp. 6228–6241, Oct. 2014, doi: 10.1021/ef5014049.

[80] A. Dehghan Monfared, M. H. Ghazanfari, M. Jamialahmadi, and A. Helalizadeh, "The Potential Application of Silica Nanoparticles for Wettability Alteration of Oil-Wet Calcite: A Mechanistic Study," *Energy Fuels*, vol. 30, Apr. 2016, doi: 10.1021/acs.energyfuels.6b00477.

[81] T. A. Chandio, M. A. Manan, K. R. Memon, G. Abbas, and G. R. Abbasi, "Enhanced Oil Recovery by Hydrophilic Silica Nanofluid: Experimental Evaluation of the Impact of Parameters and Mechanisms on Recovery Potential," *Energies*, vol. 14, no. 18, Art. no. 18, Jan. 2021, doi: 10.3390/en14185767.

[82] S. Al-Anssari, A. Barifcani, S. Wang, L. Maxim, and S. Iglauer, "Wettability alteration of oil-wet carbonate by silica nanofluid," *J. Colloid Interface Sci.*, vol. 461, pp. 435–442, Jan. 2016, doi: 10.1016/j.jcis.2015.09.051.

[83] R. O. Afolabi, "Enhanced oil recovery for emergent energy demand: challenges and prospects for a nanotechnology paradigm shift," *Int. Nano Lett.*, vol. 9, no. 1, pp. 1–15, Mar. 2019, doi: 10.1007/s40089-018-0248-0.

[84] T. A. Chandio, M. A. Manan, K. R. Memon, G. Abbas, and G. R. Abbasi, "Enhanced Oil Recovery by Hydrophilic Silica Nanofluid: Experimental Evaluation of the Impact of Parameters and Mechanisms on Recovery Potential," *Energies*, vol. 14, no. 18, Art. no. 18, Jan. 2021, doi: 10.3390/en14185767.

[85] "Viscosity Reduction of Heavy Oil Using Nanocatalyst in Aquathermolysis Reaction." Accessed: May 18, 2024. [Online]. Available: https://www.jstage.jst.go.jp/article/kona/33/0/33_2016005/_html/-char/en

[86] "(PDF) On the Role of Water in Natural-Zeolite-Catalyzed Cracking of Athabasca Oilsands Bitumen." Accessed: May 18, 2024. [Online]. Available: https://www.researchgate.net/publication/262068366_On_the_Role_of_Water_in_Natural-Zeolite-Catalyzed_Cracking_of_Athabasca_Oilsands_Bitumen

[87] "(PDF) Use of Nickel Nanoparticles for Promoting Aquathermolysis Reaction During Cyclic Steam Stimulation." Accessed: May 18, 2024. [Online]. Available: https://www.researchgate.net/publication/318334009_Use_of_Nickel_Nanoparticles_for_Promoting_Aquathermolysis_Reaction_During_Cyclic_Steam_Stimulation

[88] M. Tajmiri and M. R. Ehsani, "The Potential of ZnO Nanoparticles to Reduce Water Consuming in Iranian Heavy Oil Reservoir," *J. Water Environ. Nanotechnol.*, vol. 1, no. 2, pp. 84–90, Nov. 2016, doi: 10.7508/jwent.2016.02.002.

[89] "Effect of Fe2O3 and WO3 nanoparticle on steam injection recovery | Dr. Mohammad Reza Ehsani." Accessed: May 18, 2024. [Online]. Available: https://ehsani.iut.ac.ir/effect-fe2o3-and-wo3-nanoparticle-steam-injection-recovery

[90] "Impact of Nanotechnology on Enhanced Oil Recovery: A Mini-Review." Accessed: Jun. 08, 2024. [Online]. Available: https://www.researchgate.net/publication/335144433_Impact_of_Nanotechnology_on_Enhanced_Oil_Recovery_A_Mini-Review

[91] O. Tavakkoli, H. Kamyab, M. Shariati, A. Mustafa Mohamed, and R. Junin, "Effect of nanoparticles on the performance of polymer/surfactant flooding for enhanced oil recovery: A review," *Fuel*, vol. 312, p. 122867, Mar. 2022, doi: 10.1016/j.fuel.2021.122867.

[92] A. Z. Abidin, T. Puspasari, and W. A. Nugroho, "Polymers for Enhanced Oil Recovery Technology," *Procedia Chem.*, vol. 4, pp. 11–16, Jan. 2012, doi: 10.1016/j.proche.2012.06.002.

[93] S. A. Farzaneh and M. Sohrabi, "A Review of the Status of Foam Application in Enhanced Oil Recovery," Jun. 2013, doi: 10.2118/164917-MS.

[94] "Energies | Free Full-Text | Aqueous Hybrids of Silica Nanoparticles and Hydrophobically Associating Hydrolyzed Polyacrylamide Used for EOR in High-Temperature and High-Salinity

Reservoirs." Accessed: May 18, 2024. [Online]. Available: https://www.mdpi.com/1996-1073/7/6/3858

[95] "(PDF) Enhanced Oil Recovery Using Polymer/nanosilica." Accessed: May 18, 2024. [Online]. Available: https://www.researchgate.net/publication/283984166_Enhanced_Oil_Recovery_Using_Polymernanosilica

[96] "Improving heavy oil recovery in the polymer flooding process by utilizing hydrophilic silica nanoparticles | Request PDF." Accessed: May 18, 2024. [Online]. Available: https://www.researchgate.net/publication/316077821_Improving_heavy_oil_recovery_in_the_polymer_flooding_process_by_utilizing_hydrophilic_silica_nanoparticles

[97] "Effect of nano titanium dioxide on heavy oil recovery during polymer flooding: Petroleum Science and Technology: Vol 34 , No 7 - Get Access." Accessed: May 18, 2024. [Online]. Available: https://www.tandfonline.com/doi/full/10.1080/10916466.2016.1156125

[98] "Hybrid suspension of polymer and nanoparticles for enhanced oil recovery | Polymer Bulletin." Accessed: May 18, 2024. [Online]. Available: https://link.springer.com/article/10.1007/s00289-019-02713-2

[99] Munshi, A. M.; Singh, V. N.; Kumar, M.; Singh, J. P., "Effect of nanoparticle size on sessile droplet contact angle.," *J Appl Phys*, 2008.

[100] Ravera, F.; Santini, E.; Loglio, G.; Ferrari, M.; Liggieri, L., "Effect of Nanoparticles on the Interfacial Properties of Liquid/Liquid and Liquid/Air Surface Layers.," *J Phys Chem B*, 2006.

[101] Barron, A. R.Cheraghian, G.; Kiani, S.; Nassar, N. N.; Alexander, S.;, "Silica Nanoparticle Enhancement in the Efficiency of Surfactant Flooding of Heavy Oil in a Glass Micromodel.," *Ind Eng Chem Res*, 2017.

[102] Ahmed, A.; Saaid, I. M.; Pilus, R. M.; Ahmed, A. A.; Tunio, A. and H.; Baig, M. K., "Development of surface treated nanosilica for wettability alteration and interfacial tension reduction.," *J Dispers. Sci Technol 2018*.

[103] Cheraghian, G., "Effects of titanium dioxide nanoparticles on the efficiency of surfactant flooding of heavy oil in a glass micromodel," *Pet Sci Technol*, 2016.

[104] Zaid, H. M.; Latiff, N. R. A.; Yahya, N., "The Effect of Zinc Oxide and Aluminum Oxide Nanoparticles on Interfacial Tension and Viscosity of Nanofluids for Enhanced Oil Recovery," *Adv Mater Res*, 2014.

[105] A. Rezaei, M. Riazi, M. Escrochi, and R. Elhaei, "Integrating surfactant, alkali and nano-fluid flooding for enhanced oil recovery: A mechanistic experimental study of novel chemical combinations," *J. Mol. Liq.*, vol. 308, p. 113106, Jun. 2020, doi: 10.1016/j.molliq.2020.113106.

[106] Fakoya M.F., Shah S.N., "Emergence of nanotechnology in the oil and gas industry: Emphasis on the application of silica nanoparticles," *Pet. 3*, 2017.

[107] Taoutaou S., Goh S.H., Bermea J.A.V., Vinaipanit M., and McClure J., "Achieving zonal isolation by using new generation mud removal chemistry and design methodology to displace non-aqueous drilling fluid," *Soc. Pet. Eng.*, 2015.

[108] Dwight K.S., *Cementing, Second printing, SPE, New York City.* 1990.

[109] Santra A.K., Boul P., Pang X., "Influence of nanomaterials in oilwell cement hydration and mechanical properties," *SPE Int. Oilfield Nanotechnol. Conf Exh Noordwijk Neth.*, 2012.

[110] Chithra S., Kumar S., Chinnaraju K., "The effect of colloidal nano-silica on workability, mechanical and durability properties of high performance concrete with copper slag as partial fine aggregate," 2016.

[111] M. T. Maagi and G. Jun, “Application of nanoparticles for strengthening wellbore cement-formation bonding,” *Oil Gas Sci. Technol. - Rev. IFP Energ. Nouv.*, vol. 75, p. 64, 2020, doi: 10.2516/ogst/2020052.

[112] i Thomas Maagi, Gu Jun., “Application of nanoparticles for strengthening wellbore cement formation bonding.,” *Oil Gas Sci. Technol. - Rev. D’IFP Energ. Nouv. 2020 75 Pp64 Ff102516ogst2020052ff Ffhal-02949707f*, 2022.

[113] Silvestre J.P.T., “Nanotechnology in construction: Towards structural applications,” *MSc Thesis Lisbon Univ. Technol. Lisbon Port.*, 2015.

[114] M. T. Alsaba, M. F. Al Dushaishi, and A. K. Abbas, “A comprehensive review of nanoparticles applications in the oil and gas industry,” *J. Pet. Explor. Prod. Technol.*, vol. 10, no. 4, pp. 1389–1399, Apr. 2020, doi: 10.1007/s13202-019-00825-z.

[115] S. Linley *et al.*, “Targeted nanoparticle binding & detection in petroleum hydrocarbon impacted porous media,” *Chemosphere*, vol. 215, pp. 353–361, Jan. 2019, doi: 10.1016/j.chemosphere.2018.10.046.

[116] A. El-Diasty and A. Salem, *Applications of Nanotechnology in the Oil & Gas Industry: Latest Trends Worldwide & Future Challenges in Egypt*, vol. 2. 2013. doi: 10.2118/164716-MS.

[117] M. T. Alsaba, M. F. Al Dushaishi, and A. K. Abbas, “A comprehensive review of nanoparticles applications in the oil and gas industry,” *J. Pet. Explor. Prod. Technol.*, vol. 10, no. 4, pp. 1389–1399, Apr. 2020, doi: 10.1007/s13202-019-00825-z.

[118] A. H. Abdullah *et al.*, “A comprehensive review of nanoparticles: Effect on water-based drilling fluids and wellbore stability,” *Chemosphere*, vol. 308, no. Pt 1, p. 136274, Dec. 2022, doi: 10.1016/j.chemosphere.2022.136274.

[119] Z. Tahr, J. A. Ali, and A. S. Mohammed, “Sustainable aspects behind nano-biodegradable drilling fluids: A critical review,” *Geoenergy Sci. Eng.*, vol. 222, p. 211443, Mar. 2023, doi: 10.1016/j.geoen.2023.211443.

[120] R. Rafati, S. R. Smith, A. Sharifi Haddad, R. Novara, and H. Hamidi, “Effect of nanoparticles on the modifications of drilling fluids properties: A review of recent advances,” *J. Pet. Sci. Eng.*, vol. 161, pp. 61–76, Feb. 2018, doi: 10.1016/j.petrol.2017.11.067.

[121] “A comprehensive review of nanoparticles: Effect on water-based drilling fluids and wellbore stability - PubMed.” Accessed: Jun. 08, 2024. [Online]. Available: https://pubmed.ncbi.nlm.nih.gov/36058368/

[122] “Wellbore instability: Causes and consequences.” Accessed: Jun. 08, 2024. [Online]. Available: https://www.researchgate.net/publication/26494059_Wellbore_instability_Causes_and_consequences

[123] J. Xu, Z. Qiu, X. Zhao, H. Zhong, G. Li, and W. Huang, “Synthesis and characterization of shale stabilizer based on polyethylene glycol grafted nano-silica composite in water-based drilling fluids,” *J. Pet. Sci. Eng.*, vol. 163, Apr. 2018, doi: 10.1016/j.petrol.2018.01.007.

[124] “Smart Pickering Water-in-Oil Emulsion by Manipulating Interactions between Nanoparticles and Surfactant as Potential Oil-Based Drilling Fluid.” Accessed: Jun. 08, 2024. [Online]. Available: https://www.researchgate.net/publication/337349823_Smart_Pickering_Water-in-Oil_Emulsion_by_Manipulating_Interactions_between_Nanoparticles_and_Surfactant_as_Potential_Oil-Based_Drilling_Fluid

[125] “Effect of Nano ZnO on wellbore stability in shale: An experimental investigation | Ali Nakhaee - Academia.edu.” Accessed: Jun. 08, 2024. [Online]. Available: https://www.academia.edu/84358501/Effect_of_Nano_ZnO_on_wellbore_stability_in_shale_An_experimental_investigation?uc-sb-sw=21956560

[126] C. Zamora-Ledezma, C. Narváez Muñoz, V. Guerrero, E. Medina Dagger, and L. Meseguer-Olmo, “Nanofluid Formulations Based on Two-Dimensional Nanoparticles, Their Performance,

and Potential Application as Water-Based Drilling Fluids," *ACS Omega*, vol. 7, p. 20457−20476, Jun. 2022, doi: 10.1021/acsomega.2c02082.

[127] "Jagar A.Ali Araz Bayaz Hamadamin Shwan Mohamed *Energy Fuels*, Feb. 2022, Accessed: Jun. 08, 2024. [Online]. Available: https://www.researcher-app.com/paper/10419854

[128] "Jeffrey O.Oseh Norddin MNA Mohd Afeez O. GbadamosiPolymer nanocomposites application in drilling fluids: A review - ScienceDirect." Accessed: Jun. 08, 2024. [Online]. Available: https://www.sciencedirect.com/science/article/abs/pii/S2949891023000027

[129] E. I. Mikhienkova, A. V. Minakov, V. A. Zhigarev, and A. V. Matveev, "The effect of nanoparticles additives on filtration properties of drilling muds with microparticles," *J. Phys. Conf. Ser.*, vol. 1105, no. 1, p. 012127, Nov. 2018, doi: 10.1088/1742-6596/1105/1/012127.

[130] E. Veisi, M. Hajipour, and E. B. Delijani, "Experimental study on thermal, rheological and filtration control characteristics of drilling fluids: effect of nanoadditives," *Oil Gas Sci. Technol. – Rev. D'IFP Energ. Nouv.*, vol. 75, p. 36, 2020, doi: 10.2516/ogst/2020033.

[131] S. Ponmani, R. . Nagarajan, and J. S. Sangwai, "Effect of Nanofluids of CuO and ZnO in Polyethylene Glycol and Polyvinylpyrrolidone on the Thermal, Electrical, and Filtration-Loss Properties of Water-Based Drilling Fluids," *SPE J.*, vol. 21, no. 02, pp. 405–415, Apr. 2016, doi: 10.2118/178919-PA.

[132] Z. Vryzas and V. C. Kelessidis, "Nano-Based Drilling Fluids: A Review," *Energies*, vol. 10, no. 4, Art. no. 4, Apr. 2017, doi: 10.3390/en10040540.

[133] "An Introduction To Machine Learning - Mycloudplace." Accessed: Jun. 19, 2024. [Online]. Available: https://mycloudplace.com/an-introduction-to-machine-learning/

[134] "Deep Learning: A Comprehensive Overview on Techniques, Taxonomy, Applications and Research Directions | SN Computer Science." Accessed: Jun. 19, 2024. [Online]. Available: https://link.springer.com/article/10.1007/s42979-021-00815-1

[135] "LinkedIn." Accessed: Jun. 19, 2024. [Online]. Available: https://www.linkedin.com/posts/rukshan-manorathna-700a3916b_systematic-classification-of-neural-network-activity-7198197362526228481-8iKw

[136] "Machine Learning and Data Science in the Oil and Gas Industry: Best Practices, Tools, and Case Studies 0128207140, 9780128207147 - DOKUMEN.PUB." Accessed: Jun. 19, 2024. [Online]. Available: https://dokumen.pub/machine-learning-and-data-science-in-the-oil-and-gas-industry-best-practices-tools-and-case-studies-0128207140-9780128207147.html

[137] "(PDF) Solving Inverse Kinematics Using Neural Networks." Accessed: Jun. 19, 2024. [Online]. Available: https://www.researchgate.net/publication/344705494_Solving_Inverse_Kinematics_Using_Neural_Networks/figures?lo=1&utm_source=google&utm_medium=organic

[138] "Neural Network Design (2nd Edition): Hagan, Martin T, Demuth, Howard B, Beale, Mark H, De Jesús, Orlando: 9780971732117: Amazon.com: Books." Accessed: Jun. 20, 2024. [Online]. Available: https://www.amazon.com/Neural-Network-Design-Martin-Hagan/dp/0971732116

[139] H. Jacobsson, "Inversion of an Artificial Neural Network Mapping by Evolutionary Algorithms with Sharing".

[140] "(PDF) A Hybrid Multi-Objective Evolutionary Algorithm Using an Inverse Neural Network." Accessed: Jun. 19, 2024. [Online]. Available: https://www.researchgate.net/publication/221411175_A_Hybrid_Multi-Objective_Evolutionary_Algorithm_Using_an_Inverse_Neural_Network

[141] J. Kindermann and A. Linden, "Inversion of neural networks by gradient descent," *Parallel Comput.*, vol. 14, no. 3, pp. 277–286, Aug. 1990, doi: 10.1016/0167-8191(90)90081-J.

[142] J. J. Grefenstette, *Genetic Algorithms and their Applications: Proceedings of the Second International Conference on Genetic Algorithms*. Psychology Press, 2013.

[143] "Moamen Gasser Ahmed Naguib Artificial Neural Network Model to Predict Filtrate Invasion of Nanoparticle-Based Drilling Fluids." Accessed: Jun. 01, 2024. [Online]. Available: https://www.researchgate.net/publication/369156693_Artificial_Neural_Network_Model_to_Predict_Filtrate_Invasion_of_Nanoparticle-Based_Drilling_Fluids

[144] A. Parizad, K. Shahbazi, and A. A. Tanha, "SiO2 nanoparticle and KCl salt effects on filtration and thixotropical behavior of polymeric water based drilling fluid: With zeta potential and size analysis," *Results Phys.*, vol. 9, pp. 1656–1665, Jun. 2018, doi: 10.1016/j.rinp.2018.04.037.

[145] "Pitt, M. The Marsh funnel and drilling fluid viscosity: A new equation for field use. SPE Drill. Complet. 2000, 15, 3–6. - Recherche Google." Accessed: Jun. 19, 2024. [Online]. Available:

wi Ahmed Zarzor Al-Yaseri Apparent Viscosity Direct from Marsh Funnel Test | Iraqi Journal of Chemical and Petroleum Engineering." Accessed: Jun. 19, 2024. [Online]. Available: https://ijcpe.uobaghdad.edu.iq/index.php/ijcpe/article/view/268

[147] A. Gowida, S. Elkatatny, K. Abdelgawad, and R. Gajbhiye, "Newly Developed Correlations to Predict the Rheological Parameters of High-Bentonite Drilling Fluid Using Neural Networks," *Sensors*, vol. 20, p. 2787, May 2020, doi: 10.3390/s20102787.

[148] "FS alkabri Energies | Free Full-Text | Apparent Viscosity Prediction of Water-Based Muds Using Empirical Correlation and an Artificial Neural Network." Accessed: Jun. 19, 2024. [Online]. Available: https://www.mdpi.com/1996-1073/12/16/3067

[149] A. Alsabaa, H. Gamal, S. Elkatatny, and A. Abdulraheem, "Real-Time Prediction of Rheological Properties of Invert Emulsion Mud Using Adaptive Neuro-Fuzzy Inference System," *Sensors*, vol. 20, no. 6, Art. no. 6, Jan. 2020, doi: 10.3390/s20061669.

[150] "Nada Sabah Asawar A;Alswasiti Massara SalamImproving Drilling Fluid Properties at High Pressure Conditions Using Selected Nanomaterials - IOPscience." Accessed: Jun. 19, 2024. [Online]. Available: https://iopscience.iop.org/article/10.1088/1757-899X/579/1/012004

[151] M. T. Alsaba, M. F. Al Dushaishi, and A. K. Abbas, "Application of nano water-based drilling fluid in improving hole cleaning," *SN Appl. Sci.*, vol. 2, no. 5, p. 905, Apr. 2020, doi: 10.1007/s42452-020-2723-2.